UNIVERSIDADE D
COIMBRA

Bárbara Daniela Araújo Pinheiro Teixeira

# *ELUCIDATING AUTOPROCESSING ACTIVITY AND FUNCTION OF THE RICKETTSIAL RETROPEPSIN APRC IN MAMMALIAN CELLS*

**Tese realizada no Centro de Neurociências e Biologia Celular da Universidade de Coimbra no âmbito do Mestrado em Biologia Celular e Molecular, orientada pela Doutora Isaura Simões e Doutora Ana Luísa Carvalho apresentada ao Departamento de Ciências da Vida da Faculdade de Ciências e Tecnologia da Universidade de Coimbra**

Outubro de 2020

UNIVERSIDADE D
COIMBRA

Bárbara Daniela Araújo Pinheiro Teixeira

# *ELUCIDATING AUTOPROCESSING ACTIVITY AND FUNCTION OF THE RICKETTSIAL RETROPEPSIN APRC IN MAMMALIAN CELLS*

**Tese realizada no Centro de Neurociências e Biologia Celular da Universidade de Coimbra no âmbito do Mestrado em Biologia Celular e Molecular, orientada pela Doutora Isaura Simões e Doutora Ana Luísa Carvalho apresentada ao Departamento de Ciências da Vida da Faculdade de Ciências e Tecnologia da Universidade de Coimbra**

Outubro de 2020

This work was concluded at the Center for Neuroscience and Cell Biology (CNC) of the University of Coimbra, under the scientific supervision of Professor Isaura Simões and Professor Ana Luísa Carvalho, with the support of the Faculty of Science and Technology of the University of Coimbra.

This work was financed through the COMPETE 2020 - Operational Programme for Competitiveness and Internationalisation and Portuguese national funds via FCT – Fundação para a Ciência e a Tecnologia, under project POCI-01-0145-FEDER-029592 (aka PTDC/SAU-INF/29592/2017) (UndoHijack) and UIDB/04539/2020.

## Resumo

As espécies do género *Rickettsia* são bactérias intracelulares obrigatórias transmitidas a mamíferos através de vetores artrópodes, causando doenças infeciosas, como a febre maculosa das Montanhas Rochosas, a febre escaro-nodular e o tifo epidémico. A elevada patogenicidade e a falta de terapêuticas eficazes, associadas ao progressivo aumento da resistência a antibióticos, reforçam a importância da pesquisa de novos fatores de *Rickettsia* para o desenvolvimento de estratégias terapêuticas inovadoras. Neste contexto, a protease aspártica de *Rickettsia conorii* (APRc) emerge como um potencial alvo, tendo sido demonstrado que catalisa o processamento *in vitro* de duas proteínas autotransportadoras envolvidas na adesão e invasão de *Rickettsia* (Sca5/OmpB e Sca0/OmpA), antecipando o seu potencial envolvimento na modulação de fatores de virulência de *Rickettsia*. A APRc é uma protease membranar do tipo retropepsina, partilhando várias características com esta família de proteases aspárticas. Estas evidências experimentais marcam o início do estudo da APRc como um potencial alvo terapêutico em rickettsioses. No entanto, ainda existem várias questões em aberto relativamente à relação estrutura-função, sobretudo relativamente ao mecanismo e à dinâmica da atividade autolítica da APRc, bem como da natureza dos seus substratos. Até ao momento, a atividade de autoprocessamento da APRc apenas foi estudada *in vitro* e em *E. coli*. No entanto, e dada a relevância de células de mamífero na infeção por *Rickettsia*, importa avaliar a atividade da APRc também neste contexto. Neste trabalho, demonstrámos que diferentes construções do domínio solúvel da protease são autoprocessadas após expressão transiente em células HEK293, sendo este processo dependente da atividade catalítica da APRc. Além disso, a expressão de APRc induziu alterações morfológicas, como condensação nuclear, alteração da forma nuclear e aparecimento de material celular fragmentado, também dependente da sua atividade catalítica. Estas características são geralmente observadas em células apoptóticas e ensaios adicionais parecem corroborar este fenótipo de apoptose, observando-se um aumento na percentagem de células positivas para caspase-3 clivada e PARP clivada, e na percentagem de células anexina V-APC$^{+}$/DAPI$^{-}$, após a expressão da APRc.

Com este trabalho demonstramos o autoprocessamento da APRc em células HEK293 e antecipamos uma nova putativa função biológica desta protease de *Rickettsia* na modulação de processos de morte celular.



**Palavras-chave:** *Rickettsia* | retropepsina APRc | atividade de processamento da APRc | células de mamífero | morte celular

## Abstract

*Rickettsia* species are obligate intracellular bacteria that are transmitted to mammals through arthropod vectors, causing infectious diseases, such as Rocky Mountain spotted fever, Mediterranean spotted fever, and epidemic typhus. The life-threatening character of rickettsioses, the lack of specific therapeutics, and the progressive increase in antimicrobial resistance due to inappropriate use of antibiotics reinforces the importance of searching for new rickettsial factors to develop innovative therapeutic strategies. In this context, the aspartic protease from *Rickettsia conorii* (APRc) emerges as a candidate target for intervention since it was shown that this enzyme is able to catalyze the *in vitro* processing of two autotransporter adhesin/invasion proteins, Sca5/OmpB and Sca0/OmpA, anticipating its potential participation as a modulator of rickettsial surface virulence factors. APRc is a membrane-embedded retropepsin-like homologue, sharing several features of this family of aspartic proteases. This experimental evidence marks the beginning of exploring APRc as a target for developing new strategies to combat rickettsioses. However, there are still several open questions regarding structure-function relationships of APRc, namely in what concerns the mechanisms and dynamics of its autoactivation/activity and the nature of its substrates, which would help us to infer the functional relevance of this protease during infection. Until now, the autoprocessing activity of APRc was only studied *in vitro* and *E. coli*. However, the relevance of mammalian cells in rickettsial infection supports extending research to explore APRc activity in this context. Herein, we demonstrate that different GFP-APRc fusion constructs undergo autoprocessing upon transient expression in HEK293 cells, and that this process is dependent on the catalytic aspartate. Moreover, the expression of the different forms of APRc induced morphological alterations, such as nuclear condensation, alterations of nuclear shape, and the presence of fragmented cellular material, again dependent on APRc proteolytic activity. These features resemble an apoptotic phenotype, which our additional assays appear to corroborate by showing an increase in nuclear condensation, on the percentage of cleaved caspase-3 and cleaved PARP-positive cells, and of annexin V-$APC^+$/$DAPI^-$ cells, upon expression of APRc.

Taken together, the evidence presented in this work confirms APRc autoprocessing in HEK293 cells and suggest that induction of cell death may be one of the putative functions of this highly conserved rickettsial protease.

**Keywords:** *Rickettsia* | rickettsial retropepsin APRc | APRc autoprocessing activity | mammalian cells | cell death

# Table of Contents

## List of Abbreviations

| | |
|---|---|
| **AG** | Ancestral group |
| **AIDS** | Acquired immunodeficiency syndrome |
| **ANXA2** | Annexin A2 |
| **AP-SWATH** | Affinity-purification SWATH mass spectrometry |
| **Apaf** | Apoptotic protease activating factor |
| **APRc** | Aspartic protease from *Rickettsia conorii* |
| **Arfs** | ADP-ribosylation factors |
| **coxABC** | Cytochrome *c* oxidase |
| **cydAB** | Cytochrome *d* ubiquinol oxidase |
| **DAMPs** | Damage-associated molecular pattern molecules |
| **DMEM** | Dulbecco's modified eagle medium |
| **eIF4G** | Eukaryotic initiation factor 4G |
| **eIF3d** | Eukaryotic initiation factor 3 subunit d |
| **Epac1** | Exchange protein directly activated by cAMP |
| **ER** | Endoplasmic reticulum |
| **FBS** | Fetal bovine serum |
| **FGFR** | Fibroblast growth factor receptor |
| **FN1** | Fibronectin |
| **GEF** | Guanine nucleotide exchange factors |
| **HEK293** | Human embryonic kidney 293 cells |
| **HIV** | Human immunodeficiency virus |
| **HUVEC** | Human umbilical vein endothelial cell |
| **ICAM** | Intercellular adhesion molecule |
| **JAK-STAT** | Janus kinase-signal transducer and activator of transcription |
| **LB** | Luria-Bertani |
| **LPS** | Lipopolysaccharides |

| | |
|---|---|
| **MAC** | Membrane attack complex |
| **MD2** | Myeloid differentiation factor 2 |
| **MSF** | Mediterranean spotted fever |
| **MX1** | MX dynamin-like GTPase |
| **NF-κB** | Nuclear factor-kappa B |
| **PABP** | Poly(A)-binding protein |
| **PAMPs** | Pathogen-associated molecular pattern molecules |
| **PARP** | Poly(ADP-ribose) polymerase |
| **PIP5K** | Phosphatidylinositol 4-phosphate 5-kinase |
| **PI(4,5)$P_2$** | Phosphatidylinositol 4,5-biphosphate |
| **qPCR** | Real-time quantitative polymerase chain reaction |
| **RARP-2** | *Rickettsia* ankyrin repeat protein 2 |
| **RIPK** | Receptor interacting protein kinase |
| **RMSF** | Rocky Mountain spotted fever |
| **ROS** | Reactive oxygen species |
| **Sca** | Surface cell antigen |
| **SFG** | Spotted fever group |
| **SQSTM1** | Sequestosome-1 |
| **sodB** | Superoxide dismutase |
| **SOD** | Mitochondrial protein superoxide dismutase |
| **STAT** | Signal transducer and activator of transcription |
| **T4SSs** | Type IV secretion systems |
| **TCA** | Tricarboxylic acid cycle |
| **TG** | Typhus group |
| **TLR4** | Toll-like receptor 4 (TLR4) |
| **TRG** | Transitional group |
| **WT** | Wild-type |

# List of Figures

## List of Tables

# Chapter I

# 1. Introduction

## 1.1. *Rickettsia* and rickettsioses

*Rickettsia* species belong to the bacteria domain known for causing infectious diseases in humans, such as Rocky Mountain spotted fever (RMSF, caused by *Rickettsia rickettsii*), Mediterranean spotted fever (MSF) (*Rickettsia conorii*), and epidemic typhus (*Rickettsia prowazekii).* Based on the development of new cellular and molecular biology tools and whole genome sequence analysis, these species are organized in four different genetic groups, the ancestral group (AG), the spotted fever group (SFG), the typhus group (TG), and the transitional group (TRG). Most of the known species belong to the SFG, and most of the species which belong to SFG and also TG are pathogenic to humans, causing the previously mentioned diseases as well as milder forms of rickettsioses. These organisms are obligatory intracellular parasites, and have arthropod hosts (ticks, fleas or lice) as part of their life-cycle, allowing the transmission of the parasite to animals and humans (Walker and Ismail, 2008; Weinert et al., 2009; Cruz et al., 2014).

Over the last years, the impact of rickettsial diseases on global health has been increasing since it was reported that more than 50% of the emerging infectious diseases events occurred between 1940 and 2004 were caused by different bacteria, such as *Rickettsia* (Jones et al., 2008). Rickettsiae possess distinctive biological characteristics, like aerosol transmission, persistence in infected hosts and low infectious doses, and therefore are considered dangerous pathogens (Azad, 2007). In this way, in the last years, *Rickettsia* and rickettsioses have been the target of different studies with the goal of developing new therapeutics.

### 1.1.1. Epidemiology

Rickettsial microorganisms have been reported all over the world (except Antarctica), but most of them are restricted to a specific region due to vector constraints and also climatic conditions. From 2000 to 2017, the number of rickettsioses cases reported in the United States has been increasing but remarkably the case fatality rate has declined since 1940, when the tetracycline antibiotics start to became available (Centers for Disease Control and Prevention (CDC), 2020). The increase in reported cases and the decrease in death rates may be likely associated with the increase of *R. parkeri* rickettsioses, a milder form of rickettsioses when compared with the ones caused

by *R. rickettsii*, the etiologic agent of RMSF (Blanton, 2019; Centers for Disease Control and Prevention (CDC), 2019, 2020).

Several deathly outbreaks of RMSF were documented in Mexico during the 1940s, being that most of the patients belonged to economically disadvantaged communities characterized by many tick-infested domesticated and free-ranging dogs. Since the mid-2000s, there has been a resurgence of RMSF outbreaks in several regions of Mexico, predominantly driven by the same poor living conditions of the populations as during the 1940s (Parola et al., 2013; Álvarez-Hernández et al., 2017). The reported cases of RMSF have also been increasing in Mexico but, unlike the North American case, the case fatality rates also increased over the years, achieving 40% of case fatality in 2016 (Álvarez-Hernández et al., 2017).

Regarding MSF, in 1997, a fatality rate of 32.3% was reported in Portugal; however, in the 2000-2010 period, the number of reported cases of rickettsioses decreased (Sousa et al., 2003; European Centre for Disease Prevention and Control (ECDC), 2013). In the last years, new rickettsial species associated with human disease have been identified and diagnosed in Europe, reinforcing the idea that rickettsial infections are still not well recognized and that the magnitude of these diseases in Europe may be underappreciated (European Centre for Disease Prevention and Control (ECDC), 2013).

Regarding epidemic typhus, which is caused by *R. prowazekii*, it is responsible for epidemics in populations with poor sanitary and overcrowded conditions. Without antibiotic treatment, it can have case fatality rates up to 60% but can be reduced to below 5% with antibiotic treatment (Bechah et al., 2008).

With the increase of international travels and ecotourism, associated with an expansion in geographic distribution of vectors due to climate change, tick-borne rickettsioses are likely to increase in the next years, increasing even more the need for identifying and studying the different rickettsial species, particularly the pathogenic ones (Parola et al., 2013).

### 1.1.2. Pathogenesis and virulence factors

In order to fight bacterial diseases such as rickettsioses, it is relevant to identify and characterize the molecular strategies used by bacteria to infect and cause disease in a host. Pathogenic bacteria produce different types of molecules known as virulence factors, which help them to invade and colonize the host. These factors are either unique to specific species or conserved throughout different microorganisms (Wilson et al., 2002; Sharma et al., 2016). Depending on their function, virulence factors can be classified into distinct groups, including cytosolic factors, membrane-associated factors,

and secretory factors. The cytosolic factors allow bacteria to adapt to the host environment, leading to changes in bacteria metabolism, morphology, and physiology. On the other hand, the membrane-associated factors facilitate bacteria adhesion to and invasion of the host cells. To evade from host's innate and adaptive immune system, bacteria also produce secretory factors, that can also be involved in host tissue damage (Baron, 1996; Sharma et al., 2016).

#### 1.1.2.1. Life cycle

Rickettsiae are arthropod-transmitted bacteria, and arthropods can act as reservoirs, as amplifiers of these microorganisms as well as vectors. *Ixodes* ticks are considered the main reservoirs and vectors of SFG *Rickettsia,* but it has also been reported their association with mites, fleas, and lice (Raoult and Roux, 1997; Walker and Ismail, 2008). Besides *Ixodes* ticks, *Dermacentor* and *Rhipicephalus* ticks were also found to be vectors of *Rickettsia* (Socolovschi et al., 2009).

Although these bacteria occur in nature associated with arthropod vectors, *Rickettsia* can also infect vertebrates, including humans. When *Rickettsia* infect the arthropod, they start to grow and multiply in almost all organs. Ovaries of adult female ticks are one of these infected organs, and therefore the oocytes are also infected, giving rise to a transovarial transmission. Since the egg is infected, the infection is maintained across all following stages of the arthropod life cycle (transstadial transmission), leading to the maintenance of infection through several generations. Beyond the ovaries, the salivary glands can also be infected by bacteria. *Ixodes* ticks are obligate hematophagous, requiring blood to survive and reach the adult life stage (Raoult and Roux, 1997). When the tick damages the mammalian host skin, the host organism rapidly reacts with the formation of a hemostatic plug, activating the coagulation cascade, vasoconstriction, and inflammatory response to induce wound healing and tissue repair. These host responses would lead to the disruption of tick feeding and the rejection of the tick, having negative effects on tick feeding and development. Therefore, during host-tick co-evolution, ticks developed mechanisms that overcome both hemostatic and immune responses. The salivary secretion of ticks contains several biologically active molecules such as anticoagulants, anesthetics, immunomodulating molecules and, in case of infected ticks, *Rickettsia* that can be transmitted to vertebrate hosts (Raoult and Roux, 1997; Azad and Beard, 1998; Walker and Ismail, 2008; Kazimírová and Štibrániová, 2013). Relative to these saliva components, it is known that they can interfere with the complement system, with the activity of natural killer cells and macrophages, inhibit neutrophil function, and can even decrease the production of

cytokines in the host organism (Ferreira and Silva, 1999; Montgomery et al., 2004; Valenzuela, 2004; Kazimírová and Štibrániová, 2013).

Once *Rickettsia* are internalized by host cells, they have to escape from the phagosome before replication. After this, in the cytosol, bacteria start to replicate by binary fission and redistribute inside the cell. To complete their life cycle, these bacteria must lyse the host cell or infect neighbor cells since, depending on the species, they can also spread intercellularly (McClure et al., 2017) (**Figure 1**).

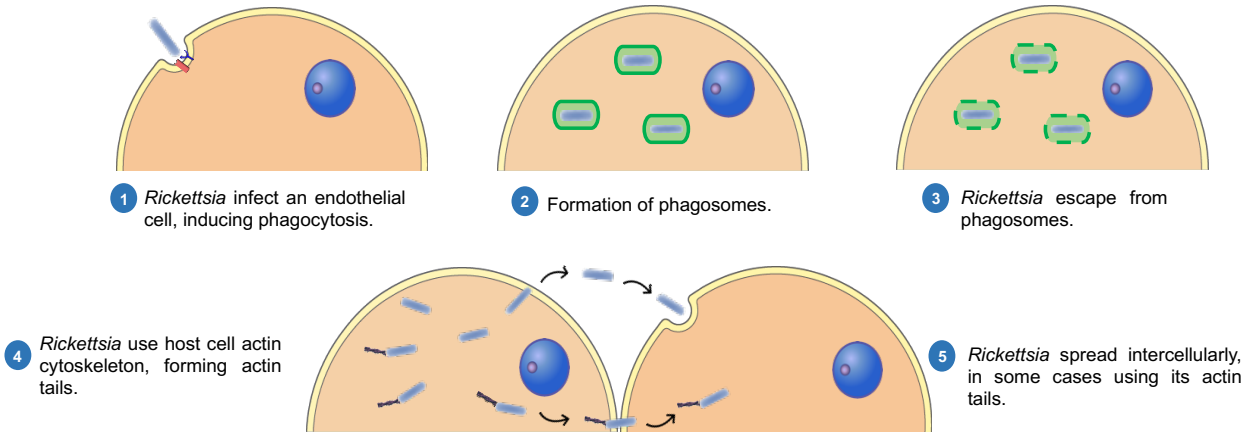


**Figure 1.** Life cycle of *Rickettsia* inside the host cell.
When *Rickettsia* contact with the host's cell membrane, it is recognized and phagocytosed by the host cell (**1** and **2**). However, *Rickettsia* disrupt the phagosomal membrane (**3**) and enter the host cytosol. Once *Rickettsia* gain access to the host cytosol, bacteria start to spread intra and intercellularly using the host cell actin cytoskeleton (in the case of TG members, they spread through lysis of the host cell not forming actin tails) (**4**). Therefore, bacteria that form actin tails move through the cytoplasm and into the membrane where they can escape to the neighbor cells (**5**).

Rickettsiae can also be harbored and transmitted by blood-sucking insects such as fleas and lice, but in these organisms the infection is not transmitted transovarially since *Rickettsia* kill their carrier host. In these cases, bacteria are thought to have mammal reservoirs, such as humans (proposed in the case of *R. prowazekii*), cats (*R. felis*) or rodents (*R. typhi*), and so they can spread bacteria through horizontal transmission (Gillespie et al., 2009b). Nonetheless, different research groups detected *R. felis* in mosquitoes, changing our knowledge of rickettsial vectors and its transmission to humans (Socolovschi et al., 2012a, 2012b; Dieme et al., 2015; Zhang et al., 2019). Mosquitos are able to carry and spread a significant number of pathogens and parasites that cause disease to humans throughout the world, such as malaria, dengue, Zika, yellow fever, and chikungunya (Maina et al., 2017; World Health Organization (WHO), 2020). With the discovery of new arthropod vectors and reservoirs of *Rickettsia*, it emerges a growing need to deepen the research on this field, namely in the study of the arthropod-human transmission mechanism (Legendre and Macaluso, 2017).

#### 1.1.2.2. Pathogenesis

Since rickettsiae are obligate intracellular bacteria, they evolved in such a way that they are capable of taking advantage of nutrients and energy available in the cytosol of the host cells. Due to this, throughout evolution, these species have lost several genes associated with the synthesis of many metabolites, presenting a highly conserved and reduced genome, and therefore making them highly dependent on the intracellular environment of the host cell to survive and proliferate. To take advantage of this intracellular environment, rickettsial species developed specific mechanisms to adhere, invade, and adapt to the host cell environment (Li and D. H. Walker, 1992; Fields et al., 2011). The main target of these pathogens is the microvascular endothelium, where they can proliferate and induce oxidative stress, injuring the endothelial cells (Walker et al., 1999). Because of this, most of the molecular components involved in host-pathogen interaction have been precisely identified in the context of rickettsiae-endothelial interactions. However, it has been uncovered that rickettsiae can infect other cell types beyond endothelial cells (*e.g.,* dendritic cells and macrophages) and, therefore, it is important the identification of the different molecular components involved in rickettsial-host cell interactions to be possible the application of this new knowledge in the prevention and treatment of rickettsioses (Fang et al., 2007; Chan et al., 2010; Curto et al., 2016).

#### 1.1.2.3. Virulence factors

The identification of virulence genes expressed in rickettsial species, the interpretation of their function on the host cell, and its validation *in vivo* have not been easy due to the difficult genetic manipulation of these species (Wood and Azad, 2000). Despite these difficulties, recent studies have been able to identify some putative factors that can be associated with the pathogenicity of *Rickettsia*, such as molecular components involved in the attachment to the host cell, phagosomal escape, and actin-based motility, as well as secreted effectors and other mediators that may be involved in other functions essential to rickettsial survival (Walker and Ismail, 2008).

To survive, *Rickettsia* must enter host cells, and so bacteria need to adhere to and invade host cells. The adherence process occurs due to the binding of rickettsial proteins to host cell receptors. Several rickettsial outer membrane proteins involved in this process belong to the surface cell antigen (Sca) autotransporter proteins family, such as Sca1, Sca2, Sca0/rOmpA, and Sca5/rOmpB (Li and Walker, 1998; Uchiyama et al., 2006; Cardwell and Martinez, 2009; Riley et al., 2010). Adr2 may be another protein that promotes the adhesion of rickettsiae to the host cells (Vellaiswamy et al., 2011); however, there is not much consensus on this hypothesis since Garza and colleagues

were not able to conclude that this protein is involved in the rickettsial attachment to host cell (Garza et al., 2017). These adhesion-mediating proteins promote close interaction between bacteria and the host, likely augmenting signaling events mediated by other rickettsial proteins involved in the invasion process (Riley et al., 2010). Some of these proteins only mediate adhesion to host cells but others, like Sca2, rOmpA, and rOmpB, also participate in the invasion process, allowing the entrance of bacteria. However, it is not yet described the mammalian host receptor of Sca2 (Cardwell and Martinez, 2009). On the contrary, the mammalian host receptors for rOmpB and rOmpA have been identified. Rickettsial OmpB plays a role in the invasion of the host cells through interaction with its mammalian host receptor, Ku70. The bacterial invasion induced by rOmpB-Ku70 interaction is dependent on clathrin and caveolin-2 and involves the ubiquitination of Ku70 by the ubiquitin ligase c-Cbl (Martinez et al., 2005; Uchiyama et al., 2006; Chan et al., 2009). Besides this, actin rearrangements are essential for the invasion, being ultimately dependent on Arp2/3 complex, activated by host signaling pathways involving GTPase Cdc42, phosphoinositide 3-kinase, c-Src, and the activity of other protein tyrosine kinases (Martinez and Cossart, 2004; Chan et al., 2009).

Cardwell and Martinez observed similarities between Sca2 and rOmpB-mediated invasion of mammalian cells through scanning and transmission electron microscopy. These results suggest that two different receptors at the plasma membrane can trigger invasion signals. However, these signals eventually converge in a single response, which is the local recruitment of actin filaments and components of the endocytic machinery (caveolin-2, clathrin, and c-Cbl) to invade the host cell (Cardwell and Martinez, 2009). He and colleagues concluded that rOmpB also interacts with host annexin A2 (ANXA2) present on the host cell surface, showing that the depletion of *ANXA2* gene hampered rickettsial adhesion to the host cells *in vitro*. Therefore, this data suggests that ANXA2 might play a key role in rickettsial adhesion to the host cells (He et al., 2019). Recently, it was reported that rOmpB is also capable of binding to factor H, the major soluble inhibitor of complement, which prevents complement activation and amplification on the host surface (Riley et al., 2012). As we can observe, some proteins exhibit more than one function, apparently using different mechanisms. Therefore, these proteins possess moonlight activity, being denominated as moonlighting proteins (Jeffery, 1999).

Regarding rOmpA, it was recently described that this conserved rickettsial protein interacts with α2β1 integrin heterodimer (Hillman et al., 2013). Nonetheless, it was not yet described if rOmpA-α2β1 integrin-mediated invasion activates the different signaling cascades associated with β1integrin activation. Also, it was reported that the $\beta$-peptide of rOmpA can associate with fibroblast growth factor receptor (FGFR)1 that, when

activated by phosphorylation, binds to caveolin-1, facilitating the entry of *Rickettsia* through endocytosis mediated by caveolin-1. This endocytic mechanism is also mediated by the presence of heparan sulfate proteoglycans (HSPGs) since the presence of HSPGs and also FGFR1 inhibitors resulted in the decrease of rickettsial internalization into host cells (Sahni et al., 2017).

As described before, several host proteins are involved in rickettsial adhesion to and/or invasion into host cells, such as Ku70 (Martinez et al., 2005), α2β1 integrin (Hillman et al., 2013), caveolin-2 (Chan et al., 2009), and clathrin (Chan et al., 2009). Another host protein was recently described that might also play a role in rickettsial adhesion to and invasion into host cells, the exchange protein directly activated by cAMP (Epac)1. Gong and colleagues demonstrated that both *Epac1* gene knockout and pharmacological inhibition of Epac1 *in vivo* suppress rickettsial adhesion and invasion, suggesting that this host protein might play an important role in rickettsial infection (Gong et al., 2013). Until now, the molecular mechanisms underlying the Epac1-mediated rickettsial adhesion and invasion are still unknown.

The outer membrane proteins rOmpB and rOmpA can be cleaved *in vitro* by APRc, a protease found in the outer membrane of *Rickettsia*. Therefore, this protease can also have a role in rickettsial virulence and might be another example of a moonlighting protein, which will be further developed later in this chapter (Cruz et al., 2014). *Rickettsia* also express an outer membrane glycoprotein named Adr1 that binds vitronectin, which is another complement inhibitory protein. This interaction prevents the membrane-damaging effect of the terminal complement pathway (there is no formation of the membrane attack complex (MAC) on bacteria surface), therefore promoting resistance to the host anti-bacterial effects. Also, Adr1-vitronectin interaction may contribute to rickettsial adhesion to host cells (Riley et al., 2014; Fish et al., 2017). Adr2, a protein related to Adr1, seems to be also involved in the evasion from the host immune system. When Adr2 was expressed in serum-sensitive *E. coli* cells, they became serum-resistant, suggesting that this protein is involved in rickettsial serum-resistance mechanisms. In addition, researchers observed that Adr2 binds to vitronectin, similar to what has been observed for Adr1 (Garza et al., 2017).

After the adhesion and invasion processes, attached *Rickettsia* are engulfed since there is the activation of intracellular signaling pathways, inducing actin polymerization and membrane reorganization. It occurs the internalization of bacteria and they are phagocytosed in a clathrin and caveolin-dependent way (Uchlyama, 2012). Once phagocytized by host cells, rickettsiae rapidly escape from the phagosome and enter the host cytosol. To disrupt the phagosomal membrane, rickettsial species use membranolytic proteins such as phospholipase D and hemolysin C (Whitworth et al.,

2005). It is also anticipated that this membrane disruption is mediated by phospholipase A2, another possible moonlighting protein since it has been reported to mediate host entry and host lysis for intercellular spread (Rahman et al., 2013) .

Once *Rickettsia* gain access to the host cytosol, bacteria start to spread intra and intercellularly using the host cell actin cytoskeleton. SFG *Rickettsia* express the surface molecules RickA and Sca2, which activate actin nucleation and recruit the Arp2/3 complex to form an actin tail (Sahni et al., 2013). Recently, Reed and colleagues reported that RickA and Sca2 are responsible for rickettsial motility at different times during infection. In early stages, bacterial motility is slow and winding, promoted by a short and curved actin tail, requiring both RickA and the Arp2/3 complex. In contrast, late motility requires only Sca2, promoting fast and directionally persistent movement due to a straight and long actin tail (Reed et al., 2014). In this specific case, Sca2 has a function similar to eukaryotic formins, facilitating the elongation of pre-existing actin filaments (Haglund et al., 2010). Kleba and colleagues recently reported that the disruption of Sca2 protein in *R. rickettsii* inhibits actin-based motility *in vitro*, not being observed the formation of actin comet tails, with intercellular spread also being affected. They also inoculated guinea pigs with *R. rickettsii* Sca2 mutant, observing that these animals did not develop fevers, a metric used for virulence. Therefore, this experimental evidence suggests that Sca2 is essential for rickettsial actin-based motility and intercellular spread, and it can be considered a virulence factor for this rickettsial species (Kleba et al., 2010). From these observations, we can conclude that Sca2 is another example of a moonlighting protein since it is involved in adherence, invasion, and actin-based motility, probably through independent cellular processes. Nonetheless, rickettsial species belonging to TG can only form short actin tails, as they do not possess *rickA,* and *sca2* encodes a divergent protein. These data suggest that to infect adjacent cells, TG bacteria use a distinct mechanism. Due to a high accumulation related to intercellular replication, TG species cause the lysis of the infected cells, thereby disseminating to the neighbor cells (Hackstadt, 1996; Reed et al., 2014).

To survive inside the host cells, intracellular bacteria can subvert and exploit the eukaryotic machinery. These bacteria possess refined secretion systems, which allow them to inject effector molecules into the host cell and modulate several host proteins (Sahni et al., 2013). Thus, some bacteria such as *Rickettsia* use a membrane-associated transporter system named type IV secretion system (T4SS), allowing the translocation of virulence factors into host cells. These translocated effector molecules have a wide range of host-changing functions, such as introgression of genome, modification of cytoskeleton and ubiquitination system, and sequestration of vesicular trafficking (Gillespie et al., 2009a). One example of these effector molecules is RalF, a protein only

found in some *Rickettsia* and *Legionella* species. This protein contains a Sec7 domain, which is conserved in eukaryotic guanine nucleotide exchange factors (GEFs), responsible for activating ADP-ribosylation factors (Arfs), proteins associated with actin cytoskeleton remodeling (in *Rickettsia* species) and vesicle trafficking (in *Legionella* species) (Alix et al., 2012). It is already described that RalF interacts and activates specifically Arf6, inducing the endocytosis of bacteria *via* phosphatidylinositol 4-phosphate 5-kinase (PIP5K) and phosphatidylinositol 4,5-biphosphate ($PI(4,5)P_2$) (Rennoll-Bankert et al., 2016). In this way, since *Rickettsia* can manipulate the actin cytoskeleton *via* RalF, this effector protein may be involved in the invasion of host cells. Recently, it was showed that *Rickettsia* ankyrin repeat protein (RARP)-2 is another type IV secreted effector. It was shown to be released into the host cytosol, where it interacts with the endoplasmic reticulum (ER) manipulating its structure to form membranous structures (Lehman et al., 2018). Recently, RARP-2 was also associated with selective fragmentation of the *trans*-Golgi network, compromising protein trafficking to the different subcellular destinations, which might be another rickettsial strategy to escape from host cell immune surveillance (Aistleitner et al., 2020).

In response to cellular stress, such as bacteria invasion, a defense mechanism called autophagy is activated in host cells to eliminate the invading bacteria. However, several intracellular bacteria have evolved mechanisms to evade autophagy (Wu and Li, 2019). For instance, some bacterial pathogens are capable of avoiding the formation of a polyubiquitin coat by recruiting host proteins to the bacteria surface, shielding themselves from autophagy recognition (Ogawa et al., 2005; Yoshikawa et al., 2009; Dortet et al., 2011). Regarding rickettsial species, it was recently reported that rOmpB blocks the formation of a polyubiquitin coat, protecting rickettsiae against autophagic recognition by host cells, both in macrophages and endothelial cells. When cells were co-infected with wild type (WT) and *ompB* mutant *R. parkeri,* Engström and colleagues observed that, while mutant bacteria were polyubiquitylated, WT bacteria were not stained for polyubiquitin, suggesting that rOmpB acts specifically on the surface of bacteria, without globally affecting the host ubiquitylation machinery. This research group was also interested in determining whether rOmpB was an *R. parkeri* virulence factor *in vivo,* similar to that observed *in vitro* in cell cultures. Using the mouse as an animal model, they concluded that rOmpB promotes autophagy evasion in host immune cells, allowing the colonization of animal organs (spleen, lungs, liver, and kidneys) by *R. parkeri* (Engström et al., 2019). In addition to playing a role in adhesion to and invasion into host cells and serum resistance, rOmpB also seems to be important in evasion from the host's autophagy machinery, thus reinforcing the idea rOmpB is another example of a moonlighting protein.

*Rickettsia* express other possible virulence factors that might also be involved in other processes essential to their intracellular survival, such as cytochrome *c* oxidase (coxABC) and cytochrome *d* ubiquinol oxidase (cydAB), enzymes used for aerobic respiration under different oxygen concentrations (coxABC is used under optimal aerobic conditions, and cydAB is used under low-oxygen concentrations) (McLeod et al., 2004; Narra et al., 2016). *Rickettsia* also express superoxide dismutase (sodB) that neutralizes reactive oxygen species (ROS) produced by the host cells as a response to an infection (Walker and Ismail, 2008). It was recently identified a peptidoglycan amidase in *R. conorii* (RC0497) that is mainly localized on the cell wall, on the periplasmic space, and on cell separation junctions during the division of rickettsiae (Patel et al., 2020). Through *in vitro* assays, Patel and colleagues concluded that this rickettsial enzyme can cleave peptidoglycan, the major component of the bacterial cell envelope and one of the most important pathogen-associated molecular pattern molecules (PAMPs) recognized by the host innate immune system (Wolf and Underhill, 2018; Patel et al., 2020). The cleavage of peptidoglycan molecules, importing it into the rickettsial cytoplasm, may be an effective strategy to escape the host immune system developed by rickettsiae and other bacteria (Humann and Lenz, 2009; Patel et al., 2020). By being able to degrade peptidoglycans present on the cell wall, RC0497 may also be involved in the rickettsial cell wall recycling (Patel et al., 2020). The turnover of cell wall seems to be a conserved and important mechanism present in several bacteria, conferring several advantages, such as the recovery of resources and detection of antibiotics targeting cell wall (Mayer, 2012; Johnson et al., 2013).

During a rickettsial infection, it is observed eruption, pyrexia, and endotoxin shock in the infected mammalian. It is thought that these symptoms might be mediated by lipopolysaccharide (LPS) found on the outer membrane of *Rickettsia* since this endotoxin triggers an inflammatory response through the Toll-like receptor 4 (TLR4) / myeloid differentiation factor 2 (MD-2) receptor complex in many host cell types (Uchlyama, 2012; Guillotte et al., 2018).

In order to identify putative virulence factors and taking into account the limitations in genetic manipulation of rickettsial species, research groups resort to different approaches like comparative genomics between virulent (*e.g.*, *R. prowazekii* Rp22 strain) and avirulent (*e.g.*, *R. prowazekii* Madrid E strain) strains (Sahni et al., 2013). However, genomic comparisons alone are not sufficient for associating genotype with phenotype since, for example, the autotransporter Sca2 is present and functional in several avirulent rickettsial species and, nevertheless, its disruption in virulent strains decrease their virulence (Kleba et al., 2010). Therefore, it is necessary to resort to complementary methodologies to obtain a complete inventory of rickettsial virulence

factors and their mechanisms of action, allowing potential targets for therapeutic intervention to be unveiled.

The majority of the studies mentioned above regarding the identification of the rickettsial virulence factors have been performed with endothelial cells. However, results from different research groups have shown that other cell types are also infected by *Rickettsia*, namely dendritic cells and macrophages (Fang et al., 2007; Chan et al., 2010; Curto et al., 2016). This evidence anticipates a much more complex network of host-pathogen interactions, and opens several questions regarding the putative function(s) of the already identified and those yet unknown rickettsial virulence factors in different cell types.

#### 1.1.2.4. Manipulation of host cells by *Rickettsia*

As previously stated, rickettsiae can infect other cell types beyond endothelial cells (Fang et al., 2007; Chan et al., 2010; Curto et al., 2016). Assuming this, it is plausible to hypothesize that there are probably many other rickettsial virulence factors whose function is still unknown, given the high level of manipulation that has been described in host cells upon rickettsial infection (Zhao et al., 2016, 2020; Curto et al., 2019b, 2019a).

When THP-1 cells (macrophage-like cells) were infected with *R. conorii*, a pathogenic member of SFG *Rickettsia*, researchers observed an alteration in the proteomic profile and the host gene expression profile of infected cells. These data provide new insights about some pathogenesis mechanisms of rickettsial species and how these bacteria hijack host cells to own advantage (Curto et al., 2019a, 2019b). At 24h post-infection, it was observed that the infection of THP-1 cells by *R. conorii* induces the enrichment of several enzymes involved in the tricarboxylic acid cycle (TCA) (such as citrate synthase and fumarate hydratase), as well as some members of oxidative phosphorylation (like cytochrome c and ubiquinol-cytochrome c redutase core protein 1) (Curto et al., 2019a). The upregulation of enzymes implicated in these metabolic pathways associated with ATP production suggests that the infection by *Rickettsia* reprograms the metabolism of the host to increase ATP production for a successful intracellular replication of bacteria. Besides these host metabolic pathways, rickettsial infection also promotes an increase in several enzymes of fatty acid β-oxidation, a catabolic process in which fatty acid molecules are degraded to generate acetyl-CoA, one of the intermediates of TCA (Curto et al., 2019a). Glutaminolysis is another metabolic pathway that generates intermediates of TCA, converting glutamate in α-ketoglutarate. In *R. conorii*-infected cells, some enzymes involved in this protein catabolism process are increased, such as glutamate dehydrogenase I (Curto et al., 2019a). Taking into account these data, it can be assumed that *R. conorii* manipulates

different host pathways, all involved in the generation of intermediates of TCA, with the ultimate goal of increasing the levels of ATP. The idea that *Rickettsia* may modify metabolic supply and demand in host cells is also supported by the evidence that several types of inner and outer mitochondrial membrane transporters are found increased in cells infected by *R. conorii*. All of these metabolic alterations triggered by *R. conorii* infection are characteristic of an M2-like, anti-inflammatory activation program, beneficial for the pathogen survival and proliferation inside host cells (Curto et al., 2019a). In parallel with *R. conorii*-infected THP-1 cells, researchers also evaluated the proteome of THP-1 cells infected with *R. montanensis,* a non-pathogenic member of SFG *Rickettsia*. Infection of these cells either with *R. conorii* or *R. montanensis* induced a decrease of multiple subunits of the proteasome and immunoproteasome, which can be considered a rickettsial mechanism to escape from antigen peptide presentation in immune cells (Curto et al., 2019a). However, the impairment of the proteasome may lead to the accumulation of misfolded and toxic proteins in the ER, resulting in ER stress and compromising the host cell viability. To avoid this harmful effect in host cells, and to be able to replicate inside the macrophages, *R. conorii* appears to be able to increase the ER folding capacity by increasing host protein content involved in protein processing and quality control (Curto et al., 2019a). This counteracting rickettsial mechanism was not observed in *R. montanensis*-infected cells, which may explain why this rickettsial species cannot establish a successful infection within macrophages (Curto et al., 2016, 2019a).

Besides modulating several metabolic pathways of the host cells, *R. conorii* can also interfere with the host gene expression as early as 1h post-infection, altering the expression of several genes that may contribute to the survival and proliferation of this pathogen within macrophages (Curto et al., 2019b). Some of the transcripts that were found increased in THP-1 cells infected with *R. conorii* are associated with pro-survival pathways, such as Bcl-2 protein family members MCL1 and BCL2A1 (Curto et al., 2019b). The infection of THP-1 cells by *R. conorii* also induced an enrichment in PIM3 transcripts, that are involved with the prevention of apoptosis, promotion of cell survival, and protein translation (Mukaida et al., 2011; Curto et al., 2019b). mRNA levels of the mitochondrial protein superoxide dismutase (SOD) 2, known to have a crucial role in the protection against oxidative stress and cell death, were also upregulated in *R. conorii*-infected cells (Drane et al., 2001; Curto et al., 2019b). The profound modulation of host gene expression machinery by *R. conorii* is also reflected in the alteration of non-coding RNAs, molecules with key roles in the control of gene expression and also in the modulation of the activity of several transcription factors, that might alter the expression of other genes (Mattick and Makunin, 2006; Curto et al., 2019b). This experimental evidence opens several questions regarding the relevance of immune cells in the

progression of infection since rickettsiae can profoundly manipulate the transcriptional apparatus of the host to extend host cell survival, as well as pathogen survival and proliferation within macrophages.

Since endothelial cells are considered the first target of *Rickettsia*, researchers analyzed the proteome and secretome profiles in *R. conorii*-infected endothelial cells (Zhao et al., 2016, 2020). When the proteome of total cellular lysates of endothelial cells infected for 10 days with *R. conorii* was analyzed, it was reported the accumulation of several proteins associated with Janus kinase-signal transducer and activator of transcription (JAK-STAT) pathway, such as signal transducer and activator of transcription (STAT)1, MX dynamin-like GTPase (MX1), and ISG15 ubiquitin-like modifier (Zhao et al., 2016). In these whole-cell lysates, several proteins involved in the pyrimidine and arginine biosynthetic pathways were found decreased, suggesting that rickettsiae may perturb different metabolic pathways of host cells (Zhao et al., 2016). Besides analyzing total cellular lysates, Zhao and colleagues also explored the proteome of plasma membrane of *R. conorii*-infected endothelial cells, detecting a decrease on the expression of α-actin 1, which may explain the formation of gaps on adherens junctions of endothelial cells after rickettsial infection (Valbuena and Walker, 2005; Zhao et al., 2016). Analysis of the Golgi fraction resulted in the identification of downregulated proteins involved in cadherin signaling, consistent with the endothelial cell detachment observed upon rickettsial infection, resulting in tissue invasion (George et al., 1993; Zhao et al., 2016). In this fraction, it was also reported the increase of several proteins involved in platelet-endothelial adhesion, such as intercellular adhesion molecule (ICAM)-1 and fibronectin (FN1) (Zhao et al., 2016).

A proteomics approach was also applied to analyze the secretome of *R. conorii*-infected endothelial cells (Zhao et al., 2020). At 24h post-infection, several proteins were found upregulated on the secretome of infected endothelial cells, such as cytokines and chemokines, molecules with a crucial role in cell signaling. Besides these proteins, it was also reported the secretion of sequestosome-1 (SQSTM1), a scaffold protein with an important role in the autophagic degradation of ubiquitinated substrates (Sebastiani et al., 2017; Zhao et al., 2020).

Based on these experimental data, it can be assumed that the host cell is extremely manipulated during rickettsial infection. Therefore, many more rickettsial effectors are likely required that are still unknown, not only in number but also in the many functions that each virulence factor may eventually exert.

#### 1.1.2.5. Host cell death regulation by *Rickettsia*

In response to bacterial infection, the host cell activates an immune defense mechanism intrinsic to several organisms, which is the death of infected cells. There are different types of cell death already described, such as necrosis, pyroptosis, and apoptosis (Ashida et al., 2011). Necrosis is an uncontrolled form of cell death, triggered by an external insult, such as bacterial infection or physical injury. Inside the cell, the increase in ROS production and the triggering of danger signals result in several collateral damages, including nuclear swelling, membrane rupture and, consequently, the release of cellular contents. In the end, this type of cell death leads to the activation of an inflammation cascade independent of caspase-1, resulting in tissue damage (D'Arcy, 2019). Like necrosis, pyroptosis is also a pro-inflammatory type of cell death, being the major difference its dependence on caspase-1. Pyroptosis is triggered by the presence of PAMPs and damage-associated molecular pattern molecules (DAMPs) (Ashida et al., 2011). The recognition of these molecules results in the assembly of the inflammasome, with the activation of caspase-1. The activation of this cellular death pathway results in nuclear condensation, membrane rupture, and the release of pro-inflammatory cytokines into the surrounding area (Ashida et al., 2011; D'Arcy, 2019). Bacterial infection may also trigger apoptosis, a noninflammatory type of programmed cell death. Morphologically, apoptotic cells are characterized by membrane blebbing, nuclear condensation, DNA fragmentation, and cell shrinkage (Ashida et al., 2011; Atkin-Smith and Poon, 2017). At the later stages of apoptosis, the formation of apoptotic bodies retaining the pathogen is observed, which are ultimately eliminated by professional phagocytes, such as macrophages and dendritic cells (Atkin-Smith and Poon, 2017; Naderer and Fulcher, 2018; D'Arcy, 2019).

The induction of cell death may be essential to eliminating the infecting agent and destroying the pathogenic niche, preventing the replication and dissemination of the pathogen (Labbé and Saleh, 2008). Also, the death of host immune cells, such as macrophages, promotes its engulfment by dendritic cells, stimulating antigen presentation to T cells and, consequently, an effective activation of the adaptive immune system (Yrlida and Wicka, 2000). Despite these host mechanisms to fight bacterial infection, pathogens evolved strategies to inhibit cell death to achieve a successful infection (Labbé and Saleh, 2008). These strategies affect different cellular pathways associated with cell death. Some bacteria can upregulate the transcription of anti-apoptotic genes through the activation of nuclear factor-kappa B (NF-κB) pro-survival pathway or inactivation of NF-κB protein inhibitors (Ge et al., 2009; Naderer and Fulcher, 2018). Caspases play an essential role during cell death, being expressed as inactive zymogens (procaspases). Once activated, a proteolytic cascade is initiated to activate

other caspases and signaling pathways, leading to cell death (Elmore, 2007; Li and Yuan, 2008). Several pathogens target these apoptotic caspases by secreting factors similar to inhibitors of apoptosis. These factors interact with host caspases, preventing its activation by molecular mimicry (Blasche et al., 2013; Pallett et al., 2017). Pro-apoptotic proteins may also be the target of some bacterial factors that act by inhibiting their activity or even degrading them (Dong et al., 2005; Ying et al., 2005; Banga et al., 2007). Bacteria also manipulate the assembly and activation of the inflammasome, an immune system response that plays a critical role in the induction of inflammatory cascade, culminating in pyroptosis (Latz et al., 2013). This manipulation is due to the secretion of virulence factors that interfere with inflammasome's proteins, preventing its assembly (Brodsky et al., 2010; Dewoody et al., 2011).

At later stages of infection and after successful replication, pathogens may activate apoptotic signaling pathways on the host cells to escape and disseminate through the neighboring cells. The induction of apoptosis may also aim for the death of immune cells to facilitate a successful colonization (Ashida et al., 2011; Naderer and Fulcher, 2018). Mitochondria play an essential role in the regulation of cell death. Therefore, some pathogenic factors target these organelles by increasing the permeabilization of mitochondrial membranes, leading to the release of cytochrome c into the cytosol. The subsequent activation of downstream caspases induces apoptosis of these cells (Bielaszewska et al., 2013). In addition to targeting mitochondria to induce apoptosis, some bacteria interfere with the host's protein translation, thereby generating cellular stress responses, such as the activation of pro-apoptotic factors (Naderer and Fulcher, 2018). By impairing protein translation, the production of pro-survival factors might also be compromised, leading to their depletion. Consequently, the low abundance of pro-survival factors may be sufficient to induce Bax/Bak-dependent apoptosis (Goodall et al., 2016).

Since *Rickettsia* are obligate intracellular bacteria, they evolved strategies to prevent the host's cell death in order to maintain the replicative niche. During infection in endothelial cells, rickettsiae can activate NF-κB, a small family of transcription factors that influence the transcription of several genes, some of them involved in the prevention of apoptosis (Sporn et al., 1997; Clifton et al., 1998; Polager and Ginsberg, 2008). The activation of this protein complex during rickettsial infection prevents the activation of initiator caspases-8 and -9 and, consequently, the activation of executioner caspase-3 (Joshi et al., 2003). In addition, the activation of NF-κB also maintains the integrity of host cell mitochondria (Joshi et al., 2003). Joshi and colleagues have also shown that infection-induced NF-κB activation prevents host endothelial cell death by balancing the-intracellular levels of anti-apoptotic and pro-apoptotic factors (Joshi et al., 2004).

Under normal conditions, NF-κB is kept inactive at the cell cytoplasm through association with inhibitory proteins of the IκB family. As a response to a cell stimulus, the IκB proteins are phosphorylated by IKK kinase complex (IKKα and IKKβ), leading to its ubiquitination and degradation by the proteasome (Clifton et al., 2005; Israël, 2010). Consequently, NF-κB complex is redirected into the nucleus, activating the transcription of several genes involved in different cellular responses, such as cell survival (Israël, 2010). Clifton and colleagues concluded that the rickettsial infection-induced NF-κB activation was dependent on the upstream activation of the kinase complex since, 2h post-infection, the activity of both catalytic subunits (IKKα and IKKβ) was significantly increased when compared with uninfected endothelial cells (Clifton et al., 2005).

In endothelial cells infected with *R. rickettsii*, it was reported that the activation of NF-kB was firstly detected 1.5h post-infection, with a significant increase of activation levels at 3 and 24h post-infection, although it returned to baseline levels at an intermediate time-point (14h) (Sporn et al., 1997). These results suggest that the activation of NF-kB is a dynamic cellular process controlled by *R. rickettsii*.

Most previous studies on endothelial cells' survival mediated by *Rickettsia* were focused on the early stages of infection. However, it is possible that the rickettsiae-mediated prevention of apoptosis may also be a dynamic process controlled by the pathogen. Bechelli and colleagues reported that infection of endothelial cells with the "Israeli spotted fever" strain of *R. conorii* caused significant cell death at a late stage of infection (72h). The induction of cell death at this stage may be correlated with the activity of caspase-1 since its pharmacological inhibition decreases cell death significantly. However, it is possible that other cellular mechanisms may be involved in cell death since the treatment with caspase-1 inhibitor only partially decreases cytotoxicity (Bechelli et al., 2015).

As in endothelial cells, the modulation of apoptosis in macrophages may also be a dynamic process. In *R. conorii*-infected macrophages, no significant increase in cleaved poly (ADP-ribose) polymerase (PARP) positive cells (a marker of late stages of apoptosis) was observed at 24 and 120h post-infection. Nonetheless, at an intermediate time-point (72h), the number of these positive cells was significantly increased, suggesting that the regulation of host cell death may indeed be an important mechanism for *Rickettsia* survival (Curto et al., 2019b). Consistent with the idea that *Rickettsia* manipulates host survival pathways to maintain the niche, Curto and colleagues observed that at 1h post-infection, there was an upregulation of several pro-survival genes, as previously described on section 1.1.2.4. (Curto et al., 2019b).

Besides efficiently infecting endothelial cells and macrophages, it is demonstrated that *R. rickettsii* also infect neuronal cells at late stages of infection, consistent with

dysfunctions of the central nervous system reported during rickettsial infection (*e.g.*, headache and signs of meningoencephalitis) (Joshi and Kovács, 2007; Sekeyová et al., 2019). As a consequence of the rickettsial infection, neuronal apoptotic cell death is induced, being neurons more susceptible to *R. rickettsii*-induced apoptosis than endothelial cells (Joshi and Kovács, 2007).

In summary, at early stages of infection, the pathogen subverts host cell survival signaling pathways, increasing the host cell viability to allow survival and proliferation within the host. After a successful infection, the pathogen may switch host cell signaling into the activation of apoptosis signaling pathways, likely for rickettsial dissemination.

### 1.1.3. Therapeutics

Rickettsial diseases present several clinical symptoms, which vary with the causative agent and patient. The typical symptoms appear within 2-14 days of infection and include fever, headache, malaise, rash, nausea, and vomiting (Raoult and Roux, 1997). Most rickettsioses cause moderately severe illness but, in some cases, such as RMSF, MSF, and epidemic typhus, the disease can be life-threatening and even fatal in some untreated cases (Parola et al., 2005). The diagnosis of rickettsioses is based on the clinical history (tick bites, recent travel, outdoor recreational activities, contact with animals), clinical recognition, and biological tests such as serology, cell culture, and molecular tools (Parola et al., 2005; Chapman et al., 2006). The fastest and sensitive test available is real-time quantitative polymerase chain reaction (qPCR), a molecular tool that allows determining the presence of specific genes present in rickettsial DNA (Parola et al., 2005; Renvoisé et al., 2011). The treatment of patients should be started when a rickettsiosis is suspected, never waiting for the confirmatory test as some infections can be rapidly progressive. The most widely used antibiotics in these cases are bacteriostatics from the tetracycline class, most commonly doxycycline (Dobler and Wölfel, 2009).

Over the last years, the progressive increase in antibiotic resistance among pathogenic bacteria is a growing concern for global health, urging for the identification and development of novel alternatives to antibiotics. As described above, bacterial pathogenicity can be associated with several factors, among which are proteolytic enzymes. Therefore, these proteases can be considered possible targets for the development of new drugs alternative to antibiotics.

## 1.2. Retropepsin-like proteases

Proteases are enzymes responsible for catalyzing the hydrolysis of peptide bonds. When discovered, proteases were considered housekeeping enzymes involved mainly in protein catabolism, generating smaller peptides and free amino acids. However, over time, it was found that these enzymes can also catalyze precise reactions of protein post-translational processing (López-Otín and Bond, 2008). Proteases cleave specific peptide bonds of target proteins, resulting in activation, inactivation, generation of new proteins, and even alteration of protein function (Rogers and Overall, 2013).

These enzymes are classified into nine classes based on the catalytic residue: serine, cysteine, threonine, aspartic, glutamic, metalloproteases, asparagine, mixed catalytic type, and a class which includes several proteases that are not yet assigned in any particular catalytic group (Rawlings et al., 2018). Aspartic proteases are a class of proteases that cleave the peptide bond using an activated water molecule hydrogen-bonded to two aspartate residues in the active site (Ratner et al., 1985). According to the *MEROPS* database, six clans of aspartic proteases are described, each one with a common ancestry (Rawlings et al., 2018). Each clan includes several families with similar structures, functions, and significant sequence similarity. The family A2 - retropepsin-like enzymes or retroviral-like proteases - is one of the best-studied family of aspartic proteases given their relevance for human disease.

Retropepsins are essential enzymes for the survival and proliferation of retroviruses. To overcome the low size of the genome, retroviruses evolved different mechanisms of genetic economy to encode the proteins essential for their survival. The expression of polyproteins is one of these mechanisms in which, after translation, these polyproteins are cleaved into functional proteins (Konvalinka et al., 2015). The structural proteins of retroviruses, such as the matrix protein, the capsid protein, and the nucleocapsid protein, are encoded as part of Gag polyprotein. On the other hand, the viral replication enzymes, including the reverse transcriptase, the RNase H, and the integrase, are included in the Pol polyprotein (Vogt, 1997). When Gag polyprotein is translated, the viral components form the viral particles, immature and, thus, non-infectious particles. To become mature and infectious, the proteolysis of polyproteins needs to happen, with this cleavage being mediated by the protease (retropepsin) (Swanstrom and Wills, 1997) (**Figure 2**). The protease may be encoded as part of Gag polyprotein, Pol polyprotein, or even in a separate open read frame (ORF), depending on the genome structure of retroviruses (Konvalinka et al., 2015). Besides *gag* and *pol* ORF, retroviruses also have the envelope (*env*) ORF, in which the mature product is a

glycoprotein that forms the viral envelope, being subsequently cleaved into surface and transmembrane subunits (Johnson, 2011) (**Figure 2**).

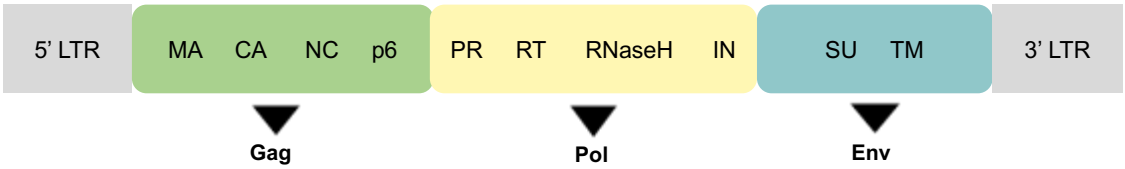


**Figure 2.** Representative genome structure of retroviruses.
Abbreviations: LTR: long terminal repeat; MA: p17 matrix protein; CA: p24 capsid protein; NC: p7 nucleocapsid; PR: protease; RT: reverse transcriptase; IN: integrase; SU: surface protein; TM: transmembrane protein.

Retropepsins were firstly described in the late 1980's with the identification of human immunodeficiency virus (HIV)-1 protease, which plays an important role in the processing of HIV proteins and, therefore, is critical for maturation of virion particles and for the progression of the acquired immunodeficiency syndrome (AIDS) (Ratner et al., 1985).

### 1.2.1. HIV-1 protease

HIV-1 protease is by far the most characterized retropepsin-type protease. In this chapter, some features that this protease shares with other members of the family A2 of aspartic proteases will be summarized.

When the HIV binds to and fuses with the host cell membrane, the virus releases its components into the host cytosol, such as RNA, the reverse transcriptase, the HIV integrase, and the mature HIV-1 protease. The reverse transcriptase is the enzyme that converts HIV RNA into HIV DNA, which is transported to the nucleus, where viral DNA is integrated into the host cell DNA by the HIV integrase (Brik and Wong, 2003).

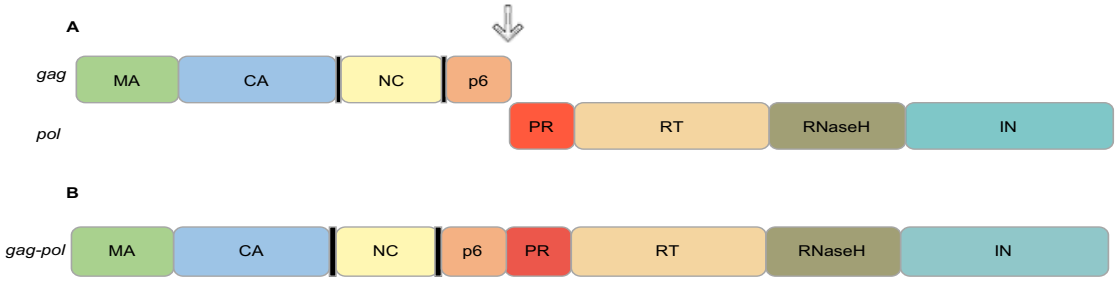


**Figure 3.** HIV-1 protease is expressed as part of the retroviral polyproteins.
**A.** Schematic representation of Gag and Pol polyproteins. The arrow indicates the site of translational frameshift, which result in the expression of the Gag-Pol polyprotein. **B.** Schematic representation of the Gag-Pol polyprotein. Spacer peptides (black vertical lines) are localized between CA and NC domains and between NC and p6 domains.
Abbreviations: MA: p17 matrix protein; CA: p24 capsid protein; NC: p7 nucleocapsid; PR: HIV-1 protease; RT: reverse transcriptase; IN: integrase.

This viral DNA must be transcribed into gag-pol mRNA and the translation of this mRNA serves both to the synthesis of the Gag and Gal-Pol polyproteins, mostly producing the Gag polyprotein. However, a translational frameshift might occur upstream of the protease gene (only 5% of the translation), resulting the Gag-Pol fusion polyprotein (**Figure 3A**). HIV-1 protease makes part of the Gag-Pol polyprotein, flanked by a transframe region at its N-terminal and by the reverse transcriptase at its C-terminal (Dunn et al., 2002; Konvalinka et al., 2015).

The polyprotein must be then cleaved at ten processing sites to generate mature active proteins, including the reverse transcriptase, integrase, RNase H, HIV-1 protease, and other proteins (**Figure 3B**). In order to release the mature protease, at least two proteolytic reactions need to occur, being these reactions catalyzed by the Gag-Pol polyprotein itself and, thus, serving as both the enzyme and substrate (protease autoprocessing). The released mature protease will hydrolyze peptide bonds on the Gag-Pol polyprotein, generating the remaining HIV proteins, essential for assembling new and mature viral particles (Dunn et al., 2002; Huang and Chen, 2010). The sequences that the protease recognizes at cleavage sites are rather promiscuous, suggesting that HIV-1 protease may catalyze several different substrates (Huang and Chen, 2013).

The mature HIV-1 protease is a homodimeric aspartic protease, with each monomer comprising 99 amino acid residues. Each Gal-Pol polyprotein contains one HIV-1 protease monomer that must associate with another monomer to form a mature protease, with a functional catalytic active site. This homodimeric protease has a single active site located between the two similar monomers, composed by three amino acids, aspartate (Asp25), threonine (Thr26) and glycine (Gly27), highly conserved among aspartic proteases (Brik and Wong, 2003). Therefore, the catalytic core of HIV-1 protease contains a pair of aspartate residues, one from each monomer, essential for proteolytic activity (Chatterjee et al., 2005). These aspartate residues are connected by a water molecule, which is involved in the catalytic mechanism of hydrolysis of the peptide bond (Brik and Wong, 2003). In terms of structure, the active site is not completely exposed, being protected by two flexible β-hairpin structures that allow the binding and release of the substrates (Huang and Chen, 2013). Additionally, this enzyme is inhibited *in vitro* by pepstatin (at least partially), a natural product that selectively inhibits members of the aspartic protease family; and the alteration of the catalytic aspartate (Asp25) to either asparagine, threonine, or alanine abolishes protease activity, all features contributing to positioning retropepsin-type proteases as members of the family A2 of aspartic proteases (Mous et al., 1988; Seelmeier et al., 1988; Darke et al., 1989).

Since HIV-1 protease plays an essential role in the HIV life cycle, allowing the viral maturation and replication, it has been the target of most anti-AIDS drugs. Some of these drugs are HIV-1 protease inhibitors that are used in combination with other anti-retroviral agents (entry inhibitors, reverse transcriptase inhibitors, and integrase inhibitors) (Huang and Chen, 2013). These protease inhibitors are substrate analogs that bind specifically to the active site, blocking protease activity (Lv et al., 2015). In the presence of these inhibitors, HIV can still replicate; however, the resulting viral particles lack the mature proteins and, therefore, cannot infect other host cells (immature virions) (Konvalinka et al., 2015). Furthermore, the delay in HIV-1 protease autoprocessing impacts the morphology of viral particles while an overactivation of this protease reduces the production of virus particles (Pan et al., 2012; Mattei et al., 2014). Taking these data, the protease processing dynamics is indeed essential for HIV maturation and thus for HIV virulence.

#### 1.2.1.1. Processing of HIV-1 protease

As previously mentioned, the autoprocessing mechanism of HIV-1 protease is a crucial step for HIV maturation and essential for the successful dissemination of the virus. Therefore, several research efforts have been made to understand the molecular and cellular mechanisms of HIV-1 protease autoprocessing.

As it is represented in **Figure 3B**, the HIV-1 protease is flanked upstream by p6 sequence and downstream by reverse transcriptase, with the release of the mature protease through these two cleavage sites. The C-terminal extension seems to have a low impact on protease activity since mutations blocking this cleavage site do not affect the generation of infectious viruses (Cherry et al., 1998). When the protease was fused at the C-terminal with fluorescent proteins, such as YFP or CFP, the catalytic activity was not compromised, suggesting again that the protease activity is not significantly affected by the downstream extension (Koh et al., 2007). In contrast, when the N-terminal cleavage site is mutated, the enzymatic activity of the protease is highly affected, leading to the generation of noninfectious viruses (Tessmer and Kräusslich, 1998). With that being said, it is plausible to suggest that the removal of the upstream sequence p6 is essential for the precursor autoprocessing process and it is likely that this sequence disrupts the protease dimerization (Huang and Chen, 2013).

When expressed in *E. coli* cells, the HIV-1 protease undergoes autoprocessing with the accumulation of the mature form in whole cell lysates (Louis et al., 1999; Huang and Chen, 2010, 2013). These cleavages observed on the full-length protease are likely mediated by the protease itself, and not by other cellular proteases since the catalytic site mutant precursor exhibited slight or even no autoprocessing at all (Huang et al.,

2009; Huang and Chen, 2010). In contrast, the mature protease is not detected when expressed on mammalian cells, suggesting that the protease is self-degraded when expressed in these cells (anticipating faster autoprocessing activity) (Lindsten et al., 2001; Huang and Chen, 2010). This idea is further supported by the evidence that in the presence of lower inhibitor concentrations, cleavage products and the mature protease become detectable; at higher concentrations of inhibitor, the autoprocessing process is significantly impaired, with the detection of the full-length precursor only (Huang and Chen, 2010; Humpolíčková et al., 2018). With this experimental evidence, it can be assumed that the impairment of the protease activity delays its degradation, being unlikely this degradation to be catalyzed by other cellular proteases.

Differences in the autoprocessing process in *E. coli vs.* mammalian cells were also observed when researchers expressed the HIV-1 protease fused with the MBP tag at the C-terminal in these two different host cells. In *E. coli*, the protease was soluble, but it did not undergo processing, whereas in mammalian cells, the MBP fusion was efficiently autoprocessed (Louis et al., 1991; Huang and Chen, 2013). Therefore, it may exist an allosteric regulation of the protease autoprocessing, dependent on the cell type (*E. coli vs.* mammalian cells).

#### 1.2.1.2. Other substrates of HIV-1 protease

Besides hydrolysis of the Gag-Pol polyprotein to generate the other HIV viral proteins, the HIV-1 protease is also capable of cleaving host cellular substrates, including cytoskeleton proteins (Shoeman et al., 1990; Adams et al., 1992), prointerleukin-1 (Adams et al., 1992), Bcl-2 (Strack et al., 1996), procaspase-8 (Nie et al., 2002), eukaryotic initiation factor 4G (eIF4G) (Ventoso et al., 2001), a subunit of eukaryotic initiation factor 3 (eIF3d) (Jäger et al., 2012), poly(A)-binding protein (PABP) (Álvarez et al., 2006), and several cellular kinases as receptor interacting protein kinase (RIPK) 1 and RIPK2 (Wagner et al., 2015).

The expression of HIV-1 protease was found to be toxic in cultured cells, although it is still uncertain the exact mechanism of cell death caused by this protease (Baum et al., 1990; Strack et al., 1996; Blanco et al., 2003; Rumlová et al., 2014; Benko et al., 2016). Strack and colleagues were the first research group suggesting that the mechanism of cell death by HIV-1 protease was based on the cleavage of the anti-apoptotic protein Bcl-2, leading to cell death through apoptosis in fibroblast, epithelial, and lymphocyte cell lines (Strack et al., 1996). Nonetheless, following studies could not confirm this observation (Nie et al., 2002; Blanco et al., 2003; Jäger et al., 2012). When HIV-1 protease was expressed in mammalian cells (fibroblast-like cell line), Blanco and colleagues identified cytopathogenic effects on these cells, including plasma membrane

damage, cytoplasm vacuolization, and loss of cell integrity, which are morphological changes characteristic of necrosis. In contrast, apoptotic markers, such as membrane blebbing, nuclear fragmentation, and the presence of apoptotic bodies were not detected (Blanco et al., 2003). Rumlová and colleagues suggested that the HIV-1 protease may indeed mediate apoptosis, namely *via* the intrinsic mitochondrial apoptotic pathway, based on observations that the protease was localized in the mitochondria, where it could be able to cleave mitochondrial proteins and decrease the mitochondrial membrane potential (Rumlová et al., 2014). Mitochondria appear to have a key role in cell death mediated by HIV-1 protease since it was observed the activation of procaspase-9, an event that is only triggered with cytochrome c release from mitochondria, that together with the activation of apoptotic protease activating factor (Apaf)-1, leads to the formation of apoptosome (Rumlová et al., 2014). Moreover, it was also identified the cleavage of PARP and DNA fragmentation, both events occurring in the execution pathway, the late phase of apoptosis that starts upon activation of caspase-3 (Elmore, 2007; Rumlová et al., 2014). The activation of this mitochondrial pathway is corroborated by data published by Nie and colleagues, in which they demonstrate that the presence of HIV-1 protease *in vitro* causes the activation of procaspase-8, the mitochondrial release of cytochrome c, the activation of procaspases-9 and -3, the cleavage of PARP, and nuclear condensation, all features of apoptosis (Nie et al., 2002). However, it is not possible to exclude the hypothesis that HIV-1 protease might also mediate apoptosis *via* the extrinsic pathway since it is recognized that caspase-8 can trigger apoptosis by directly activating caspase-3 (extrinsic pathway), apart from the indirect triggering through mitochondria with cytochrome c release and caspase-9 activation (intrinsic pathway) (Elmore, 2007).

HIV pathogenesis is profoundly associated with the depletion of $CD4^+$ T cells, which play a crucial role in the adaptive immune system with the coordination of immune responses against infections (Okoye and Picker, 2013; Vidya Vijayan et al., 2017). As previously described, HIV-1 protease is cytotoxic in expressing cells, inducing cell death. Following this idea, it is plausible to assume that the protease might be involved in the HIV-induced cell death since the treatment of HIV-infected C8166 lymphocytes with saquinavir, an HIV-1 protease inhibitor, increased cell viability (Ventoso et al., 2005). Besides this, it was reported that HIV-1 protease cleaves procaspase-8 into Casp8p41 that does not have a caspase activity, but can activate the apoptotic effector Bak, leading to the death of $CD4^+$ T cells (Sainski et al., 2014).

The initiation of translation of eukaryotic mRNAs occurs through a cap-dependent mechanism, in which several components are recruited, including eIF4G, PABP, and eiF3d. eIF4G is a scaffolding protein, essential to bridge the mRNA to ribosomes,

together with other initiation factors (Ventoso et al., 2001). Besides this role, eIF4G can bind to PABP, with the formation of a circularized mRNA, favoring its translation (Uchida et al., 2002). eIF3d is an mRNA binding protein that also plays an important role in cap-dependent translation initiation (Lee et al., 2016). During viral infection, the cap-dependent mechanism and mRNA circularization might be abolished due to the expression of viral proteases, such as HIV-1 protease. It was reported that HIV-1 protease is indeed able to cleave both eIF4G (Ventoso et al., 2001) and PABP (Álvarez et al., 2006), preventing the host's protein synthesis and, therefore, facilitating viral gene expression. As mentioned before, HIV-1 protease is also capable of cleaving eIF3d, being observed that the knockout of this initiation factor leads to an increase in the presence of the reverse transcription product. These data suggest that eIF3d might be able to bind to viral RNA, inhibiting the reverse transcription. However, in the presence of HIV-1 protease, this inhibition effect is abolished by the HIV-1 protease-mediated eIF3d cleavage (Jäger et al., 2012). To maintain the viral gene expression in a condition in which translation is globally downregulated, some RNA genomes of retroviruses include an internal ribosome entry site (IRES) that allows the translation of viral mRNA in a cap-independent manner (Guerrero et al., 2015). The downregulation of host protein synthesis is indeed advantageous to the virus, ensuring the maximal expression of viral genes and allowing evasion from host immune response (Lloyd, 2006; Walsh and Mohr, 2011).

HIV-1 protease can also interact with other host cellular proteins as a way to allow HIV to escape from host cellular defenses as well as immune defenses. Wagner and colleagues recently reported that HIV-1 protease could cleave RIPK1 and RIPK2, two members of RIPK family involved in the regulation of several cellular mechanisms, such as cell death and immune defense against viral and bacterial infections (Wagner et al., 2015).

### 1.2.2. APRc

Cruz and colleagues recently reported the identification and characterization of a novel aspartic protease highly conserved in *Rickettsia*, named aspartic protease from *Rickettsia conorii* (RC13339/APRc) (**Figure 4**), which shares several properties with retropepsin-like proteases (Cruz et al., 2014).

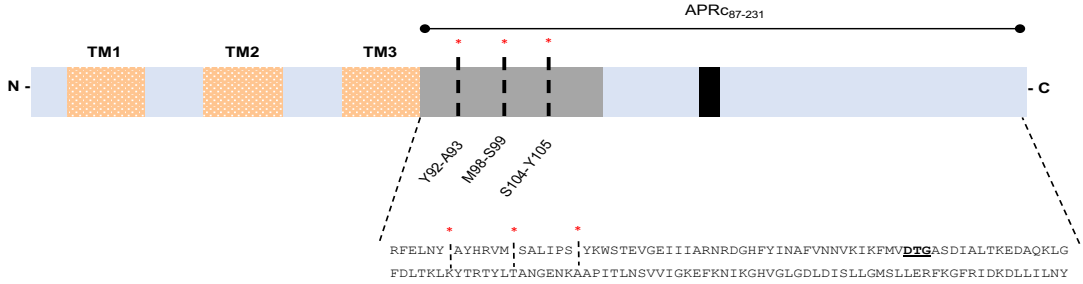

**Figure 4** (previous page)**.** Schematic representation of full-length APRc and primary structure of the soluble catalytic domain ($APRc_{87-231}$).
It is predicted that APRc has three transmembrane domains (TM1-3) at the N-terminal and a soluble catalytic domain at the C-terminal ($APRc_{87-231}$). The three autoprocessing cleavage sites identified are highlighted by * and dashed lines, both in the scheme and in the primary structure. The black box indicates on the catalytic active site (DTG).

As previously described, retropepsins need to form a homodimer to have catalytic activity. Li and colleagues obtained the crystal structures of APRc (**Figure 5**) and observed that, despite the low sequence similarity to retropepsins, the fold of the APRc monomer closely resembles one of the monomers of retropepsins (Li et al., 2015).

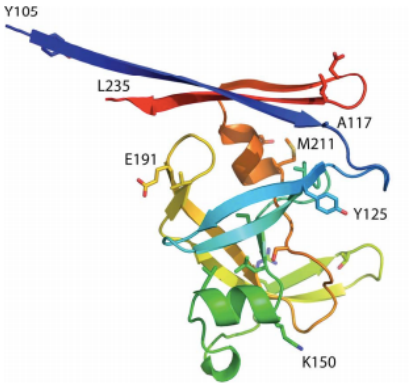


**Figure 5.** Structural representation of the monomer of APRc.
The N-terminal is represented in dark blue whereas the C-terminal is represented in red. In terms of protein secondary structures, the monomer of APRc includes ten β-strands and two α-helices. (From Li et al., 2015)

However, the observed quaternary structure of APRc's dimer is entirely different from that of retropepsins, not corresponding to the canonical active enzyme, as the catalytic aspartate residues of each monomer are not close. This non-canonical APRc dimer is probably an artifact of the crystallization conditions, the result of the extended C-terminal (with a histidine tag) of the recombinant product, or likely a combination of both (Li et al., 2015). Although the crystal structure of the dimer is still not available, it has been demonstrated that APRc shares other features with retropepsins, such as autoprocessing activity. The researchers also evaluated the effect of pepstatin, HIV-1 protease inhibitors, and EDTA on APRc's activity. Although insensitive to pepstatin, APRc was affected by several of the HIV-1 protease inhibitors, reinforcing that this protease is indeed a retropepsin-like enzyme. Regarding the results with EDTA, it was observed that this chelating agent inhibits the activity of APRc, suggesting that a metal ion must be necessary to the protease activity and/or protein folding (Cruz et al., 2014).

*E. coli* cells expressing the full-length APRc showed evidence of processing, also observed in rickettsial extracts (unpublished data). Moreover, Cruz and colleagues expressed in *E. coli* a recombinant form of APRc, consisting in a fusion construct of the complete soluble domain with a GST-tag at the N-terminal ($GST\_APRc_{87-231}$). This recombinant APRc was purified and autoprocessing analyzed by SDS-PAGE, confirming

that this protease undergoes multistep processing *in vitro*, leading to the release of the "mature" form ($APRc_{105-231}$), as observed in **Figure 6**. This autolytic activity is impaired by mutation of the catalytic aspartate by alanine, only with the accumulation of the precursor form and free GST which probably is a result of host cell proteolysis (**Figure 6**). The impairment of autolytic activity by mutating the catalytic aspartate (D140A) is another characteristic that APRc shares with retropepsins (**Figure 6**) (Cruz et al., 2014). Since oxidized insulin β-chain is usually a substrate of aspartic proteases, researchers assessed the activity of GST_$APRc_{87-231}$ towards this protein. Interestingly, the insulin cleavage products started to be detected when the final activation product ($APRc_{105-231}$) was generated, suggesting that APRc's activity is dependent on the autoprocessing process (Cruz et al., 2014).

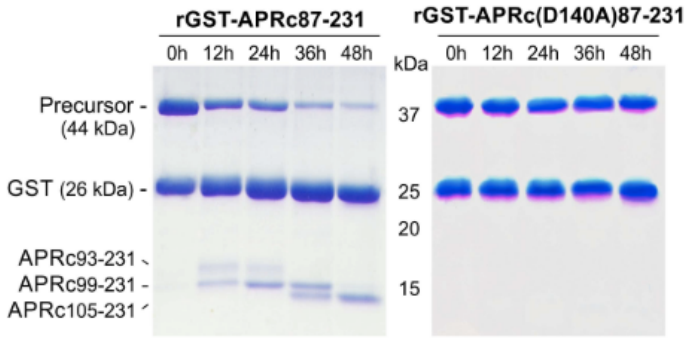


**Figure 6.** Multistep processing *in vitro* of APRc.
The recombinant form of APRc, GST_$APRc_{87-231}$, corresponds to the soluble catalytic domain of this rickettsial aspartic protease fused to GST. *In vitro* assays demonstrate that it undergoes multistep processing with the generation of its mature form, $APRc_{105-231}$. The autolytic activity of APRc is impaired by mutation of the active site catalytic aspartate by alanine (D140A), only with the detection of the larger precursor and the GST tag. (From Cruz et al., 2014)

Globally, this experimental evidence suggests that the processing at the N-terminal is a requirement for protease activation and, therefore, it is plausible to presume that this N-terminal sequence might be involved in the regulation of the enzymatic activity, presumably through a conformational change that allows the dimer formation and activity. This protease likely undergoes some conformational change along with the processing mechanism, since no proteolytic activity was observed towards the same substrate when the final mature form $APRc_{105-231}$ was expressed in *E. coli* (unpublished data). Because of this, the next reported studies were performed using the second intermediate of activation, $APRc_{99-231}$ (**Figure 4**). When the *in vitro* processing of this activation intermediate was assessed, the conversion into the final product of activation was apparent. Indeed, when the cleavage site (S104-Y105) was truncated, or even with the mutation on the catalytic aspartate, there was no obvious detection of processed forms, suggesting that the N-terminal processing observed on the precursor is indeed sequence-dependent (unpublished data).

The length of the β-strand localized at the N-terminal (highlighted in dark blue in **Figure 5**) seems to be crucial for the stability of the protease and, consequently, to dimer formation. The generation of different truncated constructs at the N-terminal ($APRc_{105-231}$, $APRc_{110-231}$, $APRc_{115-231}$, and $APRc_{122-231}$) and the analysis of the different forms by analytical size-exclusion chromatography revealed that only the form $APRc_{110-231}$ accumulated as a dimer, whereas the remaining three forms accumulated mostly as monomers. Moreover, there was a pronounced reduction in recombinant protein yields for the shorter constructs, anticipating lower stability for these recombinant forms. Interestingly, the C-terminal extensions may not significantly impact the formation of the dimer since all of the constructs studied above were fused to an histidine tag and $APRc_{110-231}$ still accumulated as a dimer (unpublished data).

In order to determine the subcellular localization of APRc in *E. coli*, the full-length protease was produced in this working model. From these assays, it was concluded that APRc accumulates in the outer membrane with the soluble catalytic domain of the protease exposed to the cell surface. These results were confirmed in rickettsial species, where APRc also accumulates at the outer membrane with the catalytic domain oriented towards the extracellular environment (Cruz et al., 2014).

As previously reported, proteases have an important role in bacteria life cycle, and thus, like other proteases, APRc might also be involved in different stages of the rickettsial infectious process. In the last years, it has emerged the concept that proteins with moonlighting activity may be involved in bacterial pathogenicity (Henderson and Martin, 2011). In this way, it is plausible to hypothesize that APRc can also be a moonlighting protein, performing more than one function in rickettsial infection progression, as highlighted below.

Throughout evolution, mammalians and other animals developed a system composed of a complex network of cells and humoral factors, named immune system, capable of detecting and destroying pathogens. To achieve this, the immune system is constituted by several components, including immunoglobulins, complement proteins, and antimicrobial peptides (Müller et al., 2008; Yatim and Lakkis, 2015). Some bacteria have evolved complex and efficient methods to subvert these host immune mechanisms, - where bacterial proteases are included - affecting some of the immunological defense mechanisms. This may include the downregulation of inflammation pathways, and binding to and degradation of immunoglobulins, antimicrobial peptides, or other crucial complement components (Finlay and McFadden, 2006). Taking into account this information, APRc may also affect some of these host immune system components. Indeed, recent evidence suggests that APRc may act as a novel evasin through non-immune IgG-binding (unpublished data).

Moreover, it was shown that APRc catalyzes the processing of Sca0/rOmpA and Sca5/rOmpB *in vitro*, a process likely important for the maturation of these proteins (Cruz et al., 2014). Therefore, it is reasonable to suggest that APRc may also be implicated in the degradation/maturation of other rickettsial proteins, especially those located at the outer membrane, impacting bacteria adherence to and invasion of host cells. Once rickettsial cells are phagocytosed by host cells, these bacteria can escape from phagosomes due to the presence of rickettsial membranolytic effectors, such as phospholipase D and hemolysin C (Whitworth et al., 2005). Since APRc is a proteolytic enzyme, it is possible that this protease might interfere with phagosomal membrane proteins, leading to the destruction of the phagosomal membrane and, consequently, to the release of rickettsiae into the host cytosol. To survive inside the host cells, *Rickettsia* require several supplies for growth and proliferation. Rickettsial species have a small number of genes required for amino acid biosynthesis. Thus, they likely evolved proteolytic pathways that hydrolyze host proteins into smaller molecules that bacteria use as nutrients (Andersson et al., 1998). Proteases involved in these proteolytic pathways contribute to bacterial pathogenesis, being considered by some authors as the main virulence factors among all the bacterial extracellular factors (Secades and Guijarro, 1999). In this way, APRc might possess similar characteristics to other extracellular proteases secreted by pathogens, degrading host proteins to supply *Rickettsia* with nutrients. Also, one cannot exclude that APRc might target specific host proteins to interfere with cellular responses during infection. *Rickettsia* are obligate intracellular bacteria that have the vascular endothelium as one of the main targets, invading adjacent cells using actin polymerization mechanisms. Therefore, rickettsial infection leads to endothelial dysfunction and increased microvascular permeability with the disruption of the interendothelial adherens junctions (development of interendothelial gaps) (Valbuena and Walker, 2005). Although the mechanistic aspects inherent to the formation of these gaps are still not well understood and proteases have not yet been associated with these processes, APRc could also be implicated in the damage of host cell structures, such as extracellular matrices, promoting intercellular spread and rickettsial dissemination.

Proteins with moonlighting activity are a prevalent phenomenon in bacterial pathogens. It remains to be fully demonstrated that APRc is indeed a moonlighting protein exerting some of the functions hypothesized above (Henderson and Martin, 2011)

## 1.3. Research objectives

There are still several open questions regarding structure-function relationships of APRc, namely in what concerns the mechanisms and dynamics of its autoactivation as well as the nature of its substrates. Although there are multiple challenges ahead before we fully understand the role of this strictly conserved retropepsin in the life-cycle of *Rickettsia*, we believe that a more in-depth knowledge of the unique features and function(s) of APRc will reveal novel aspects on the role of bacterial retropepsin-type proteases as virulence factors and, therefore, as potential therapeutic targets.

With this work, we aimed at elucidating the autoprocessing activity and function of the rickettsial protease APRc in mammalian cells. To explore this, the objectives of this work were to:

i. Assess if the proteolytic processing of APRc is dependent on cell type (compare processing in mammalian cells with available evidence from *E. coli*);
ii. Evaluate the impact of the transient expression of APRc in mammalian cells;
iii. Evaluate if the expression of precursor *vs.* mature forms of APRc impacts protease function in the host cell;
iv. Unravel the functional role of the protease in mammalian cells.

# Chapter II

# 2. Material and Methods

## 2.1. Material

Oligonucleotides were purchased from GenScript (Piscataway, NJ, USA). Phusion High-Fidelity DNA polymerase, T4 DNA ligase, and T4 DNA kinase PNK were purchased from New England Biolabs (Ipswich, MA, USA). PfuTurbo DNA polymerase was purchased from Agilent Technologies (Santa Clara, CA, USA). Synthetic genes encoding the predicted soluble catalytic domain of RC1339/APRc were produced by GenScript. The sequencing analyses were performed by Eurofins Genomics (Ebersberg, Germany). The rabbit polyclonal anti-GFP antibody (A01388) and the rabbit polyclonal anti-APRc antibody (antibody towards APRc sequence Tyr-Thr-Arg-Thr-Tyr-Leu-Thr-Ala-Asn-Gly-Glu-Asn-Lys-Ala) were produced by GenScript. The mouse monoclonal anti-β-actin antibody (A5441), the rabbit anti-mouse IgG (whole molecule)-peroxidase antibody (A9044), and the goat anti-rabbit IgG (whole molecule)-peroxidase antibody (A0545) were purchased from Sigma-Aldrich (St. Louis, MO, USA). The mouse polyclonal anti-TOM20 antibody (sc-17764) was produced by Santa Cruz Biotechnology (Dallas, TX, USA). The Alexa Fluor 647-conjugated goat anti-mouse Ig (51-9006588) was produced by BD Biosciences (San Jose, CA, USA). The antibodies used for the analysis of apoptosis-related proteins belong to the Apoptosis Antibody Sampler kit (Cell Signaling Technology, Danvers, MA, USA). The Alexa Fluor 568-conjugated goat anti-rabbit IgG [H+L] secondary antibody (A11036) and the annexin V – APC conjugate (A35110) were produced by Invitrogen (Carlsbad, CA, USA). *E. coli* TOP10F' competent cells were prepared according with the calcium chloride method.

## 2.2. Methods

### 2.2.1. PCR-based cloning

The mammalian gene expression plasmid pcDNA3.1(+)-N-eGFP (GenScript), which carries an ampicillin-resistant gene, was used to clone the coding sequence for the predicted soluble catalytic domain of APRc (construct coding amino acids 87-231, codon optimized for expression in human cells) in frame with a C-terminal tag, TwinStrep tag (WSHPQFEKGGGSGGGSGGSAWSHPQFEK) or 3xFLAG tag (DYKDHDGDYKDHDIDYKDDDK) (constructs hereby named: GFP_APRc$_{87-231}$_TwinStrep or GFP_APRc$_{87-231}$_3xFLAG).

In order to generate the expression constructs harboring the sequence encoding the shorter forms APRc$_{99-231}$ and APRc$_{110-231}$, both sequences were firstly amplified using

the construct $APRc_{87-231}$ as the template. The PCR-based cloning technique was used to generate the constructs. The constructs were amplified by PCR, following the conditions showed in **Table 1** and using the program described in **Figure 7**. The template DNA and the primers used for each construct are described in **Table 4**.

**Table 1.** PCR conditions used in PCR-based cloning technique.

| **PCR conditions for PCR-based cloning** | |
|---|---|
| **Phusion High-Fidelity Reaction Buffer 10x** | 10 µL |
| **dNTPs** (10 mM) | 1 µL |
| **Primer Forward** (10 µM) | 2.5 µL |
| **Primer Reverse** (10 µM) | 2.5 µL |
| **Template DNA** | 100 ng |
| **Phusion High-Fidelity DNA Polymerase** | 0.5 µL |
| **Autoclaved Milli-Q $H_2O$** | Up to 50 µL |

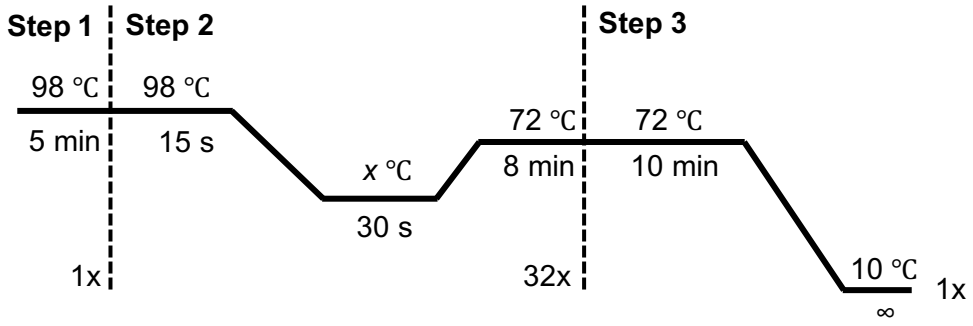


**Figure 7.** PCR program steps for the amplification of the constructs.
The temperature value *x* is the annealing temperature that depends on the melting temperature (Tm) of the primers used **(Table 4)**. Both values were calculated using New England Biolabs (NEB) Tm calculator available on https://tmcalculator.neb.com/#!/main.

To confirm if the PCR amplification was successful, 5 µL of each PCR reaction was run on a 1% agarose gel with ethidium bromide in a Mini-Sub Cell GT Horizontal Electrophoresis System (Bio-Rad, Hercules, CA, USA) and visualized on Gel Doc XR+ System (Bio-Rad). Next, 1 µL of DpnI (20,000 U/mL, New England Biolabs) was added to each PCR reaction and incubated at 37℃ for 7h. For purification of each PCR product, the NucleoSpin Gel and PCR Clean-up kit (Macherey-Nagel, Dueren, Germany) was used, following the manufacturer's instructions. This kit method is based on binding of plasmid DNA to the silica membrane column with the removal of contaminants through salt/ethanol washing steps. After purification, DNA phosphorylation and ligation were performed to promote the recircularization of each PCR product, resulting in the DNA

product with the desired sequence deleted. Each reaction was incubated at room temperature for 3h, with the conditions of the reaction described in **Table 2**.

**Table 2**. Phosphorylation and ligation conditions used to recircularize the PCR products.

| Phosphorylation and ligation conditions | |
|---|---|
| **T4 DNA Ligase Buffer 10x** | 2 µL |
| **T4 DNA Ligase** | 1 µL |
| **T4 DNA Kinase PNK** | 2 µL |
| **PCR purified product** | 100 ng |
| **Autoclaved Milli-Q $H_2O$** | Up to 20 µL |

Then, 10 µL of each ligation reaction was transformed in a 150 µL aliquot of TOP10F' *E. coli* competent cells with a recovery time of 1h30min. For each construct, 2 colonies were picked and grown overnight in 3 mL of Luria-Bertani (LB) medium with ampicillin (1:1,000).

**Note:** The mammalian gene expression plasmid pcDNA3.1(+)-N-eGFP is a high copy number type vector and growing the colonies in 3 mL of LB medium with ampicillin is sufficient to obtain a high concentration of plasmid DNA on the miniprep kit used. In case of having a low copy type vector, it is advised to use a higher volume of LB medium (10 mL).

For plasmid DNA isolation, the NucleoSpin Plasmid QuickPure (Macherey-Nagel) was used, following the manufacturer's instructions. This isolation method is based on the alkaline lysis of *E. coli* cells followed by binding of plasmid DNA to the silica membrane column. The plasmid DNA was eluted in autoclaved Milli-Q $H_2O$ and quantified using NanoDrop® ND-1000 UV-Vis Spectrophotometer (ThermoFisher Scientific, Waltham, MA, USA). Plasmid DNA was sequenced to confirm that it contained the desired deletion.

### 2.2.2. Site-directed mutagenesis

To generate the untagged constructs at the C-terminal, a site-directed mutagenesis protocol was performed to include the TGA stop codon at the end of the predicted soluble catalytic domain (GFP_APRc$_{87-231}$), and at the end of the sequence encoding the shorter versions APRc$_{99-231}$ and APRc$_{110-231}$. This protocol was also used to generate the active-site mutants of the APRc fusion constructs, APRc$_{87-231}$(D140N), APRc$_{99-231}$(D140N), and APRc$_{110-231}$(D140N), replacing the active-site aspartic acid residue by an asparagine.

The conditions of the site-directed mutagenesis technique are described in **Table 3** and the PCR program is described in **Figure 8**. The template DNA and the primers used for each construct are described in **Table 4**.

**Table 3.** PCR conditions used in the site-directed mutagenesis protocol.

| PCR conditions for site-directed mutagenesis | |
|---|---|
| ***PfuTurbo* Reaction Buffer 10x** | 5 µL |
| **dNTPs** (10 mM) | 1 µL |
| **Primer Forward** (10 µM) | 1 µL |
| **Primer Reverse** (10 µM) | 1 µL |
| **Template DNA** | 100 ng |
| ***PfuTurbo* DNA Polymerase** | 1 µL |
| **Autoclaved Milli-Q $H_2O$** | Up to 50 µL |

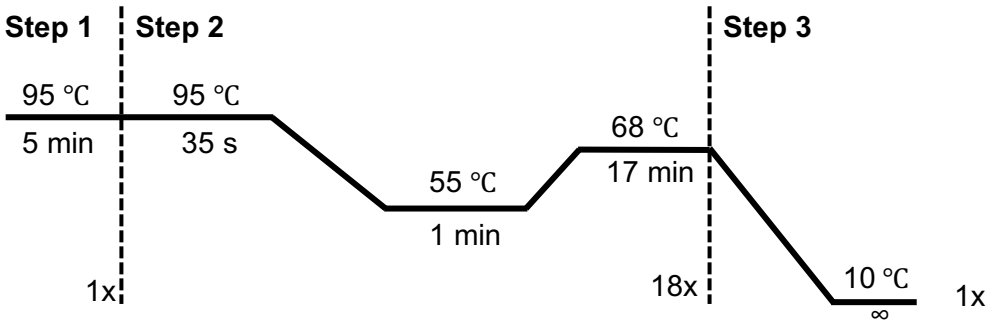


**Figure 8.** PCR program steps for the amplification of the constructs, used in the site-directed mutagenesis protocol.

Next, 1 µL of DpnI was added to each PCR reaction and incubated at 37℃ for 7h. Then, 10 µL of each PCR reaction was transformed in a 150 µL aliquot of TOP10F' *E. coli* competent cells with a recovery time of 1h30min. For each construct, 2 colonies were picked and grown overnight in 3 mL of LB medium with ampicillin (1:1,000). For plasmid DNA isolation, the NucleoSpin Plasmid QuickPure was used, following the manufacturer's instructions. The plasmid DNA was eluted in autoclaved Milli-Q $H_2O$ and quantified using NanoDrop spectrophotometer. The plasmid DNA was sequenced to confirm that it contained the mutation.

### 2.2.3. Isolation of plasmid DNA for transfection

The plasmids confirmed by sequencing were transformed in a 150 µL aliquot of TOP10F' *E. coli* competent cells without recovery time. For each construct, one colony was picked and grown overnight in 10 mL of LB medium with ampicillin (1:1,000). For plasmid DNA isolation, the Monarch Plasmid Miniprep Kit (New England Biolabs) was

used, following the manufacturer's instructions. The plasmid DNA was eluted in autoclaved Milli-Q $H_2O$ and quantified using NanoDrop spectrophotometer. By using this isolation kit, it is ensured that the obtained plasmid DNA is of high quality and endotoxin-free, allowing its use in transfection assays using mammalian cells.

**Table 4.** Template constructs and primers used to generate the expression constructs used in this work.
Constructs marked with [1] were generated by PCR-based cloning while the ones marked with [2] were generated by site-directed mutagenesis.

| Expression construct | Primer Forward | Primer Reverse | Template DNA |
|---|---|---|---|
| [2]GFP_APRc$_{87-231}$_TwinStrep_D140N | 5' AAGATCAAGTTCATGGTGAACACCGGCGCCAGCG 3' | 5' CGCTGGCGCCGGTGTTCACCATGAACTTGATCTT 3' | GFP_APRc$_{87-231}$_TwinStrep |
| [2]GFP_APRc$_{87-231}$_3xFLAG_D140N | 5' AAGATCAAGTTCATGGTGAACACCGGCGCCTCCG 3' | 5' CGGAGGCGCCGGTGTTCACCATGAACTTGATCTT 3' | GFP_APRc$_{87-231}$_3xFLAG |
| [2]GFP_APRc$_{87-231}$ | 5' GATCTGCTGATCCTGAATTACTGATATAAGGACCACGATGGCGAC 3' | 5' GTCGCCATCGTGGTCCTTATATCAGTAATTCAGGATCAGCAGATC 3' | GFP_APRc$_{87-231}$_3xFLAG |
| [2]GFP_APRc$_{87-231}$_D140N | 5' AAGATCAAGTTCATGGTGAACACCGGCGCCTCCG 3' | 5' CGGAGGCGCCGGTGTTCACCATGAACTTGATCTT 3' | GFP_APRc$_{87-231}$ |
| [1]GFP_APRc$_{99-231}$_TwinStrep | 5' TCTGCCCTGATCCCAAGCTA 3' | 5' CTTGTACAGCTCGTCCATGCC 3' | GFP_APRc$_{87-231}$_TwinStrep |
| [1]GFP_APRc$_{99-231}$_3xFLAG | 5' AGCGCCCTGATCCCCAGC 3' | 5' CTTGTACAGCTCGTCCATGCC 3' | GFP_APRc$_{87-231}$_3xFLAG |
| [2]GFP_APRc$_{99-231}$_TwinStrep_D140N | 5' AAGATCAAGTTCATGGTGAACACCGGCGCCAGCG 3' | 5' CGCTGGCGCCGGTGTTCACCATGAACTTGATCTT 3' | GFP_APRc$_{99-231}$_TwinStrep |
| [2]GFP_APRc$_{99-231}$_3xFLAG_D140N | 5' AAGATCAAGTTCATGGTGAACACCGGCGCCTCCG 3' | 5' CGGAGGCGCCGGTGTTCACCATGAACTTGATCTT 3' | GFP_APRc$_{99-231}$_3xFLAG |
| [2]GFP_APRc$_{99-231}$ | 5' AAGATCAAGTTCATGGTGAACACCGGCGCCTCCG 3' | 5' CGGAGGCGCCGGTGTTCACCATGAACTTGATCTT 3' | GFP_APRc$_{99-231}$_3xFLAG |
| [2]GFP_APRc$_{99-231}$_D140N | 5' AAGATCAAGTTCATGGTGAACACCGGCGCCTCCG 3' | 5' CGGAGGCGCCGGTGTTCACCATGAACTTGATCTT 3' | GFP_APRc$_{99-231}$ |
| [1]GFP_APRc$_{110-231}$_TwinStrep | 5' GAAGTGGGCGAGATCATCATC 3' | 5' CTTGTACAGCTCGTCCATGCC 3' | GFP_APRc$_{87-231}$_TwinStrep |
| [1]GFP_APRc$_{110-231}$_3xFLAG | 5' GAAGTGGGCGAGATCATCATC 3' | 5' CTTGTACAGCTCGTCCATGCC 3' | GFP_APRc$_{87-231}$_3xFLAG |
| [2]GFP_APRc$_{110-231}$_TwinStrep_D140N | 5' AAGATCAAGTTCATGGTGAACACCGGCGCCAGCG 3' | 5' CGCTGGCGCCGGTGTTCACCATGAACTTGATCTT 3' | GFP_APRc$_{110-231}$_TwinStrep |
| [2]GFP_APRc$_{110-231}$_3xFLAG_D140N | 5' AAGATCAAGTTCATGGTGAACACCGGCGCCTCCG 3' | 5' CGGAGGCGCCGGTGTTCACCATGAACTTGATCTT 3' | GFP_APRc$_{110-231}$_3xFLAG |
| [2]GFP_APRc$_{110-231}$ | 5' CTGCTGATCCTGAATTACTGATCCCACCCACAGTTCGAG 3' | 5' CTCGAACTGTGGGTGGGATCAGTAATTCAGGATCAGCAG 3' | GFP_APRc$_{110-231}$_TwinStrep |
| [2]GFP_APRc$_{110-231}$_D140N | 5' AAGATCAAGTTCATGGTGAACACCGGCGCCAGCG 3' | 5' CGCTGGCGCCGGTGTTCACCATGAACTTGATCTT 3' | GFP_APRc$_{110-231}$ |
| [1]GFP_TwinStrep | 5' TGGTCCCACCCACAGTTCG 3' | 5' CTTGTACAGCTCGTCCATGCC 3' | GFP_APRc$_{87-231}$_TwinStrep |
| [1]GFP_3xFLAG | 5' GATTATAAGGACCACGATGGCG 3' | 5' CTTGTACAGCTCGTCCATGCC 3' | GFP_APRc$_{87-231}$_3xFLAG |

### 2.2.4. Optimization of transfection conditions

Vero cells were grown in Dulbecco's Modified Eagle Medium (DMEM; high glucose with L-glutamine and sodium pyruvate; Gibco, Carlsbad, CA, USA) supplemented with 10% heat-inactivated fetal bovine serum (FBS; ThermoFisher Scientific), 1.1% MEM nonessential amino acid solution (100mM; Corning, Corning, NY, USA), and 1.1% sodium pyruvate (Corning) at 34℃ and 5% $CO_2$. Cells were seeded in 24-well culture plates (Corning) to 60% confluency one day before transfection. The cells were then transiently transfected with the appropriate plasmid using the calcium phosphate co-precipitation method. All solutions were warmed up to room temperature. Plasmid DNA (2 µg) was mixed with Milli-Q $H_2O$ and 2 M calcium chloride, pipetting up and down, in a total volume of 50 µL. This solution was added dropwise to 50 µL of the HEPES buffered saline solution (HBS: 50 mM HEPES, 280 mM NaCl, and 1.5 mM $Na_2HPO_4$). This solution was incubated at room temperature for 30 min, vortexing for a few seconds every 10 min, to generate a precipitate containing the condensed DNA. During the incubation time, the cell medium was removed and replaced by 500 µL of fresh culture medium. Then, 100 µL/well of the transfection mixture was added dropwise to the cells, followed by gentle swirling, to distribute the precipitates in the well. The cells were placed at 34℃ and 5% $CO_2$ for 5h. After this incubation time, the cell medium was removed and replaced by 1 mL of fresh culture medium. The plates were incubated for 24h and 48h at 34℃ and 5% $CO_2$. This protocol (2 µg plasmid DNA) was also tested using EA.hy926 cells grown in DMEM (high glucose with L-glutamine and sodium pyruvate) supplemented with 10% heat-inactivated FBS; as well as using human embryonic kidney 293 (HEK293) cells grown in DMEM (low glucose with L-glutamine and sodium pyruvate; Gibco) supplemented with 10% heat-inactivated FBS. The transfection protocol was further optimized for HEK293 cells, following the same procedure described above but with different amounts of DNA (0.5 µg and 1 µg). 24h post-transfection, the cells were stained with 60 µL/well of Hoechst 33342 (1µg/mL; Sigma-Aldrich) for 15 min at 34℃ and 5% $CO_2$. Then, the cell medium was removed and replaced by new fresh culture medium. At each specified time point (24h or 48h), cell culture plates were imaged on Zeiss Axiovert 200M fluorescence microscope (Carl Zeiss, Oberkochen, Germany) using a final X20 optical zoom, and processed with ImageJ software.

### 2.2.5. Transient protein expression

HEK293 cells were grown in DMEM (low glucose with L-glutamine and sodium pyruvate) supplemented with 10% heat-inactivated FBS at 34℃ and 5% $CO_2$. The cells were seeded in 24-well culture plates to 60% confluency two days before transfection. Two days after, the cells were transiently transfected with the appropriate plasmid (0.5

µg) using calcium phosphate co-precipitation method, as described in section 2.2.4. The cells were placed at 34℃ and 5% $CO_2$ for 5h. After the incubation time, the cell medium was removed and replaced by fresh culture medium. The plates were incubated for 24h and 48h at 34℃ and 5% $CO_2$.

### 2.2.6. Preparation of protein extracts

At each specified time point (24h or 48h), the culture medium was removed, and the cells were washed 1× with PBS and lysed using 100 µL/well of protein extraction lysis buffer (25 mM Tris/HCl, 5 mM EDTA, 1% Triton X-100, and protease inhibitor cocktail tablet (Roche, Basel, Switzerland), pH 7.0). The cells were scrapped off the wells and the protein extracts were transferred to microcentrifuge tubes. The protein samples were subjected 10× to an Insulin Syringe with 23-gauge needle (BD Biosciences). Protein samples were denatured with 6× SDS sample buffer (4× Tris/HCl, 30% glycerol, 10% SDS, 0.6 M DTT, 0.012% Bromophenol Blue) and heated for 8 min at 95℃. To completely lyse the cells and shear the DNA, the samples were sonicated (60% amplification) for 2× 30 seconds, reducing the viscosity of samples. Total protein samples were frozen at -20℃ until further processing.

### 2.2.7. SDS-PAGE and Western blot

After thawing, 40 µL of total protein samples were separated by SDS-PAGE in 12% polyacrylamide gels. The gels were run in a Mini-Protean Tetra Cell system (Bio-Rad) at room temperature, at 150 V (running buffer: 100 mM Tris, 100 mM Bicine, 0.1% SDS). For Western blot analysis, the proteins were transferred onto a polyvinylidene membrane (GE Healthcare Amersham, Amersham, UK), previously activated with methanol. To transfer the proteins from the gel to the membrane, wet electroblotting method was performed, using a Mini Trans-Blot Eletrophoretic Transfer Cell (Bio-Rad) for 1h50 min at 100 V at 4℃ (transfer buffer: 25 mM Tris, 192 mM glycine, 20% methanol). The membranes were then blocked for 1h with 5% dry milk in Tris-buffered saline (TBS; 150 mM NaCl, 10 mM Tris, pH 8.0) containing 0.1% Tween 20 (TBS-T). Next, the membranes were probed with the primary antibodies: rabbit polyclonal anti-GFP antibody (A01388) (1:500), rabbit polyclonal anti-APRc antibody (1:500), and mouse monoclonal anti-β-actin antibody (A5441) (1:5,000), in TBS-T buffer containing 5% dry milk, for 1h with agitation at room temperature. After incubation with the primary antibody, the membranes were washed 5× for 5 min in 0.5% dry milk in TBS-T buffer. Rabbit anti-mouse IgG (whole molecule)-peroxidase antibody (A9044) (1:5,000) and goat anti-rabbit IgG (whole molecule)-peroxidase antibody (A0545) (1:40,000) in 5% dry milk in TBS-T buffer were used as secondary antibodies, being the membranes

incubated for 1h with agitation at room temperature. After incubation with the secondary antibody, the membranes were washed again 5× for 5 min with TBS-T buffer. The Western blots were developed using the enhanced chemiluminescent method with NZY Advanced ECL kit (NZYTech, Lisbon, Portugal), and detected on a VWR® Imager (VWR Radnor, PA, USA), according to the manufacturer's instructions.

### 2.2.8. Fluorescence confocal microscopy

HEK293 cells were grown in DMEM (low glucose with L-glutamine and sodium pyruvate) supplemented with 10% heat-inactivated FBS at 34℃ and 5% $CO_2$. The cells were seeded on glass coverslips in 24-well culture plates to 60% confluency two days before transfection. Two days later, the cells were transiently transfected with the appropriate plasmid (0.5 µg) using the calcium phosphate co-precipitation method as described in section 2.2.4. The plates were incubated at 34℃ and 5% $CO_2$, for 24h and 48h. At each specified time point (24h or 48h), the culture medium was removed, and the cells were washed 1× with PBS and fixed in 200 µL/well of 4% paraformaldehyde (PFA) for 20 min at room temperature. The cells were washed 3× with PBS, followed by permeabilization and blocking with 200 µL/well of 0.1% Triton X-100 in PBS containing 2% bovine serum albumin (BSA). The cells were then incubated for 1h with diamidino-2-phenylindole (DAPI; ThermoFisher Scientific) (1:1,000) and Rhodamine Phalloidin (ThermoFisher Scientific) (1:200) in PBS containing 2% BSA, protected from light and under agitation. After washing 3× with PBS, glass coverslips were washed with Milli-Q $H_2O$ immediately before mounting with Mowiol mounting medium. The preparations were then imaged on an LSM 710 laser scanning confocal microscope (Carl Zeiss) using a final X40 optical zoom and processed with ImageJ software.

### 2.2.9. Subcellular localization of APRc

HEK293 cells were grown in DMEM (low glucose with L-glutamine and sodium pyruvate) supplemented with 10% heat-inactivated FBS at 34℃ and 5% $CO_2$. The cells were seeded on glass coverslips in a 24-well culture plate to 60% confluency two days before transfection. Two days later, the cells were transiently transfected with the appropriate plasmid (0.5 µg) using calcium phosphate co-precipitation method as previously described in section 2.2.4. The plate was incubated for 48h at 34℃ and 5% $CO_2$. 48h post-transfection, the culture medium was removed, and the cells were washed 1× with PBS and fixed in 200 µL/well of 4% PFA for 20 min at room temperature. The cells were washed 3× with PBS, followed by permeabilization and blocking with 200 µL/well of 0.1% Triton X-100 in PBS containing 2% BSA. The cells were then incubated for 1h with the primary antibody mouse polyclonal anti-TOM20 antibody (sc-17764)

(1:500) in PBS containing 2% BSA, protected from light. After washing 3× with PBS, the cells were incubated with DAPI (1:1,000) and with the secondary antibody Alexa Fluor 647-conjugated goat anti-mouse Ig (51-9006588) (1:100) in PBS containing 2% BSA, for 1h and protected from light. After washing 3× with PBS, the glass coverslips were washed with Milli-Q $H_2O$ immediately before mounting with Mowiol mounting medium. The preparations were then imaged on an LSM 710 laser scanning confocal microscope using a final X40 optical zoom and processed with ImageJ software.

### 2.2.10. Evaluation of shape and size of nuclei

HEK293 cells were grown in DMEM (low glucose with L-glutamine and sodium pyruvate) supplemented with 10% heat-inactivated FBS at 34℃ and 5% $CO_2$. The cells were seeded on glass coverslips in a 24-well culture plate to 50% confluency two days before transfection. Two days later, the cells were transiently transfected with the appropriate plasmid using Lipofectamine 3000 (Invitrogen), according to the manufacturer's instructions. Briefly, before starting the transfection protocol, the cell medium was removed and replaced with 1 mL of fresh culture medium. Then, 0.5 µg of plasmid DNA were diluted with 1 µL of P3000 Reagent and 25 µL of DMEM without FBS. Then, the diluted DNA was mixed with 0.75 µL of Lipofectamine 3000 in 25 µL of DMEM without FBS. After 15 min of incubation at room temperature to allow DNA-Lipofectamine 3000 complexes to form, 50 µL/well of complex mixture was added dropwise, followed by gentle swirling to distribute the complexes in the well. After 24h of incubation, the cell medium was removed and replaced by fresh culture medium. The plate was incubated for 48h at 34℃ and 5% $CO_2$. 48h post-transfection, the culture medium was removed, and the cells were washed 1× with PBS and fixed in 200 µL/well of 4% PFA for 20 min at room temperature. The cells were washed 3× with PBS, followed by permeabilization and blocking with 200 µL/well of 0.1% Triton X-100 in PBS containing 2% BSA. The cells were then incubated for 1h with DAPI (1:1,000) and Rhodamine Phalloidin (1:200) in PBS containing 2% BSA, protected from light and under agitation. After washing 3× with PBS, glass coverslips were washed with Milli-Q $H_2O$ immediately before mounting with Mowiol mounting medium. The preparations were then imaged on Zeiss Axiovert 200M fluorescence microscope using a final X40 optical zoom. To evaluate nuclear condensation, the total number of cells was counted using CellProfiler software and then the number of cells that were intensely stained with DAPI was counted. To assess different parameters correlated with the form and shape of cells' nuclei, microscopy images were analyzed using CellProfiler software. The microscopy images were processed with ImageJ software.

### 2.2.11. DNA laddering assay

HEK293 cells were grown in DMEM (low glucose with L-glutamine and sodium pyruvate) supplemented with 10% heat-inactivated FBS at 34℃ and 5% $CO_2$. The cells were seeded in a 24-well culture plate to 60% confluency two days before transfection. Two days later, the cells were transiently transfected with the appropriate plasmid using Lipofectamine 3000 as previously described (section 2.2.10). The DNA laddering assay was performed as described by Zhu and Wang, 1997. Briefly, 48h post-transfection, the culture medium was removed, and the cells were collected adding 150 µL of trypsin-EDTA (0.25%; Gibco) and incubated for 5 min at 34℃. The cell suspensions were transferred to microcentrifuge tubes and centrifuged at 300 x g for 5 min. Then, the supernatant was removed, and the cells were washed with ice-cold PBS. The tubes were centrifuged again and, after removing the supernatants, the cells were resuspended in 30 µL of lysis buffer (10 mM Tris, 100 mM NaCl, 25 mM EDTA, 1% sarkosyl, pH 7.4) by pipetting up and down, and 4 µL of proteinase K (10 µg/µL) was added. The lysates were incubated for 2h at 45℃, after which the tubes were allowed to cool to room temperature, and then 2 µL of RNase (10 µg/µL) was added and cell lysates were incubated for 1h at room temperature. After this incubation time, 4 µL of 6× DNA sample dye was added, and the samples were run on a 2% agarose gel with ethidium bromide in a Sub Cell GT Horizontal Electrophoresis System (Bio-Rad) and visualized on Gel Doc XR+ System.

### 2.2.12. Western blot analysis of apoptosis-related proteins

HEK293 cells were grown in DMEM (low glucose with L-glutamine and sodium pyruvate) supplemented with 10% heat-inactivated FBS at 34℃ and 5% $CO_2$. The cells were seeded in a 24-well culture plate to 60% confluency two days before transfection. Two days later, the cells were transiently transfected with the appropriate plasmid using Lipofectamine 3000 as described in section 2.2.10. 48h post-transfection, the protein extracts were prepared as described in section 2.2.6. Western blot analysis was performed as described previously (section 2.2.7). The protein samples were transferred to a polyvinylidene membrane and immunodetected with the following primary antibodies: rabbit monoclonal anti-PARP antibody, rabbit monoclonal anti-cleaved PARP antibody, and rabbit monoclonal anti-caspase-3 antibody, with 1:1,000 as the dilution recommended by the manufacture. The secondary antibody used was goat anti-rabbit IgG HRP-linked antibody (1:1,500). The membranes immunodetected with anti-cleaved PARP antibody and anti-caspase-3 antibody were incubated with 2% BSA in TBS-T, while the membrane immunodetected with anti-PARP antibody was incubated with 5% dry milk in TBS-T.

The procedure above described was also applied to concentrated protein extracts. After preparation of protein extracts (section 2.2.6), 8 times the sample volume of cold (-20℃) acetone was added to the protein extracts using acetone-compatible tubes. The samples were vortexed and incubated for 30 min at -80℃. Then, the samples were centrifuged at 16,000 x g for 30 min at 4℃. After centrifugation, the supernatants were discarded, and the residual acetone was removed from pellet by air drying. The pellet should not be over-dried, or it may not dissolve properly. The pellet was resuspended in 80 µL of PBS and denatured with 6× SDS sample buffer. The samples were frozen at -20℃ until further processing. After thawing, the samples were analyzed by Western blot, using the rabbit monoclonal anti-PARP antibody and the rabbit polyclonal anti-APRc antibody.

### 2.2.13. Cell sorting by flow cytometry

Besides acetone precipitation of proteins, cell sorting by flow cytometry was also carried out in order to only analyze the protein extracts from GFP-positive cells (i.e. transfected cells). HEK293 cells were grown in DMEM (low glucose with L-glutamine and sodium pyruvate) supplemented with 10% heat-inactivated FBS at 34℃ and 5% $CO_2$. The cells were seeded in a 24-well culture plate to 50% confluency two days before transfection. Two days later, the cells were transiently transfected with the appropriate plasmid using Lipofectamine 3000 as previously described on section 2.2.10. 48h post-transfection, the cell medium was removed, and the cells were detached by adding 150 µL of trypsin/EDTA (0.25%) and incubating for 5 min at 34℃. Cell suspensions were transferred to microcentrifuge tubes and centrifuged at 300 x g for 5 min. Then, the supernatant was removed, and the cells were resuspended with 250 µL of PBS using vortex. The samples were filtered to flow cytometry tubes, and GFP-positive cells were sorted into collection tubes by flow cytometry using a FACSAria™ III Cell Sorter (BD Biosciences). The sorted cell population was then subjected to an Insulin Syringe with 23-gauge needle and denatured with 6× SDS sample and heated for 8 min at 95℃. To completely lyse the cells and shear DNA, the samples were sonicated. Protein extracts of GFP-positive cells were frozen at -20℃ until further processing. After thawing, the samples were analyzed by Western blot, using the rabbit monoclonal anti-PARP antibody and the rabbit polyclonal anti-APRc antibody (section 2.2.7).

### 2.2.14. Fluorescence confocal microscopy of apoptosis-related proteins

HEK293 cells were grown in DMEM (low glucose with L-glutamine and sodium pyruvate) supplemented with 10% heat-inactivated FBS at 34℃ and 5% $CO_2$. The cells were seeded on glass coverslips in a 24-well culture plate to 50% confluency two days

before transfection. Two days later, the cells were transiently transfected with the appropriate plasmid using Lipofectamine 3000 as previously described (section 2.2.10). The plates were incubated for 48h at 34℃ and 5% $CO_2$. 48h post-transfection, the culture medium was removed, and the cells were washed 1× with PBS and fixed in 200 µL/well of 4% PFA for 20 min at room temperature. The cells were washed 3× with PBS, followed by permeabilization and blocking with 200 µL/well of 0.1% Triton X-100 in PBS containing 2% BSA. The cells were then incubated for 1h with the primary antibodies rabbit monoclonal anti-cleaved PARP antibody (1:400) and rabbit monoclonal anti-cleaved caspase-3 antibody (1:400) in PBS containing 2% BSA, protected from light. After washing 3× with PBS, the cells were incubated with DAPI (1:1,000) and with the secondary antibody Alexa Fluor 568-conjugated goat anti-rabbit IgG [H+L] (A11036) (1:1,000) in PBS containing 2% BSA, for 1h, and protected from light. After washing 3× with PBS, glass coverslips were washed with Milli-Q $H_2O$ immediately before mounting with Mowiol mounting medium. The preparations were then imaged on an LSM 710 laser scanning confocal microscope using a final X63 optical zoom. The analysis was performed by searching specifically for the microscopy fields that include the labelling for the apoptotic-related proteins. The total number of cells and the number of cells that were stained for the apoptotic proteins were counted. The microscopy images were processed with ImageJ software.

### 2.2.15. Annexin V-APC conjugate/DAPI detection with flow cytometry

HEK293 cells were grown in DMEM (low glucose with L-glutamine and sodium pyruvate) supplemented with 10% heat-inactivated FBS at 34℃ and 5% $CO_2$. The cells were seeded on glass coverslips in a 24-well culture plate to 50% confluency two days before transfection. Two days later, the cells were transiently transfected with the appropriate plasmid using Lipofectamine 3000 as described in section 2.2.10. The plates were incubated for 48h at 34℃ and 5% $CO_2$. A positive control was prepared by incubating untransfected cells with 0.5% $H_2O_2$ for approximately 12h. The experiment was performed with some adaptations from the manufacturer's instructions. Briefly, 48h post-transfection, the cell medium was removed, and the cells were detached by adding 150 µL of 0.48 mM EDTA, incubating for 5-9 min at 34℃. After detachment, 1 mL of DMEM was added to each well, and the cell suspensions were transferred to centrifuge tubes and centrifuged at 300 x g for 5 min. For the positive control, the cell medium (with cells in suspension) was collected and centrifuged, without adding EDTA and DMEM. Then, the supernatants were removed, and the cells were washed in PBS. The tubes were centrifuged again, and the supernatants were discarded. The cells were resuspended in annexin-binding buffer (10 mM HEPES, 140 mM NaCl, 2.5 mM $CaCl_2$,

pH 7.4). The cell density was determined in order to know in which buffer volume the cells should be diluted in order to have ~ $1\times10^6$ cells/mL, preparing a sufficient volume to have 100 µL per condition. To each 100 µL of cell suspension, 5 µL of annexin V-APC conjugate (A35110) was added and incubated on ice for 15 min. After this incubation time, 400 µL of annexin-binding buffer was added and mixed using vortex, keeping samples on ice. As soon as possible, samples were filtered to flow cytometry tubes and 1 µL of DAPI was added. The stained cells (15,000 – 30,000 cells) were analyzed by flow cytometry using a FACSAria™ III Cell Sorter. Data analysis was performed with FlowJo 7.6. software.

### 2.2.16. Statistical analysis

All statistical tests were performed using GraphPad Prism 8 software (GraphPad Software, San Diego, CA, USA). $P<0.05$ was considered to indicate a statistically significant difference.

# Chapter III

# 3. Results

## 3.1. Constructs used along the study

When the soluble catalytic domain of APRc fused with GST (GST-APRc$_{87-231}$) was expressed in *E. coli*, Cruz and colleagues observed that APRc undergoes multi-step autoprocessing *in vitro*, culminating in the generation of the activated form APRc$_{105-231}$. Over time, a decrease in the precursor (GST-APRc$_{87-231}$) was observed together with an enrichment in the different intermediate forms (APRc$_{93-231}$ and APRc$_{99-231}$). After 48h, only the presence of the final activated form (APRc$_{105-231}$) was observed. In addition to these APRc fragments, the presence of free GST was also detected, which may result from proteolytic degradation by the host. This autoactivation process was confirmed *in vivo* in *E. coli*, and was shown to be impaired when researchers expressed the active site mutant of GST-APRc$_{87-231}$ (GST-APRc$_{87-231}$ (D140A)) in *E. coli*, by replacing the aspartate residue with an alanine residue (D140A), suggesting that the catalytic aspartate is indeed essential to trigger autoprocessing (Cruz et al., 2014).

Given these data, it is reasonable to hypothesize if APRc maintains this autoprocessing activity when transiently expressed in mammalian cells or if, alternatively, there might exist an allosteric regulation dependent on the cell type (*E. coli vs*. mammalian cells). To study these hypotheses, two synthetic constructs corresponding to the soluble catalytic domain of APRc (APRc$_{87-231}$) (**Figure 4**), comprising a TwinStrep tag or 3xFLAG tag fused at the C-terminal were ordered. Both constructs were codon-optimized to human codon usage and subcloned into pcDNA3.1(+)-N-eGFP vector (GFP fused at the N-terminal). Different truncated forms were generated from these longer backbones: an intermediate form (APRc$_{99-231}$) and a shorter truncated form (APRc$_{110-231}$). APRc$_{99-231}$ was one of the identified intermediate forms of APRc and may eventually correspond to the latest processing step before the generation of the mature form of APRc (Cruz et al., 2014). On the other hand, the shorter version APRc$_{110-231}$ was chosen as a control since it is already known that this form is active and a dimer in solution, and eventually will not undergo further processing at the N-terminal (unpublished data). From the three designed constructs (APRc$_{87-231}$, APRc$_{99-231}$, and APRc$_{110-231}$), C-terminally untagged constructs were subsequently generated. The constructs with or without C-terminal tags allowed to evaluate the impact of these additional tags on the processing activity of APRc, and if the protease would undergo processing at the C-terminal. The use of two different tags on the C-terminal also aimed at performing an affinity-purification SWATH mass spectrometry (AP-SWATH) analysis in order to determine APRc putative interactors in host cells and better understand how

the host's machinery is manipulated by the protease. By using two different tags on AP-SWATH, proteins that interact non-specifically with the tags could be discarded. Besides the previously mentioned constructs, the respective active-site mutants (D140N) were also generated to assess the role of the catalytic aspartate for the autoprocessing activity of APRc. In this case, the mutation on the catalytic active site consisted in replacing the aspartate residue with the asparagine residue (D140N). As negative controls, and to compare the phenotypes resulting from APRc expression, two constructs harboring only GFP fused with TwinStrep tag or 3xFLAG tag were also generated. In **Figure 9**, a representative scheme of all the constructs generated under the course of this work is presented.

Besides the previously described constructs, an *untransfected* condition was included in parallel to all transfection assays. Untransfected cells went through the transfection process without the addition of DNA, ensuring that there were any nonspecific effects caused by the transfection process.

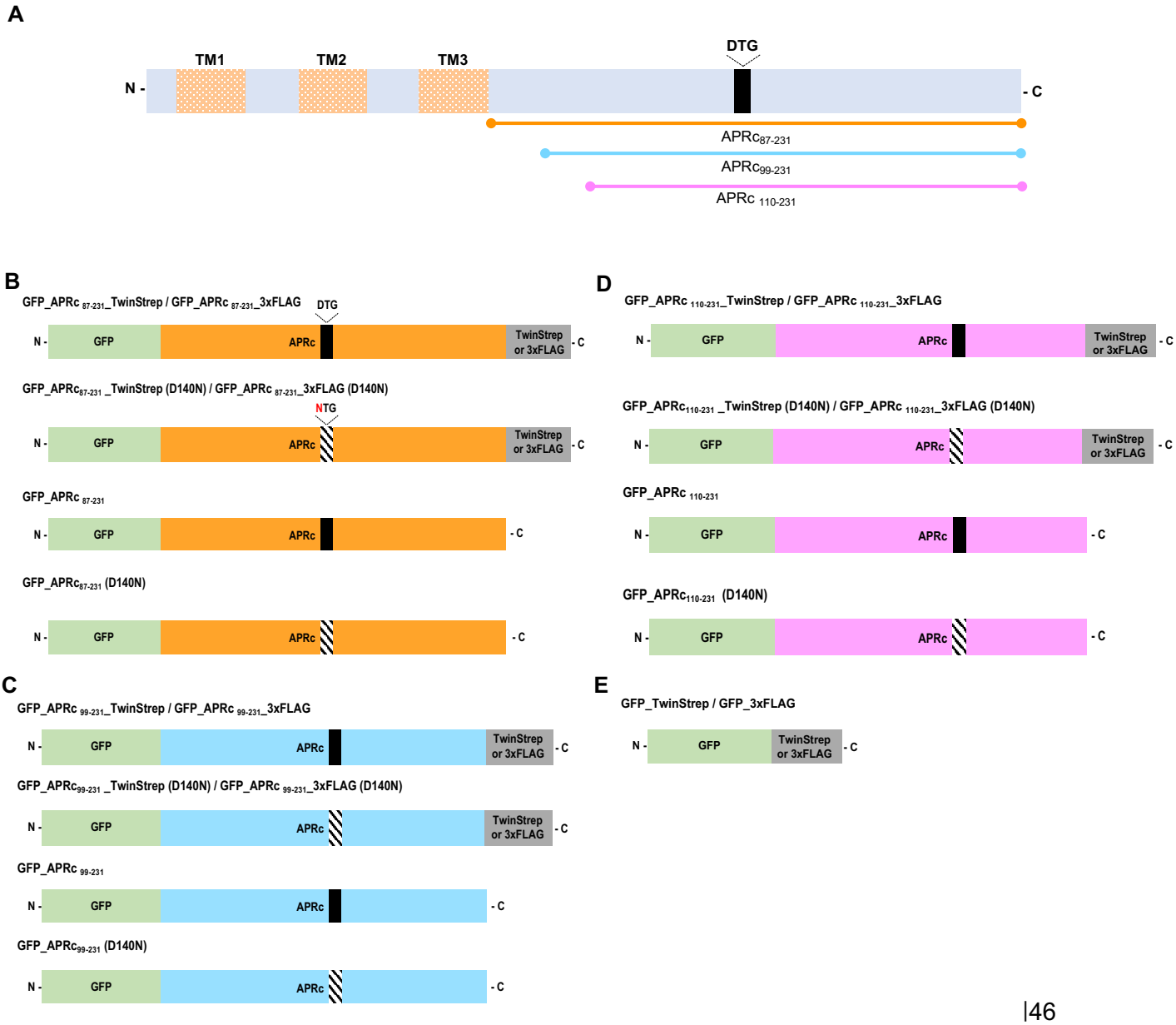

**Figure 9** (previous page)**.** Schematic representation of the full-length domain of APRc and the different constructs generated along this study.
**A.** Schematic representation of full-length APRc. It is predicted that APRc has three transmembrane domains (TM1-3) at the N-terminal and a soluble catalytic domain at the C-terminal. The three truncated forms of APRc used along this study are identified ($APRc_{87-231}$, $APRc_{99-231}$, and $APRc_{110-231}$). **B**. Schematic representation of the different constructs encoding the soluble catalytic domain of APRc (GFP_ $APRc_{87-231}$), with or without the C-terminal tag (TwinStrep tag or 3xFLAG tag). **C.** Schematic representation of the different constructs encoding an intermediate form of APRc (GFP_ $APRc_{99-231}$), with or without the C-terminal tag. **D.** Schematic representation of the different constructs encoding a shorter truncated form of APRc (GFP_ $APRc_{110-231}$), with or without the C-terminal tag. **E.** Schematic representation of the constructs encoding only GFP fused with the TwinStrep tag or 3xFLAG tag. All the constructs were cloned in pcDNA3.1(+)-N-eGFP, a mammalian expression vector that encodes green fluorescent protein (GFP). The name of each construct is indicated on the top of each schematic construct. The black box represents the catalytic active site motif (DTG). The black and white box indicates the mutation on the catalytic site, in which the aspartate residue is replaced with the asparagine residue (NTG). This amino acid substitution is highlighted in red in **B**. The numbers on the name of the truncated forms of APRc have into account the full-length amino acid sequence of APRc. The schemes are not in scale.

## 3.2. Optimization of transfection conditions

In order to start assessing the transfection conditions that would be used in this study, Vero cells and EA.hy926 cells were transiently transfected with 2 µg of the different constructs of GFP_APRc ($APRc_{87-231}$, $APRc_{99-231}$, and $APRc_{110-231}$). 24h post-transfection, the cells were stained with Hoechst, to stain nucleic acids. At two time-points (24h and 48h), the cell culture plates were observed by fluorescence microscopy, to assess the transfection efficiency regarding these two cell lines. As it can be observed in **Figure 10**, the transfection efficiency at 24h post-transfection on Vero cells was very low, with a very low number of green cells. At 48h post-transfection (**Figure 10B**), the efficiency did not increase, revealing that calcium phosphate-mediated transfection may not be an efficient method to deliver plasmid DNA into this mammalian cell line. As observed for Vero cells, calcium phosphate-mediated transfection of EA.hy926 cells also resulted in low transfection efficiency, with a reduced number of transfected cells (**Figure 11)**.

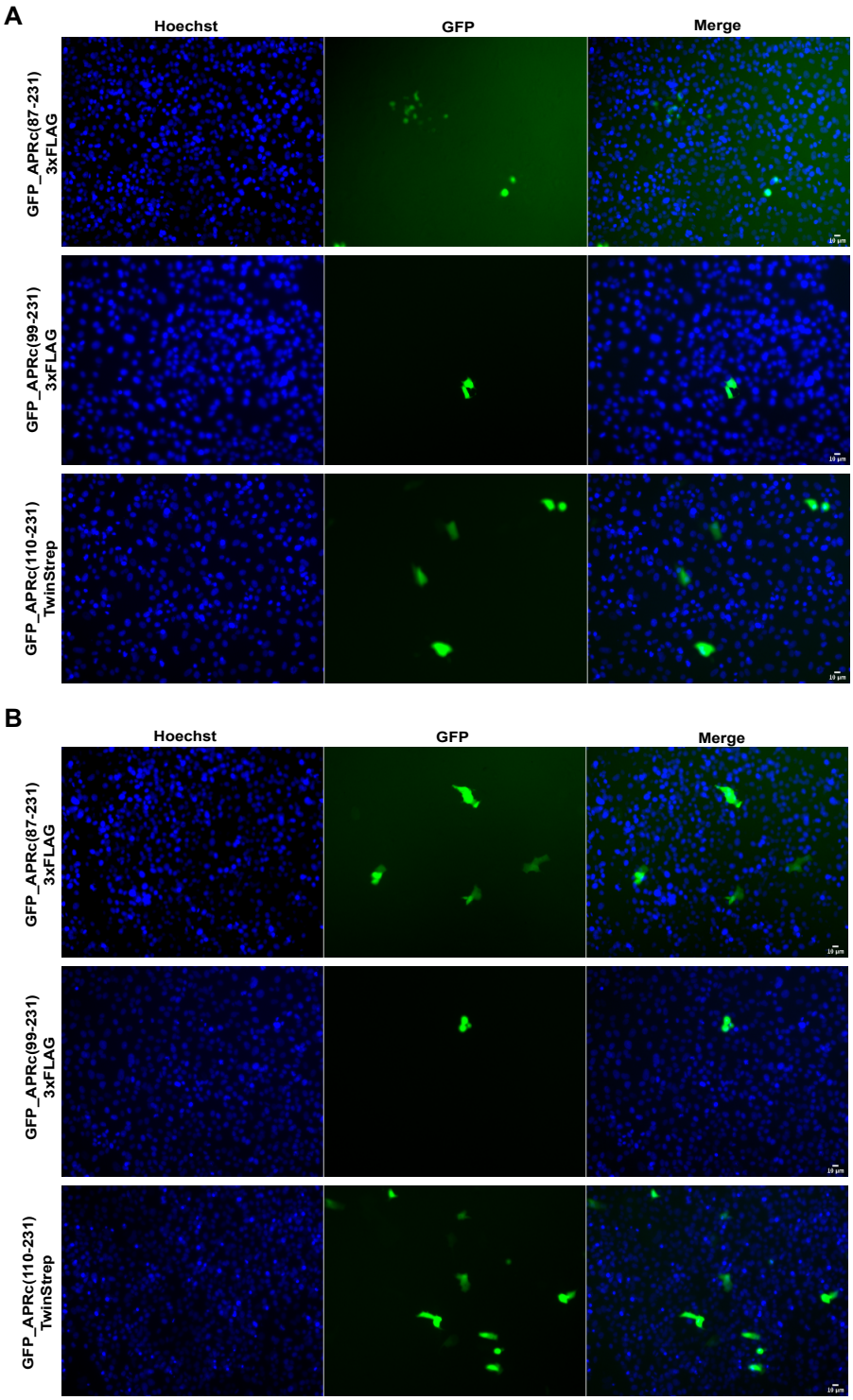


**Figure 10.** Transfection efficiency of APRc constructs in Vero cells.
Vero cells were transiently transfected with 2 µg of plasmid DNA harboring the different constructs of APRc as described in the image, using the calcium phosphate method. At 24h post-transfection, the cells were stained for microscopy analysis with Hoechst (blue) to stain the nuclei. **A.** At 24h post-transfection, the cells were observed by fluorescence microscopy. **B.** At 48h post-transfection, the cells were observed by fluorescence microscopy. The number of transfected cells was very low, suggesting that this cell line might be a difficult-to-transfect cell line. Each row shows, from left to right, nuclei staining, GFP, and the merged image. Scale bar = 10 µm.

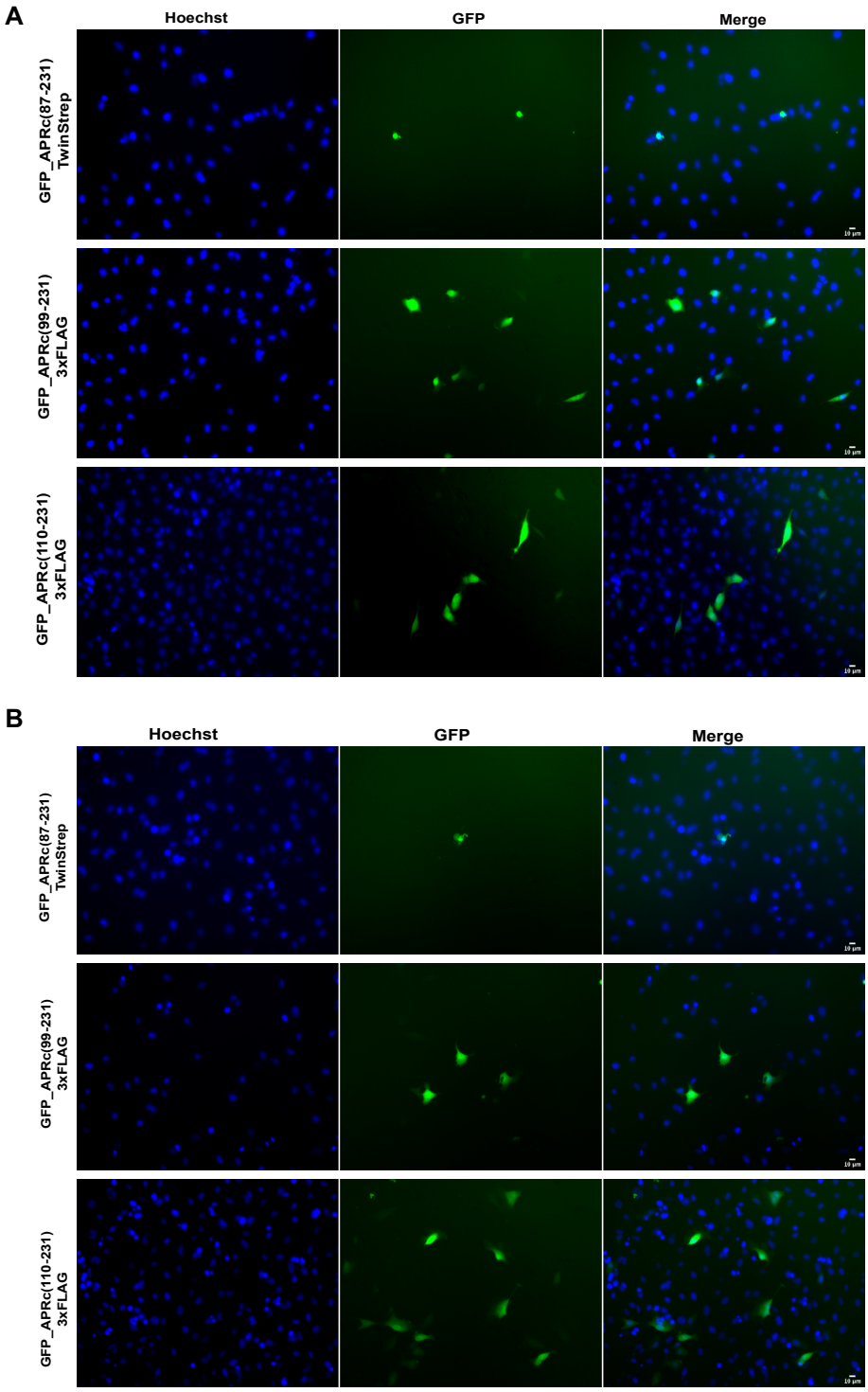


**Figure 11.** Transfection efficiency of APRc constructs in EA.hy926 cells.
EA.hy926 cells were transiently transfected with 2 µg of plasmid DNA harboring the different constructs of APRc, as described in the image, using the calcium phosphate method. At 24h post-transfection, the cells were stained for microscopy analysis with Hoechst (blue) to stain the nuclei. **(A)** At 24h post-transfection, cells were observed by fluorescence microscopy. **(B)** At 48h post-transfection, the cells were observed by fluorescence microscopy. The number of transfected cells is very low, suggesting that this cell line may be a difficult-to-transfect cell line. Each row shows, from left to right, nuclei staining, GFP, and the merged image. Scale bar = 10 µm.

Since the transfection efficiency of Vero and EA.hy926 cells was very low, which would compromise APRc processing and function analysis, we decided to switch to HEK293 cells, where the calcium phosphate transfection method is reported to be more efficient (Thomas and Smart, 2005). As shown in **Figure 12**, the transient transfection of 2 µg of selected constructs of APRc resulted indeed in a higher number of transfected cells, when analyzed at 24h post-transfection.

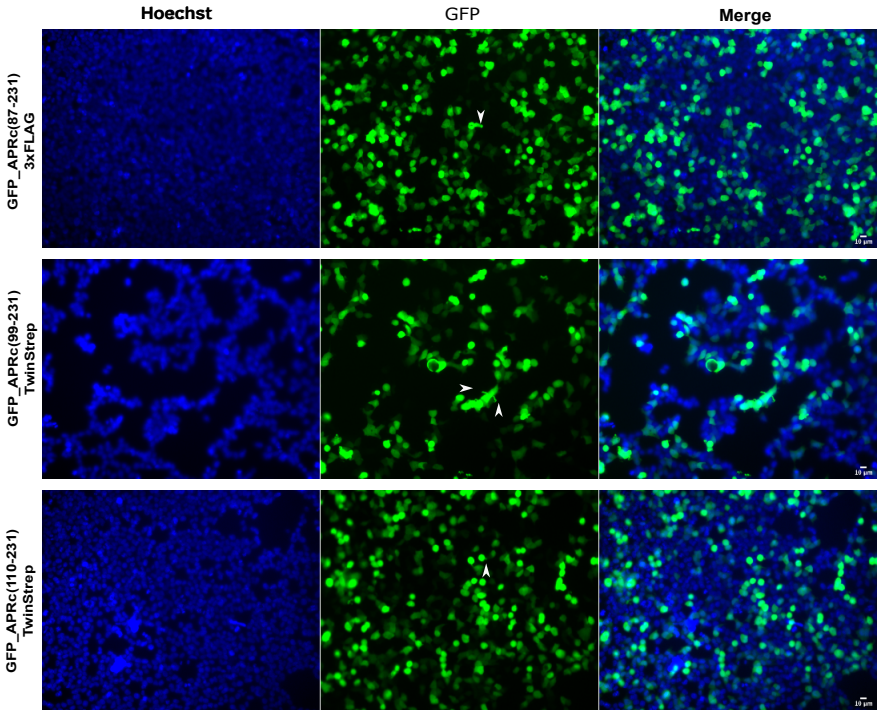


**Figure 12.** Transfection efficiency of APRc constructs in HEK293 cells.
HEK293 cells were transiently transfected with 2 µg of plasmid DNA harboring the different constructs of APRc, as described in the image, using the calcium phosphate method. At 24h post-transfection, the cells were stained for microscopy analysis with Hoechst (blue) to stain the nuclei and observed by fluorescence microscopy. White arrows indicate membrane blebbing. Each row shows, from left to right, nuclei staining, GFP, and the merged image. Scale bar = 10 µm.

As it can be observed in **Figure 12**, it was possible to detect the presence of some membrane blebbing on transfected cells. This phenotype seems to be more evident in cells expressing GFP_APRc$_{99-231}$_TwinStrep that curiously is also the construct that appears to result in a reduced number of transfected cells. Given these observations, we decided to optimize the transfection protocol to evaluate if this blebbing phenotype could be result from excess plasmid DNA in the transfection assay. Therefore, HEK293 cells were transiently transfected using the calcium phosphate protocol, reducing the amount of plasmid DNA used to 0.5 µg and 1 µg, instead of 2 µg. 24h post-transfection, the cells were stained with Hoechst and analyzed by fluorescence microscopy at two time-points (24h and 48h). Analyzing **Figures 13** and **14**, it is possible to conclude that the membrane-blebbing phenotype is still evident when using 0.5 µg of plasmid DNA, suggesting that this may indeed be a specific phenotype. Moreover, in addition to this

phenotype, some cells expressing GFP_APRc$_{87-231}$_TwinStrep (0.5 µg) present a specific localization of the GFP signal (**Figure 14**).

From these optimization assays, we decided that the best conditions to pursue with the subsequent assays were the use of HEK293 cells and 0.5 µg of plasmid DNA, analyzing the cells at 24h and 48h post-transfection.

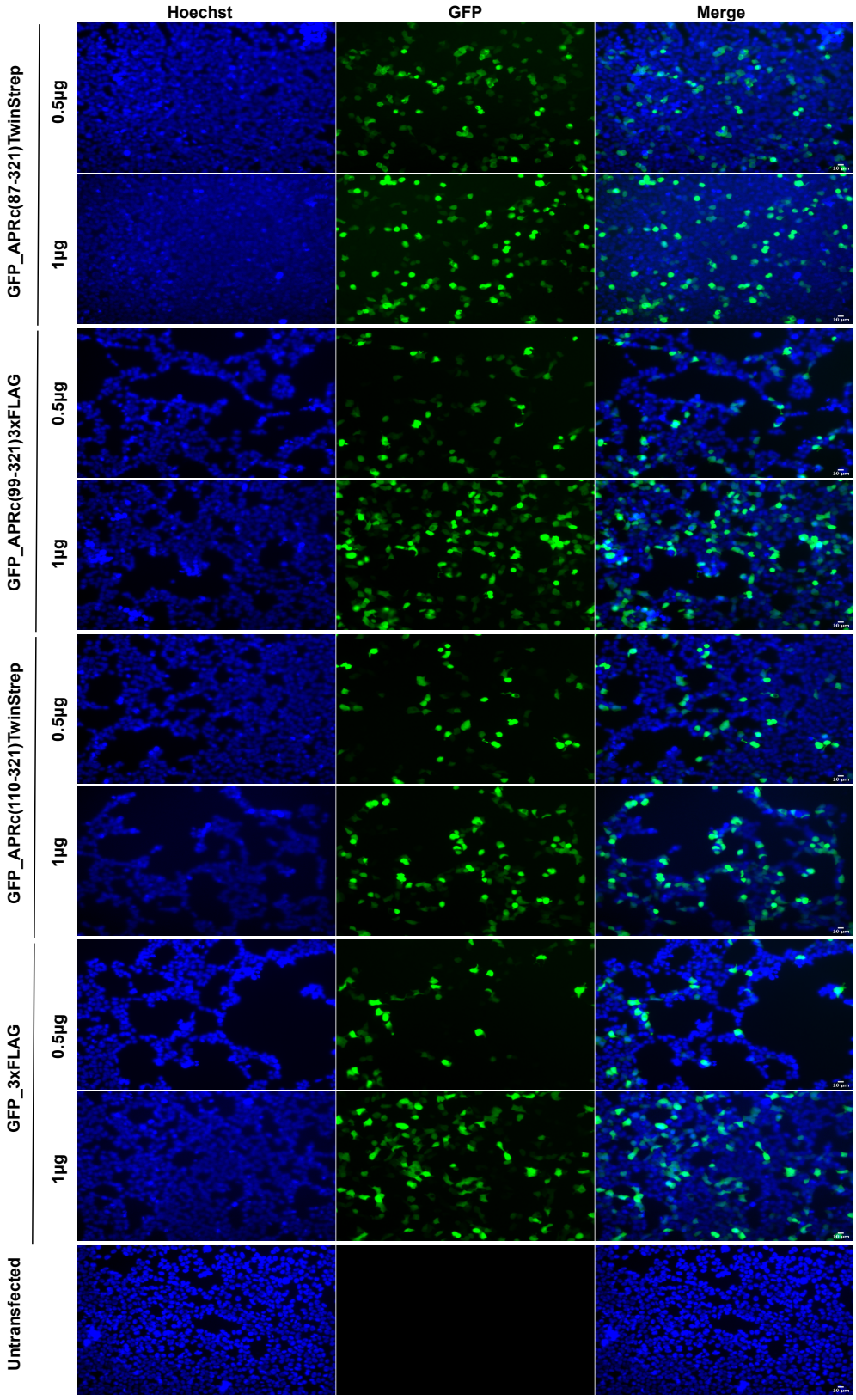


**Figure 13.** Optimization of transfection conditions of APRc constructs in HEK293 cells at 24h post-transfection.
HEK293 cells were transiently transfected with 0.5 µg and 1 µg of plasmid DNA harboring the different constructs of APRc, as described in the image, using the calcium phosphate method. At 24h post-transfection, the cells were stained for microscopy analysis with Hoechst (blue) to stain cells' nuclei. Then, the cells were observed by fluorescence microscopy. Each row shows, from left to right, nuclei staining, GFP, and the merged image. Scale bar = 10 µm.

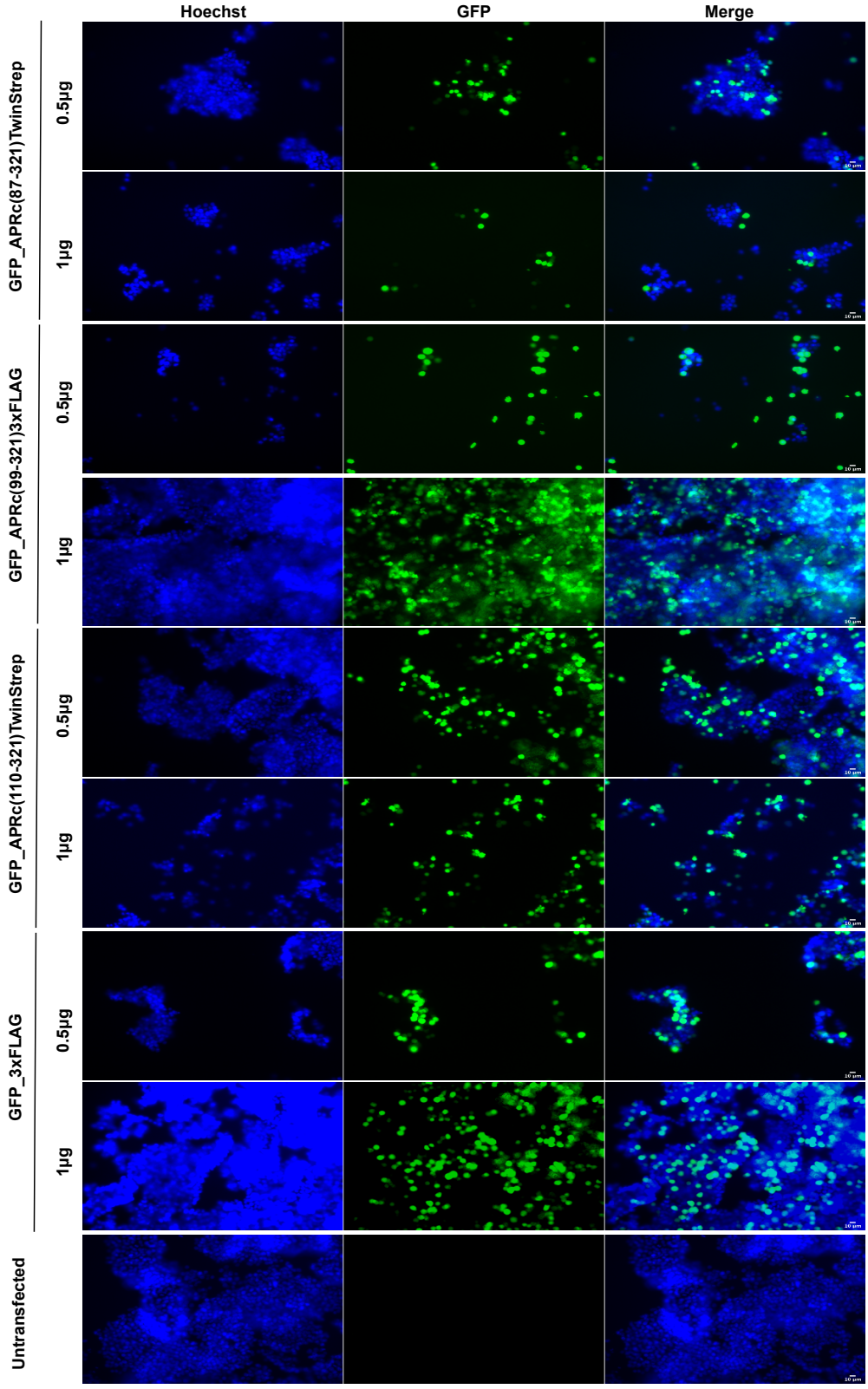


**Figure 14.** Optimization of transfection conditions of APRc constructs in HEK293 cells at 48h post-transfection.
HEK293 cells were transiently transfected with 0.5 µg and 1 µg of plasmid DNA harboring the different constructs of APRc, as described in the image, using the calcium phosphate method. At 24h post-transfection, the cells were stained for microscopy analysis with Hoechst (blue) to stain cells' nuclei. At 48h post-transfection, the cells were observed by fluorescence microscopy. Each row shows, from left to right, nuclei staining, GFP, and the merged image. Scale bar = 10 µm.

## 3.3. Evaluation of APRc autoprocessing activity *in vivo* in mammalian cells

In order to start evaluating if APRc maintains its autoprocessing activity when expressed in mammalian cells, and how the different truncated forms would impact this activity, each construct was transiently expressed in HEK293 cells, and protein expression was evaluated at two time-points post-transfection (24h and 48h). Total protein fractions were collected at each time-point and evaluated by parallel Western blot analysis. Furthermore, each construct was also transiently expressed in HEK293 cells seeded on glass coverslips. Confocal microscopy would allow us to assess if the autoprocessing/activity of APRc would result in phenotypic alterations in HEK293 cells. Therefore, at the same time-points post-transfection, the cells were fixed and stained with DAPI (for nucleic acid staining) and Rhodamine Phalloidin (for actin filaments staining), before evaluation by fluorescence microscopy.

The results obtained with the transfection of the different constructs harboring the entire soluble catalytic domain ($APRc_{87-231}$) are shown in **Figures 15-18.** Analyzing the Western blot represented in **Figure 15A** concerning 24h post-transfection, there were no significant differences between the different constructs of APRc. However, at 48h post-transfection (**Figure 15B**), the recombinant forms GFP_$APRc_{87-231}$_3xFLAG and GFP_$APRc_{87-231}$ display a low-molecular weight species when probed with anti-APRc antibody (20 and 15 kDa, respectively), consistent with processing and release of the soluble domain of APRc (tagged or untagged at the C-terminal, respectively). When probed with anti-GFP, the detection of a band with around 27 kDa in these samples that likely corresponds to GFP sustains the previous observation that APRc may be processed from the GFP fusion. To evaluate the impact of the catalytic aspartate on the autoprocessing activity, HEK293 cells were also transiently transfected with the active site mutant constructs. As expected, the mutation significantly abolished autoprocessing, with no detection of the low-molecular weight bands observed for the WT versions (**Figures 15** and **18A**), suggesting that processing of APRc is dependent on its autocatalytic activity. Furthermore, this autoprocessing activity may also be reflected on the different accumulation patterns of the GFP-fused forms observed on the Western blot at 48h post-transfection. As shown in **Figure 15B**, all the WT constructs of APRc have a lower signal of the intact fusion compared with the respective mutants. This evidence may be interpreted as excessive proteolysis of the active protease in transfected mammalian cells as a result of autoprocessing.

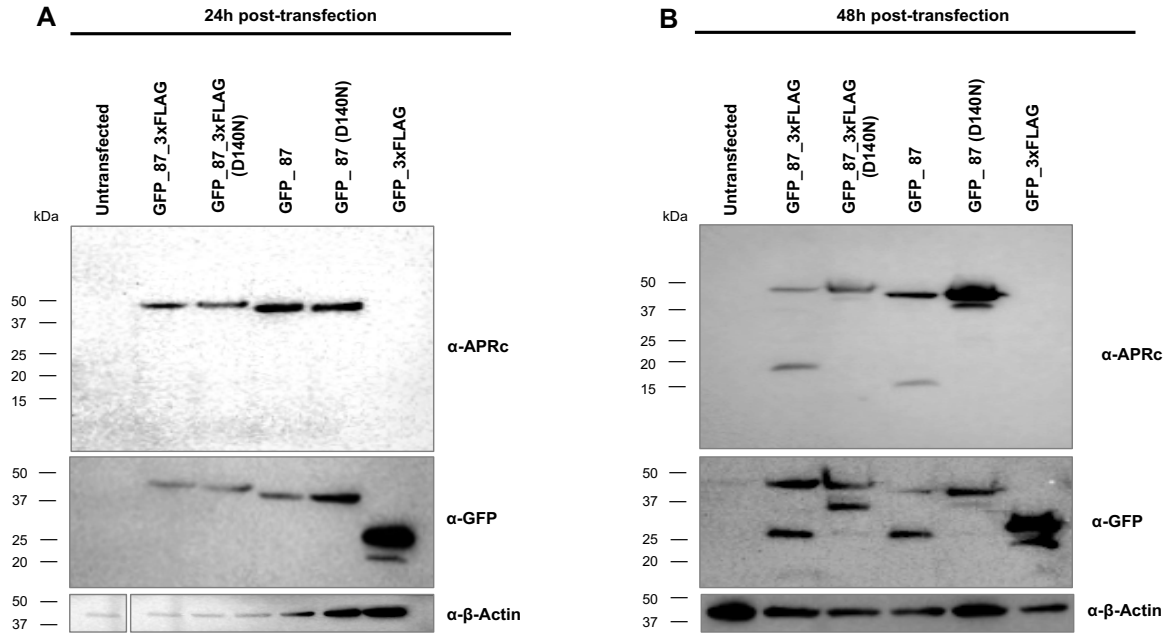


**Figure 15.** Autoprocessing of GFP_APRc $_{87-231}$-fusion proteins in HEK293 cells.
HEK293 cells were transiently transfected with pcDNA3.1+N-eGFP-derived vectors expressing the indicated constructs using the calcium phosphate method. Protein extracts were prepared at 24h (**A**) and 48h (**B**) post-transfection and analyzed by Western blotting. 40µL of each sample was examined in parallel with anti-APRc antibody, anti-GFP antibody, and anti-β-actin antibody (as a loading control). Molecular mass markers (kDa) are indicated at the left of each membrane.

Fluorescence staining of samples analyzed 24h post-transfection showed a diffuse distribution of the GFP signal for all constructs, except for the observation of a speckled-like pattern in cells transfected with GFP_APRc$_{87-231}$ (both WT and mutant forms) (**Figure 16)**. However, at 48h post-transfection, the differences between constructs start to be more evident. The speckled pattern of GFP and the presence of fragments of cells were visible in cells transfected with GFP_APRc$_{87-231}$_3xFLAG (**Figure 17**). Moreover, some membrane blebbing is also evident in cells expressing the WT constructs. This phenotype was absent in cells expressing the active site mutant, which are instead characterized by the speckled pattern. Cells expressing the untagged construct, GFP_APRc$_{87-231}$ (**Figure 17**), appear to have more fragmented cellular material as well as the speckled pattern of GFP. Again, cellular fragments were not observed in cells transfected with the untagged mutant, which only display the speckled pattern. The GFP signal in cells expressing the control construct GFP_3xFLAG (**Figure 17**), 48h post-transfection, was detected in the cytoplasm and the nucleus. This nuclear import of GFP is mainly due to the diffusion of this fluorescent protein through the nuclear pores (Seibel et al., 2007).

Interestingly, expression of the construct GFP_APRc$_{87-231}$_TwinStrep (**Figure 18A**), resulted in lower processing activity when compared with the 3xFLAG-tagged or untagged constructs, since no low-molecular weight band was detected either at 24h or

48h post-transfection. This result suggests that the TwinStrep tag may affect the conformation and/or protease activity. However, the cells transfected with GFP_APRc$_{87-231}$_TwinStrep and the respective mutant (**Figure 18B**), displayed the speckled pattern of GFP. In addition, the presence of what appears to correspond to fragmented cellular material (stained both with GFP and DAPI) was also observed in the WT.

Taking all these results, the phenotype observed in transfected cells is likely correlated with the processing/activation of APRc. At 48h post-transfection, the cells expressing GFP_APRc$_{87-231}$_3xFLAG and GFP_APRc$_{87-231}$, where the processing was evident (**Figure 15**), displayed a characteristic phenotype (**Figure 17**) with the presence of fragmented cell material. These results suggest that the autoprocessing of APRc renders the enzyme in an active form and available to cleave mammalian substrates, leading to the observed phenotype. This hypothesis is corroborated by the absence of processing and a less dramatic phenotype when the mutants are expressed. The observation of the speckled-like pattern of GFP suggests that the soluble catalytic domain of APRc may have a specific localization inside the cell that is independent of the catalytic activity.

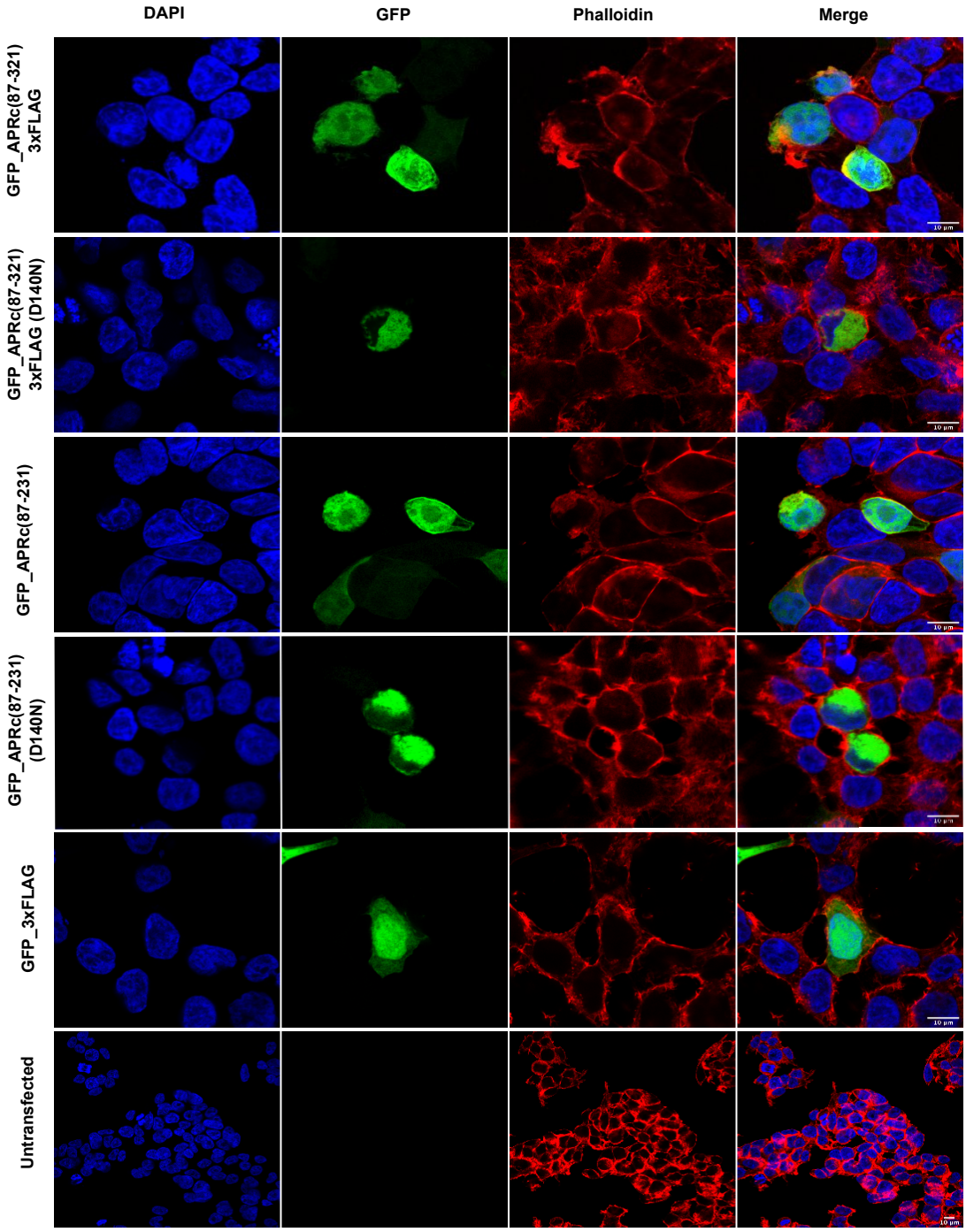


**Figure 16.** Confocal microscopy analysis of the expression of GFP_APRc$_{87-231}$-fusion constructs in HEK293 cells at 24h post-transfection.
HEK293 cells were transiently transfected with pcDNA3.1(+)-N-eGFP-derived vectors expressing the indicated constructs using the calcium phosphate method. At 24h post-transfection, the cells were fixed, permeabilized, and double stained for confocal microscopy analysis with DAPI (blue) to stain the nuclei and phalloidin (red) to stain the actin cytoskeleton. Representative images of a single slice from the z stacks. Each row shows, from left to right, nuclei staining, GFP, phalloidin staining, and the merged image. Scale bar = 10 µm.

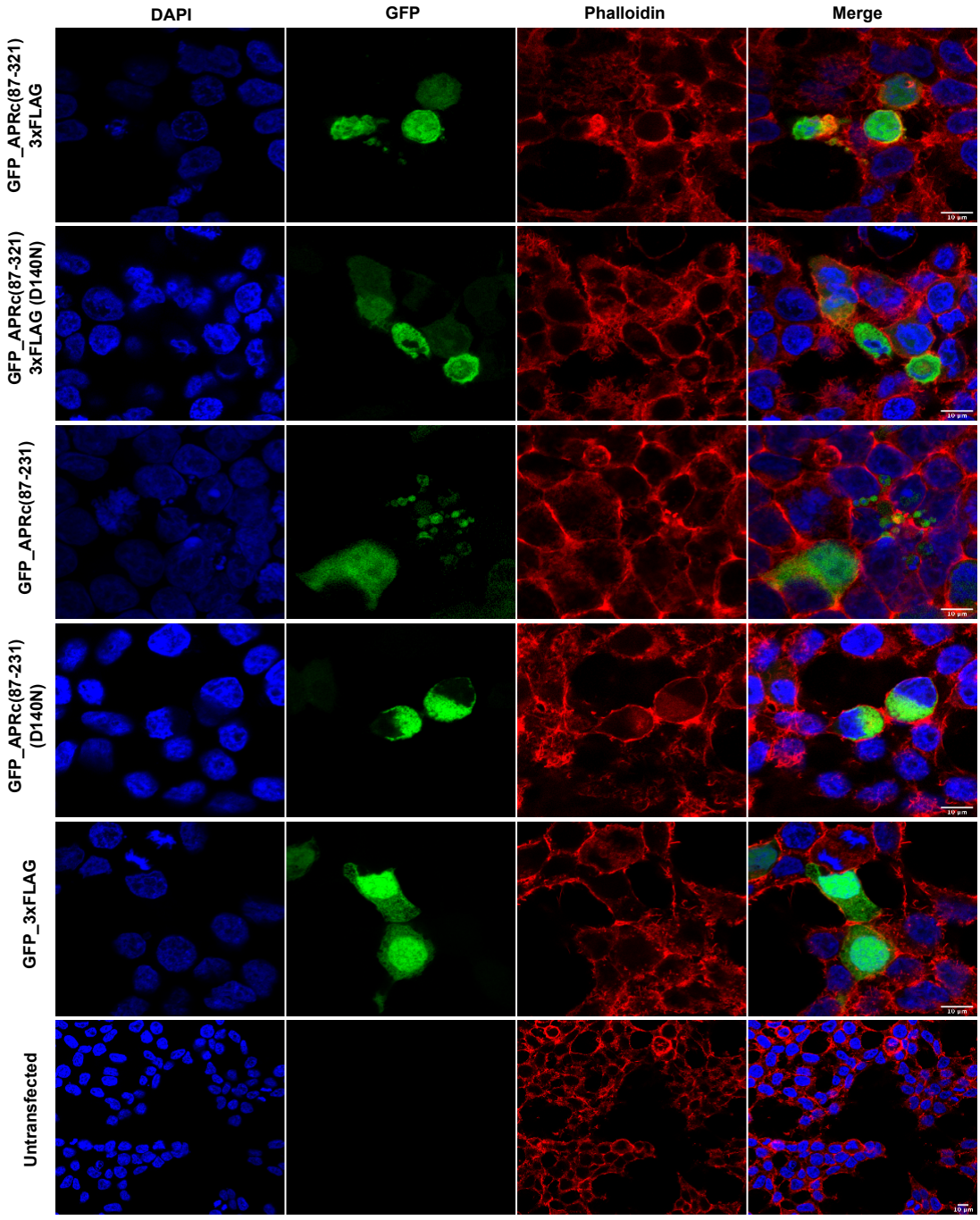


**Figure 17.** Confocal microscopy analysis of the expression of GFP_APRc$_{87-231}$ in HEK293 cells at 48h post-transfection.
HEK293 cells were transiently transfected with pcDNA3.1(+)-N-eGFP-derived vectors expressing the indicated constructs using the calcium phosphate method. At 48h post-transfection, the cells were fixed, permeabilized, and double stained for confocal microscopy analysis with DAPI (blue) to stain the nuclei and phalloidin (red) to stain the actin cytoskeleton. Representative images of a single slice from the z stacks. Each row shows, from left to right, nuclei staining, GFP, phalloidin staining, and the merged image. Scale bar = 10 μm.

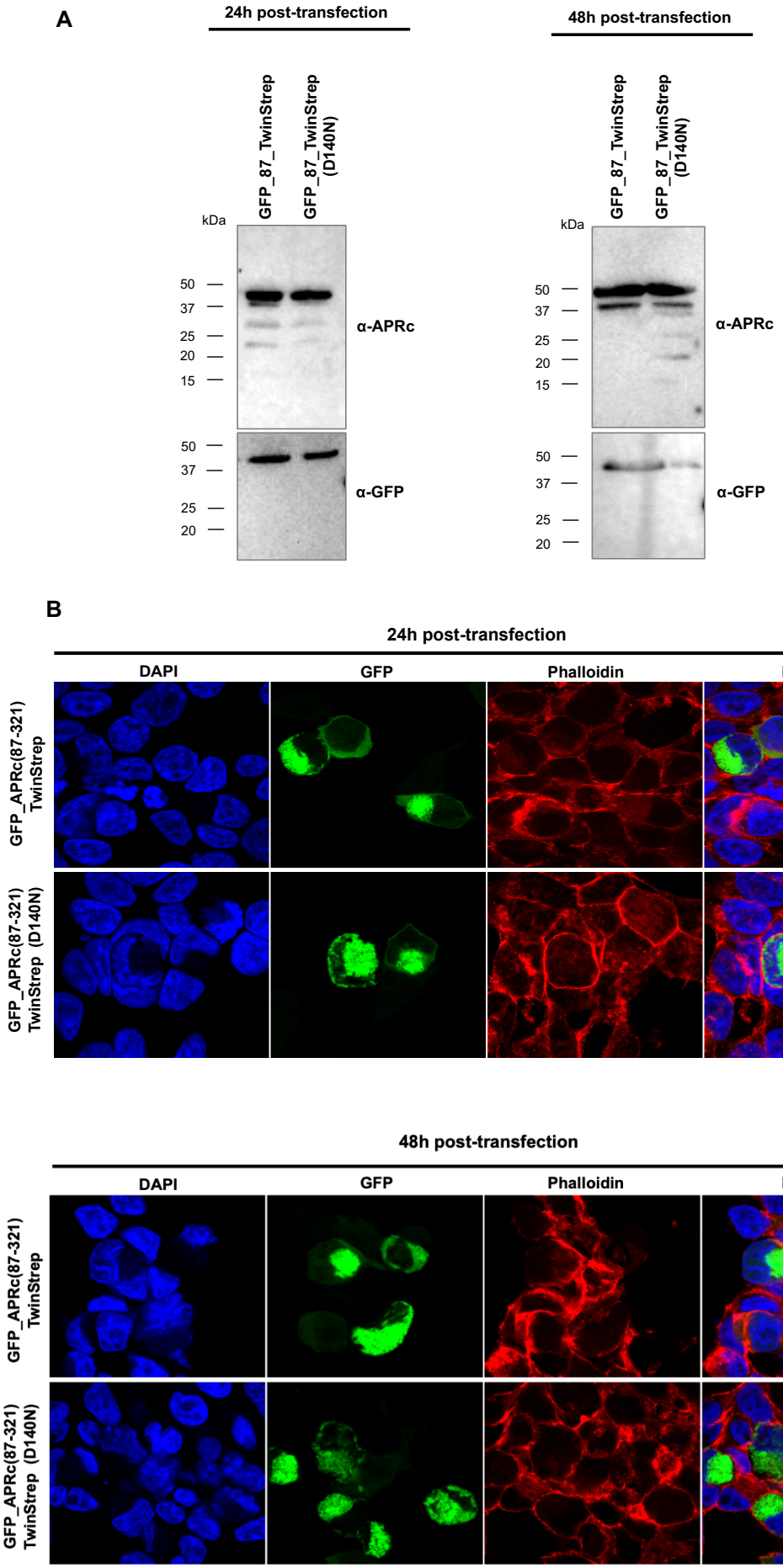
A
24h post-transfection
48h post-transfection
GFP_87_TwinStrep
GFP_87_TwinStrep (D140N)
kDa
50
37
25
20
15
α-APRc
α-GFP
B
24h post-transfection
48h post-transfection
DAPI
GFP
Phalloidin
Merge
GFP_APRc(87-321) TwinStrep
GFP_APRc(87-321) TwinStrep (D140N)

**Figure 18** (previous page)**.** Autoprocessing of GFP_APRc$_{87-231}$_TwinStrep and confocal microscopy analysis in HEK 293 cells.
HEK293 cells were transiently transfected with pcDNA3.1(+)-N-eGFP-derived vectors expressing the indicated constructs using the calcium phosphate method. **A.** Protein extracts were prepared at 24h and 48h post-transfection and analyzed by SDS-PAGE and Western blotting. 40µL of each sample was examined in parallel with anti-APRc antibody, anti-GFP antibody, and anti-β-actin antibody (as a loading control). Molecular mass markers (kDa) are indicated at the left of each membrane. **B.** At 24h and 48h post-transfection, cells were fixed, permeabilized, and double stained for confocal microscopy analysis with DAPI (blue) to stain the nuclei and phalloidin (red) to stain the actin cytoskeleton. Representative images of a single slice from the z stacks. Each row shows, from left to right, nuclei staining, GFP, phalloidin staining, and the merged image. Scale bar = 10 µm.

We next examined the results obtained upon transfection of constructs harboring the intermediate form APRc$_{99-231}$ (**Figures 19-21** and **Supplementary Figures 1-3)**.

Analyzing the Western blot represented in **Figure 19A** (and **Supplementary Figure 1A**) concerning 24h post-transfection, there were no significant differences between the different constructs of APRc, except the complete absence or faint signal of GFP_APRc$_{99-231}$_3xFLAG when immunodetected with anti-APRc or with anti-GFP antibodies, respectively. However, this likely results from lower transfection yields in this expression assay since, as shown in **Supplementary Figure 1A**, the signal was detected in the second replicate of transfection. At 48h post-transfection (**Figure 19B** and **Supplementary Figure 1B**), no processing product was observed for all tested constructs. However, it was evident a decrease in the precursor form of the 3xFLAG-tagged and untagged WT constructs compared with the corresponding mutants, as observed for the constructs harboring APRc$_{87-231}$. These results suggest that processing might indeed be occurring, but autoproteolysis might be faster for this shorter form.

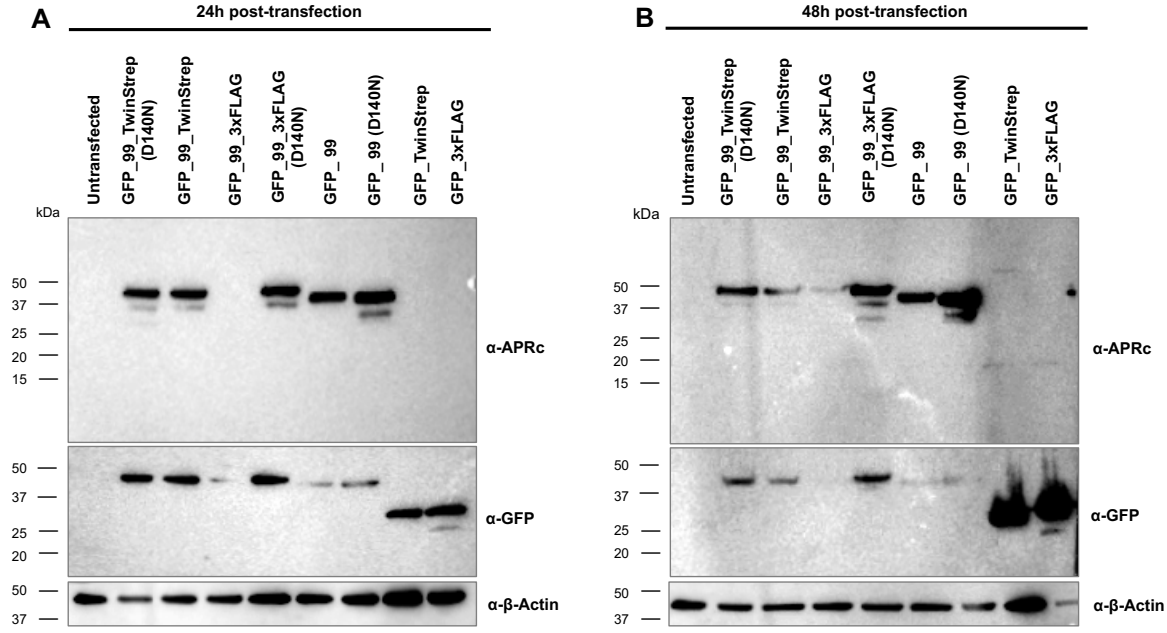


**Figure 19.** Autoprocessing of GFP_APRc$_{99-231}$-fusion proteins in HEK 293 cells.
HEK293 cells were transiently transfected with pcDNA3.1(+)-N-eGFP-derived vectors expressing the indicated constructs using the calcium phosphate method. Protein extracts were prepared at 24h (**A**) and 48h (**B**) post-transfection and analyzed by SDS-PAGE and Western blotting. 40µL of each sample was examined in parallel with anti-APRc antibody, anti-GFP antibody, and anti-β-actin antibody (as a loading control). Molecular mass markers (kDa) are indicated at the left of each membrane.

Confocal microscopy analysis of cells at 24h post-transfection showed a diffuse distribution of GFP signal in the majority of constructs, except for the presence of a speckled GFP pattern in cells transfected with GFP_APRc$_{99-231}$_TwinStrep (D140N) and the detection of some membrane blebbing in cells expressing GFP_APRc$_{99-231}$ (**Figure 20** and **Supplementary Figure 2**). At 48h post-transfection, the cellular phenotype was completely different, particularly between WT and mutants. Cells transfected with GFP_APRc$_{99-231}$_TwinStrep showed marked morphological alterations, including the presence of fragmented cellular material and some nuclear condensation (but no speckled pattern). In contrast, cell cultures expressing the GFP_APRc$_{99-231}$_TwinStrep (D140N) displayed a completely different phenotype, with the appearance of the speckled pattern (**Figure 21** and **Supplementary Figure 3**). As previously mentioned, there was a lower number of transfected cells in this first replicate for GFP_APRc$_{99-231}$_3xFLAG. However, the replicate represented in **Supplementary Figure 3** confirmed the presence of fragmented material and nuclear condensation. Moreover, membrane blebbing was more evident in these cells, when compared with cells transfected with GFP_APRc$_{99-231}$_TwinStrep. In contrast, cells expressing the mutant form of GFP_APRc$_{99-231}$_3xFLAG exhibited a diffused GFP signal distribution, without signs of nuclear condensation. In addition to membrane blebbing, cells expressing the untagged construct GFP_APRc$_{99-231}$ also showed the presence of fragmented cellular material, although not as evident as with the 3xFLAG tagged construct. The untagged mutant displayed the speckled pattern of GFP signal, without the presence of cellular fragments. As expected, the GFP signal in cells expressing the control constructs GFP_TwinStrep and GFP_3xFLAG, at 48h post-transfection, was detected in the cytoplasm and nucleus.

Globally, our results suggest that GFP_APRc$_{99-231}$_3xFLAG and GFP_APRc$_{99-231}$ were more active, compared with GFP_APRc$_{99-231}$_TwinStrep. This assumption is supported by differences in accumulation patterns of the WT and corresponding mutant precursor forms of GFP_APRc$_{99-231}$_3xFLAG and the more dramatic morphological alterations observed by confocal microscopy analysis. The fact that no activation product was detected under the evaluated conditions suggests that the activation product might be rapidly degraded by autoproteolysis. The lower number of transfected cells observed for this construct may also be related to this. We cannot discard the possibility that the generated active form may lead to cell death through a cytotoxic effect of the protease.

**Figure 20** (next page)**.** Confocal microscopy analysis of the expression of GFP_APRc$_{99-231}$-fusion constructs in HEK293 cells at 24h post-transfection.
HEK293 cells were transiently transfected with pcDNA3.1+N-eGFP-derived vectors expressing the indicated constructs using the calcium phosphate method. At 24h post-transfection, the cells were fixed, permeabilized, and double stained for confocal microscopy analysis with DAPI (blue) to stain nuclei and phalloidin (red) to stain the actin cytoskeleton. Representative images of a single slice from the z stacks. Each row shows, from left to right, nuclei staining, GFP, phalloidin staining, and the merged image. Scale bar = 10 µm.

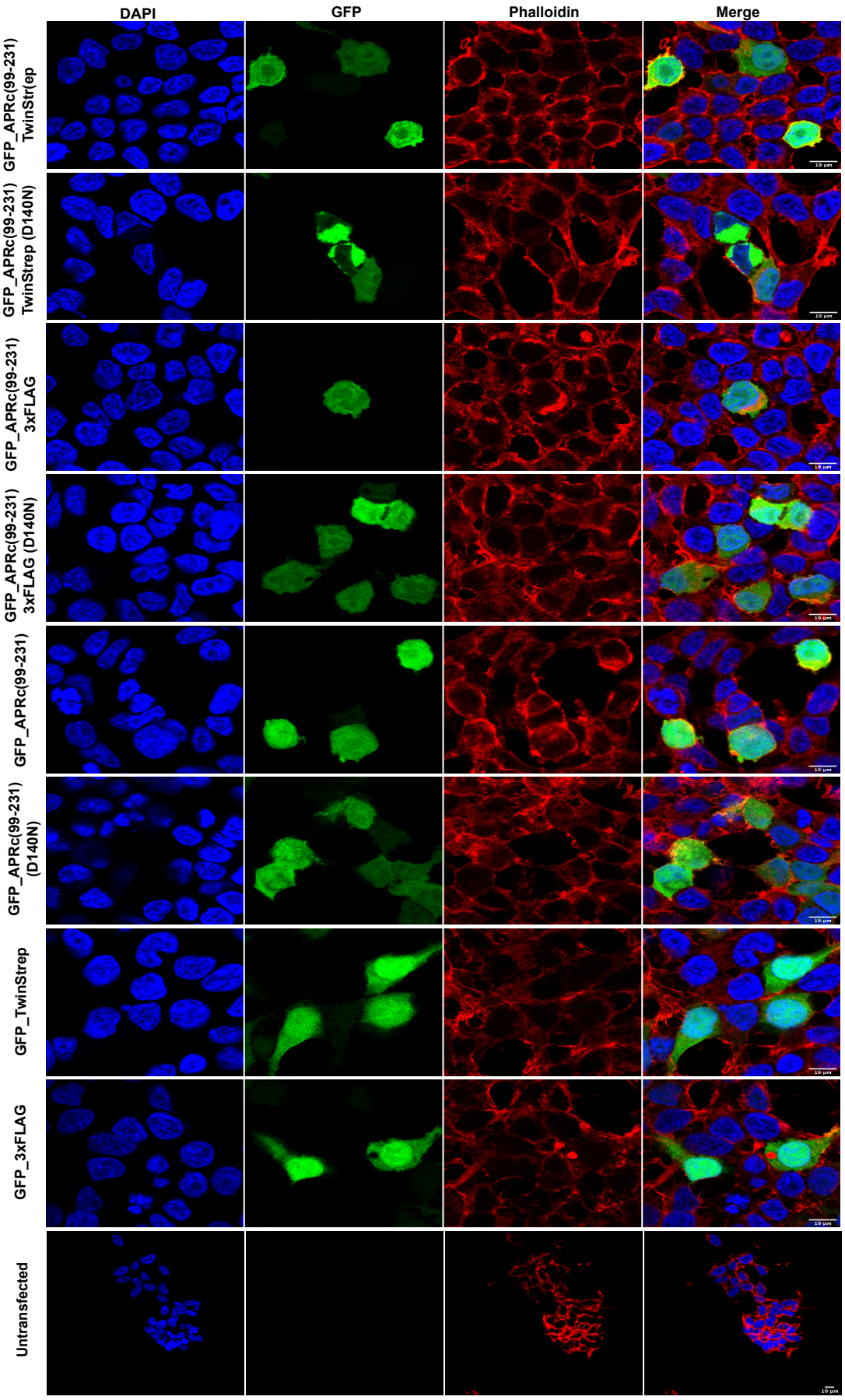
DAPI
GFP
Phalloidin
Merge
GFP_APRc(99-231) TwinStr(ep
GFP_APRc(99-231) TwinStrep (D140N)
GFP_APRc(99-231) 3xFLAG
GFP_APRc(99-231) 3xFLAG (D140N)
GFP_APRc(99-231)
GFP_APRc(99-231) (D140N)
GFP_TwinStrep
GFP_3xFLAG
Untransfected

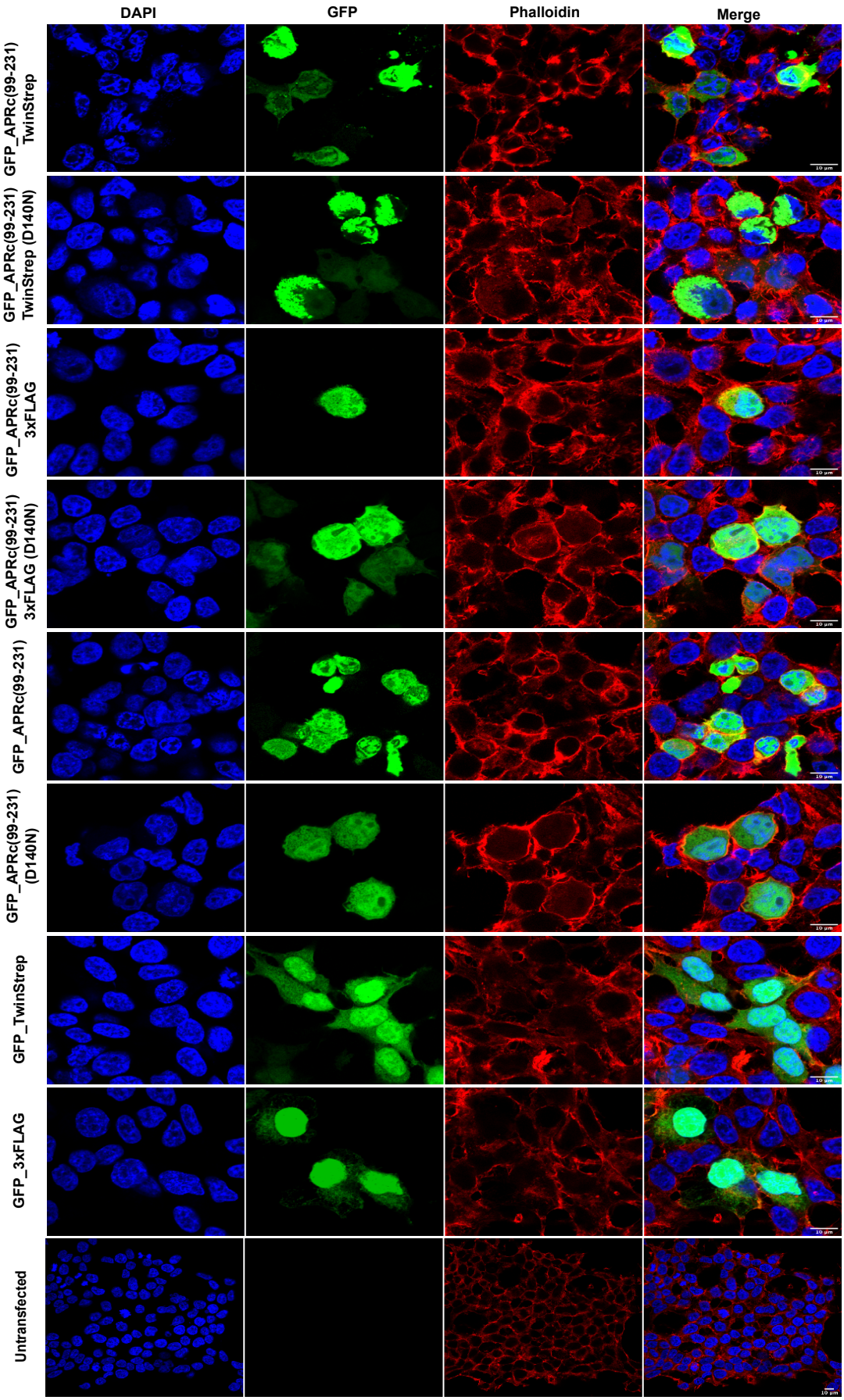
DAPI
GFP
Phalloidin
Merge
GFP_APRc(99-231) TwinStrep
GFP_APRc(99-231) TwinStrep (D140N)
GFP_APRc(99-231) 3xFLAG
GFP_APRc(99-231) 3xFLAG (D140N)
GFP_APRc(99-231)
GFP_APRc(99-231) (D140N)
GFP_TwinStrep
GFP_3xFLAG
Untransfected

**Figure 21** (previous page)**.** Confocal microscopy analysis of the expression of GFP_APRc$_{99-231}$-fusion constructs in HEK293 cells at 48h post-transfection.
HEK293 cells were transiently transfected with pcDNA3.1+N-eGFP-derived vectors expressing the indicated constructs using the calcium phosphate method. At 48h post-transfection, the cells were fixed, permeabilized, and double stained for confocal microscopy analysis with DAPI (blue) to stain the nuclei and phalloidin (red) to stain the actin cytoskeleton. Representative images of a single slice from the z stacks. Each row shows, from left to right, nuclei staining, GFP, phalloidin staining, and the merged image. Scale bar = 10 μm.

The results obtained with the transfection of the different constructs harboring the shorter truncated form of APRc (APRc$_{110-231}$) are shown in **Figures 22-24** and **Supplementary Figures 4-6**. As shown in **Figure 22**, an increased accumulation of the mutant precursor forms is again observed, compared to the respective WT constructs. Since APRc$_{110-231}$ is known to be an active dimer in solution (when purified from *E. coli*), we cannot discard the possibility that this fusion construct may not undergo further processing, which would explain the lack of processing products. However, it is also plausible that the decrease in the accumulation pattern of the WT precursor forms might result from the higher autoproteolytic activity of the activated product (which would lead to faster self-degradation).

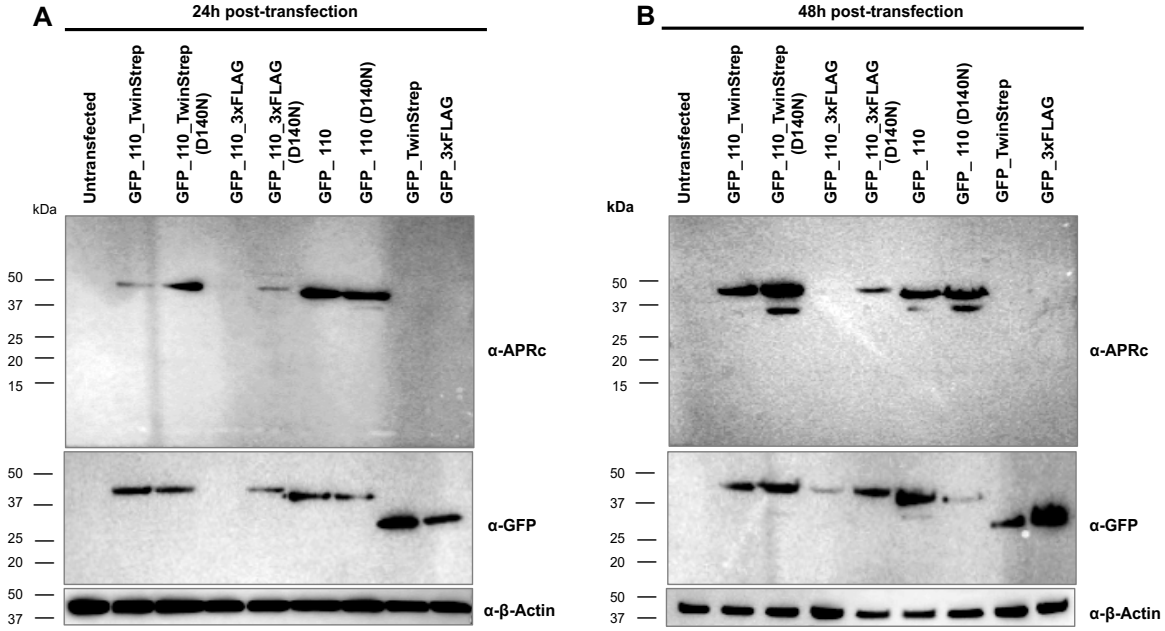


**Figure 22.** Autoprocessing of GFP_APRc$_{110-231}$-fusion proteins in HEK 293 cells.
HEK293 cells were transiently transfected with pcDNA3.1+N-eGFP-derived vectors expressing the indicated constructs using the calcium phosphate method. Protein extracts were prepared at 24h (**A**) and 48h (**B**) post-transfection and analyzed by Western blotting. 40μL of each sample was examined in parallel with anti-APRc antibody, anti-GFP antibody and anti-β-actin antibody (as a loading control). Molecular mass markers (kDa) are indicated at the left of each membrane.

Nonetheless, the impact of the protease activity on cell morphology was more evident by confocal microscopy analysis, represented in **Figures 23** and **24** (and **Supplementary Figures 5** and **6**). At 24h post-transfection (**Figure 23**), most of the transfected cells displayed a diffused distribution of GFP, except for the presence of some membrane blebbing in cells expressing GFP_APRc$_{110-231}$_TwinStrep and GFP_APRc$_{110-231}$. At 48h post-transfection (**Figure 24**), the cells expressing the WT constructs showed a considerable accumulation of fragmented cellular material and nuclear condensation, suggesting that they went through a cell death process. In contrast, the cells expressing the mutant forms of APRc$_{110-231}$ did not exhibit any of the previously mentioned phenotypes, displaying diffused distribution of GFP. Only in cells expressing GFP_APRc$_{110-231}$_TwinStrep (D140N), the speckled pattern was detected. These results contrast with the GFP signal in cells expressing the control constructs GFP_TwinStrep and GFP_3xFLAG that is, as expected, detected both in cytoplasm and nucleus.

Therefore, the decrease in the accumulation of the WT precursor forms observed in the Western blot (**Figure 22**) might be associated with the proteolytic activity of APRc that likely cleaves other targets in mammalian cells resulting in profound morphological alterations that resemble a cell death phenotype.

**Figure 23** (next page)**.** Confocal microscopy analysis of the expression of GFP_APRc$_{110-231}$-fusion constructs in HEK293 cells at 24h post-transfection.
HEK293 cells were transiently transfected with pcDNA3.1+N-eGFP-derived vectors expressing the indicated constructs using the calcium phosphate method. At 24h post-transfection, the cells were fixed, permeabilized, and double stained for confocal microscopy analysis with DAPI (blue) to stain the nuclei and phalloidin (red) to stain the actin cytoskeleton. Representative images of a single slice from the z stacks. Each row shows, from left to right, nuclei staining, GFP, phalloidin staining, and the merged image. Scale bar = 10 µm.

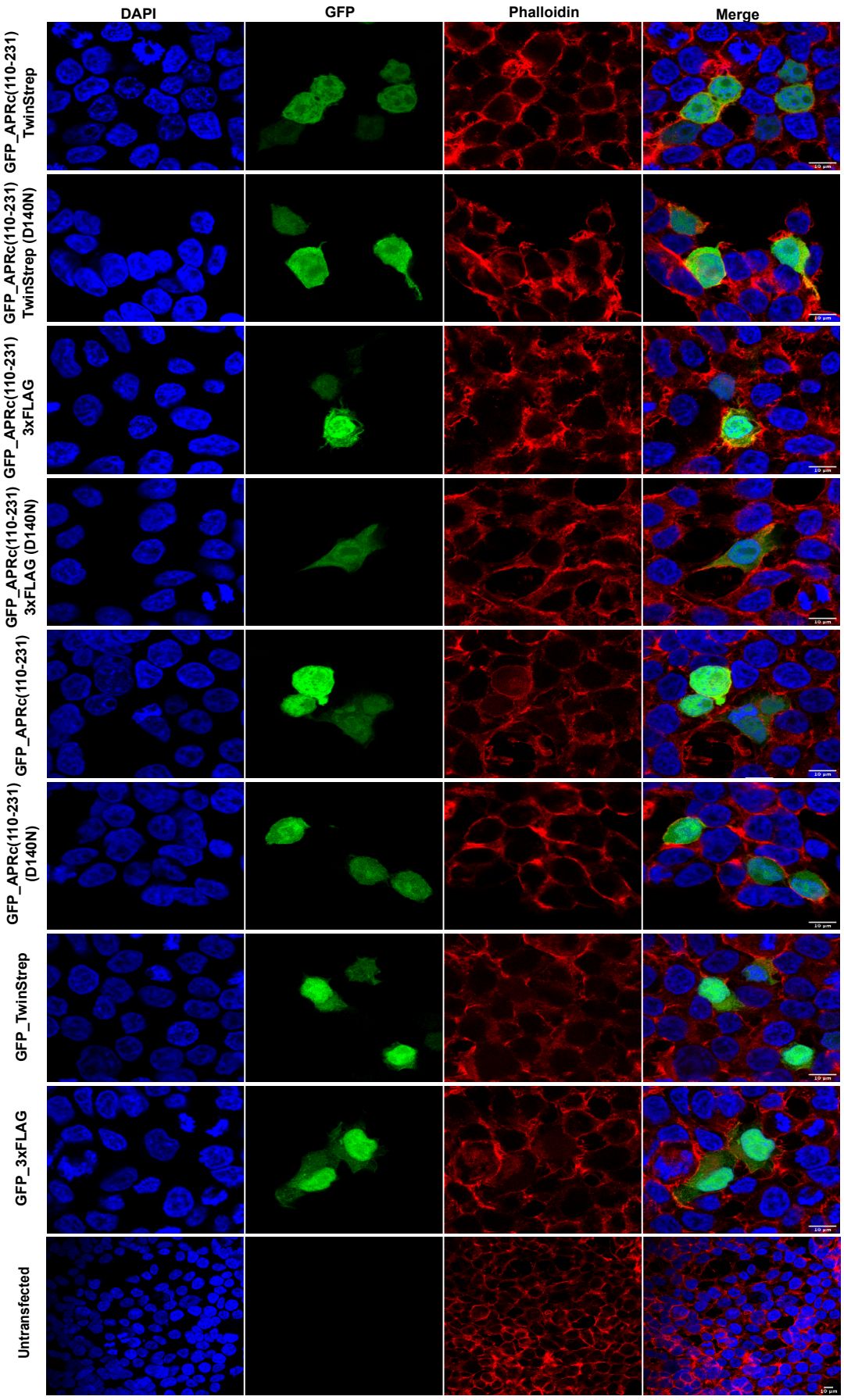
DAPI
GFP
Phalloidin
Merge
GFP_APRc(110-231) TwinStrep
GFP_APRc(110-231) TwinStrep (D140N)
GFP_APRc(110-231) 3xFLAG
GFP_APRc(110-231) 3xFLAG (D140N)
GFP_APRc(110-231)
GFP_APRc(110-231) (D140N)
GFP_TwinStrep
GFP_3xFLAG
Untransfected

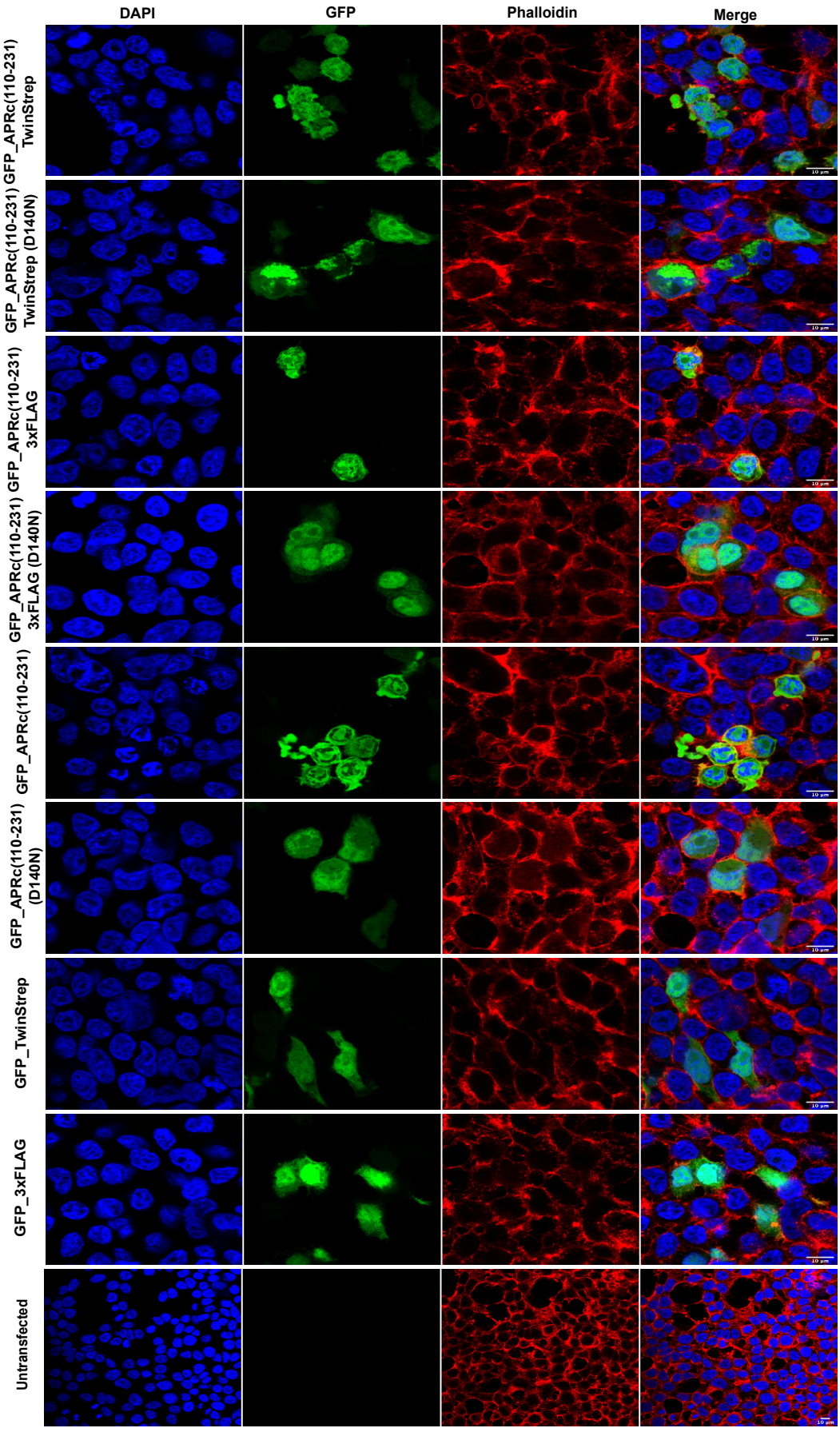
DAPI
GFP
Phalloidin
Merge
GFP_APRc(110-231) TwinStrep
GFP_APRc(110-231) TwinStrep (D140N)
GFP_APRc(110-231) 3xFLAG
GFP_APRc(110-231) 3xFLAG (D140N)
GFP_APRc(110-231)
GFP_APRc(110-231) (D140N)
GFP_TwinStrep
GFP_3xFLAG
Untransfected

**Figure 24** (previous page)**.** Confocal microscopy analysis of the expression of GFP_APRc$_{110-231}$-fusion constructs in HEK293 cells at 48h post-transfection.
HEK293 cells were transiently transfected with pcDNA3.1+N-eGFP-derived vectors expressing the indicated constructs using the calcium phosphate method. At 48h post-transfection, the cells were fixed, permeabilized, and double stained for confocal microscopy analysis with DAPI (blue) to stain the nuclei and phalloidin (red) to stain the actin cytoskeleton. Representative images of a single slice from the z stacks. Each row shows, from left to right, nuclei staining, GFP, phalloidin staining, and the merged image. Scale bar = 10 µm.

## 3.4. Subcellular localization of APRc

As previously observed at 48h post-transfection, the cells expressing APRc$_{87-231}$- and APRc$_{99-231}$-fusions displayed a speckled pattern. Moreover, this phenotype was more evident in the mutant forms, suggesting that this distribution pattern is independent of the catalytic activity. Interestingly, a speckled pattern was previously observed in HIV-1 protease-expressing cells. In fact, the protease was shown to co-localize with a mitochondrial marker, DsRed2-Mito, and detected in the mitochondrial fraction (Rumlová et al., 2014). Therefore, to analyze whether the localization of APRc could correspond to the mitochondrial compartment, the untagged constructs of the longer versions of APRc were transiently transfected in HEK293 cells and stained with DAPI and with a mouse polyclonal antibody against Tom20, a well-known mitochondrial marker (Rapaport, 2005), at 48h post-transfection.

The results obtained are represented in **Figure 25**. Immunofluorescence analysis showed that there was no co-localization of APRc with the mitochondrial protein, TOM20. Therefore, the speckled pattern observed does not correspond to a mitochondrial localization of the protease. In fact, this assay showed that the cells with membrane blebbing, nuclear condensation, and fragmented cellular material were only poorly stained with the mitochondrial marker, suggesting that these cells no longer contain mitochondria, maybe as a result of cell death.

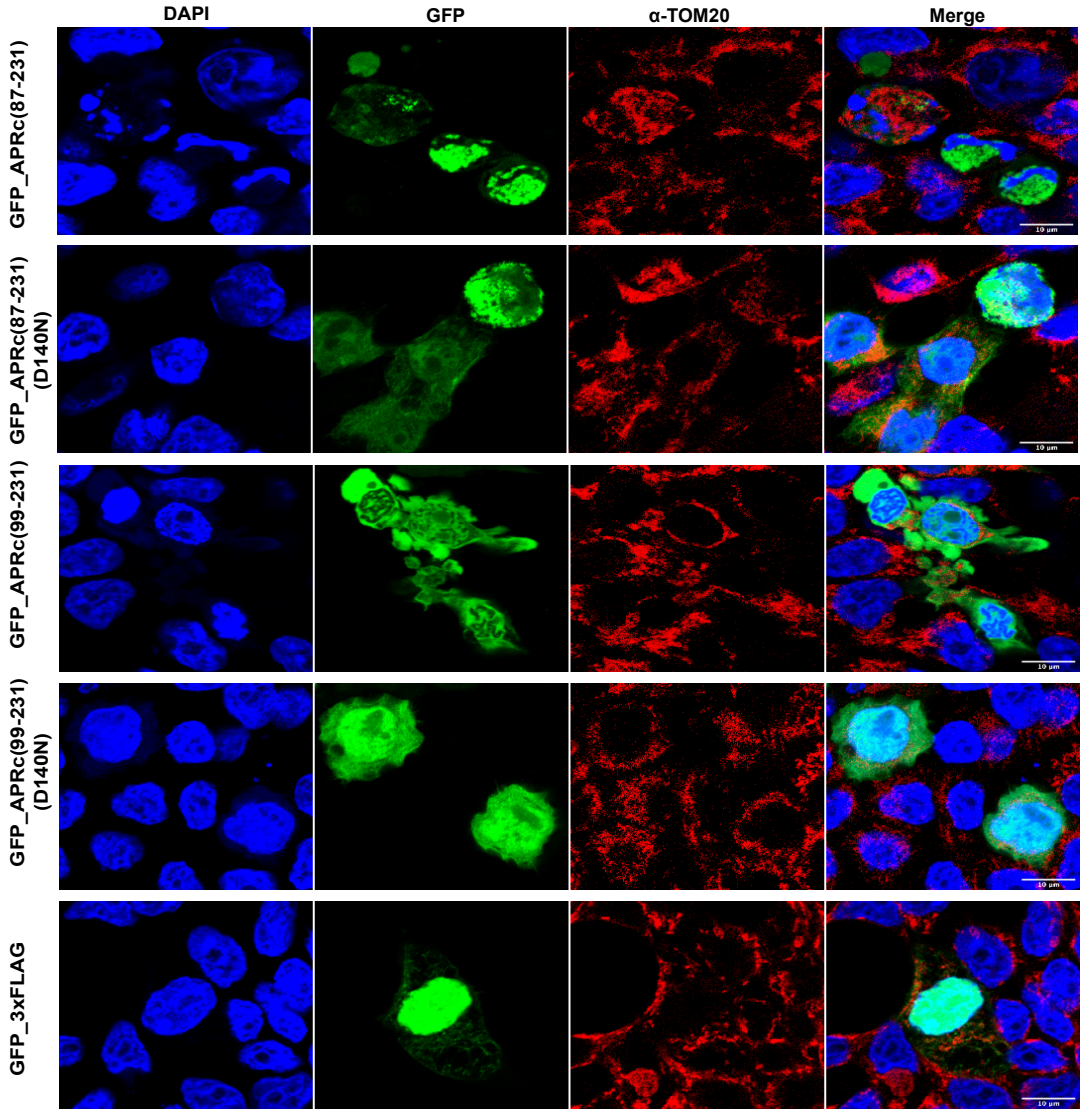


**Figure 25.** Assessing APRc co-localization with mitochondria in HEK293 cells.
HEK293 cells were transiently transfected with different untagged constructs of GFP_APRc and with the control construct, GFP_3xFLAG, using the calcium phosphate method. At 48h post-transfection, the cells were fixed, permeabilized, and stained for immunofluorescence confocal microscopy analysis with DAPI (blue) to stain the nuclei, and with anti-TOM20 antibody (red) to detect mitochondria. Representative images of a single slice from the z stacks. Each row shows, from left to right, nuclei staining, GFP, anti-TOM20 staining, and the merged image.
The merged images show that there is no co-localization of the mitochondrial marker with APRc. Scale bar = 10 μm.

## 3.5. Analysis of cell death in HEK293 cells

From our previous results, it was clear that HEK293 cells expressing the WT versions of APRc displayed a particular phenotype with morphological changes such as pseudopodia retraction, shrinkage, membrane blebbing, chromatin condensation, nuclear fragmentation, and shedding of cellular fragments that might correspond to apoptotic bodies. Since these morphological features are markers of apoptosis (Kepp et al., 2011), we next sought the use of different methodologies to evaluate if APRc was indeed triggering apoptosis in HEK293 cells.

### 3.5.1. Evaluation of parameters associated with shape and size of nuclei

Nuclear condensation is one of the features of apoptosis (Elmore, 2007). Therefore, we decided to evaluate and quantify this apoptosis hallmark, using fluorescence microscopy images. HEK293 cells were transiently transfected with GFP_APRc$_{87-231}$_3xFLAG, GFP_APRc$_{87-231}$_3xFLAG(D140N), GFP_APRc$_{99-231}$_3xFLAG, GFP_APRc$_{99-231}$_3xFLAG(D140N), GFP_APRc$_{110-231}$_TwinStrep, GFP_APRc$_{110-231}$_TwinStrep(D140N), GFP_3xFLAG, and GFP_TwinStrep, using Lipofectamine 3000. We decided to change the transfection method to increase transfection efficiency. At 48h post-transfection, the cells were fixed and then stained with DAPI. The nuclei that were intensely stained with this nuclear counterstain were considered condensed nuclei (**Figure 26A**). The constructs herein tested were selected based on the increased autoprocessing activity and more dramatic phenotypic differences observed in our previous assays (section 3.3). Cells expressing GFP_3xFLAG and GFP_TwinStrep were included as controls. As shown in **Figure 26B**, nuclear condensation was significantly increased in cells transfected with all WT constructs of APRc, compared with the respective control constructs. Interestingly, a significant reduction in nuclear condensation percentage was observed in cells expressing the corresponding active site mutants.

Globally, these data indicate that the rickettsial retropepsin APRc contributes significantly to nuclear condensation, a characteristic feature of apoptosis, and that its catalytic activity appears critical to these nuclear morphological changes, suggesting that APRc may induce an apoptotic stimulus in these mammalian cells.

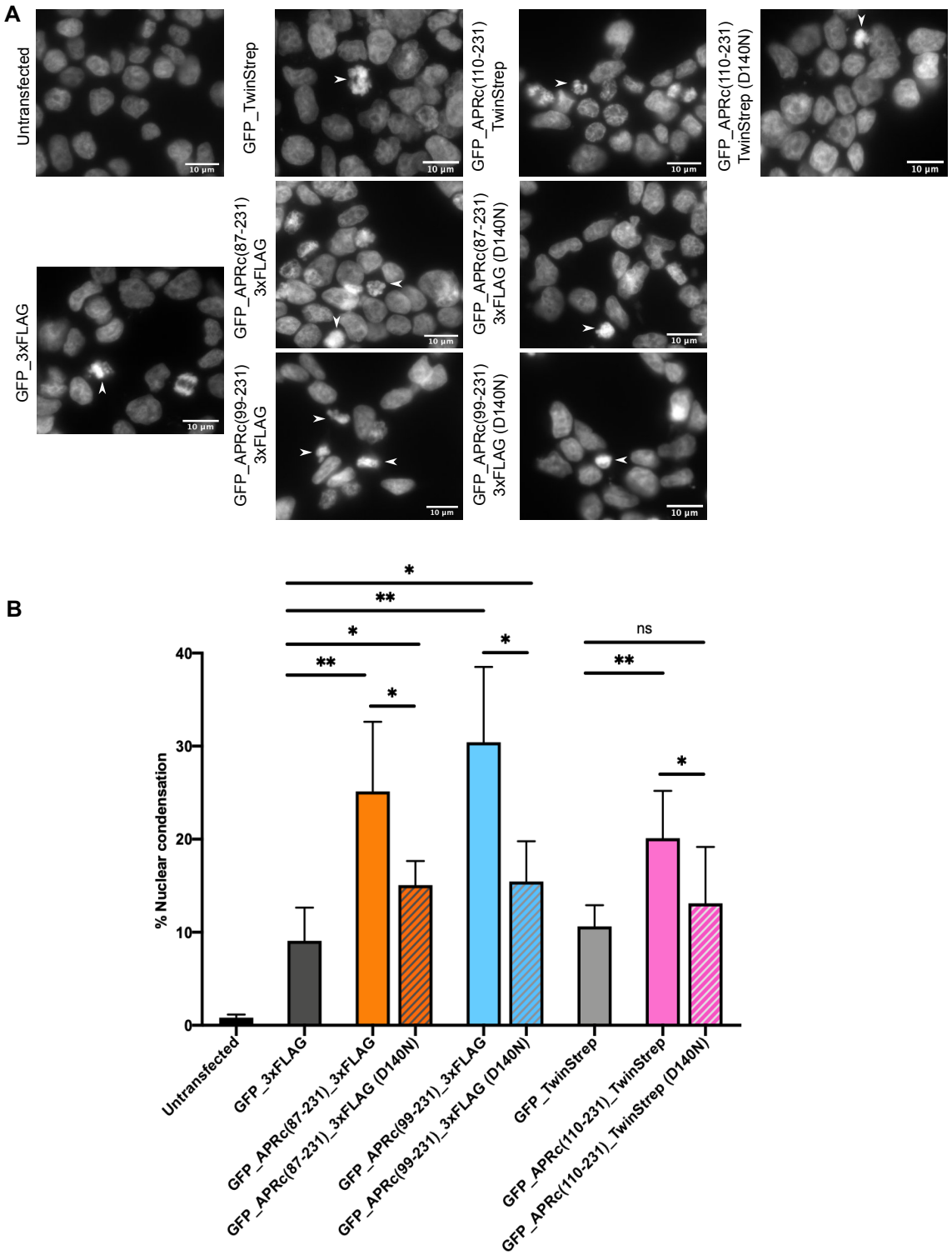


**Figure 26.** Impact of GFP_APRc-fusion constructs on nuclear condensation in HEK293 cells.
At 48h post-transfection, the cells were fixed, permeabilized, and stained for microscopy analysis with DAPI to stain nuclei. **A.** Expression of GFP_APRc-fusion constructs induced nuclear condensation (arrowheads) in HEK293 cells. Scale bar = 10 µm **B.** HEK293 cells transfected with GFP_APRc$_{87-231}$_3xFLAG, GFP_APRc$_{99-231}$_3xFLAG, and GFP_APRc$_{110-231}$_TwinStrep showed increased nuclear condensation compared with cells transfected with control constructs (GFP_3xFLAG / GFP_TwinStrep). HEK293 cells expressing the corresponding mutant constructs (D140N) partially restored the phenotype of control constructs, displaying a significant reduction in nuclear condensation compared with WT constructs. At least 400 nuclei were counted from each sample (n=2). Each value represents mean +/- SD. Brown-Forsythe and Welsh one-way ANOVA multiple-comparisons test was used to determine the significance between control constructs and APRc constructs. Welch's *t*-test was performed to determine the significance between WT and respective mutant constructs. *p<0.05 **p<0.01; ns: non-significant.

In addition to analyzing nuclear condensation, we also determined whether the expression of APRc constructs would affect other parameters related to nuclei morphology. For these, the microscopy images were then analyzed using the CellProfiler software. The results obtained for the different parameters are represented in **Figure 27**.

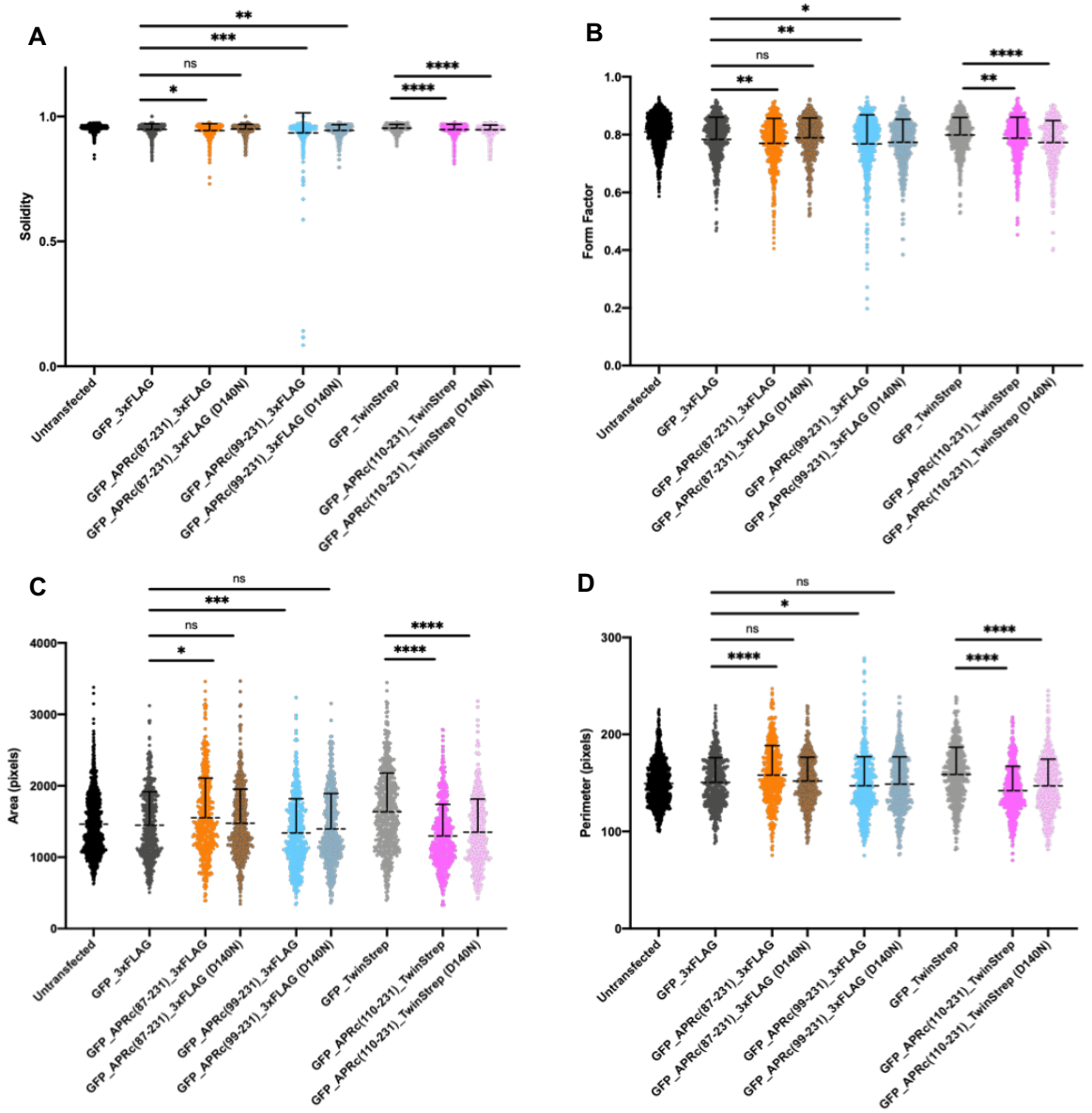


**Figure 27.** Analysis of the nuclei shape parameters solidity, form factor, area, and perimeter in HEK293 cells expressing different GFP_APRc-fusion constructs.
At 48h post-transfection, cells were fixed, permeabilized, and stained for microscopy analysis with DAPI to stain the nuclei. The microscopy images were analyzed using the CellProfiler software and the values obtained for the different nuclei shape parameters were obtained. **A** and **B.** Graphic representation of the values of nuclei shape parameters solidity **(A)** and form factor **(B)**. Solidity is calculated by Area/Convex Area, where Convex Area is the area delimited by the smallest polygon that borders all the points of the nuclei. Form factor, or circularity, is calculated by $4\pi \times \text{Area}/\text{Perimeter}^2$. Nuclei of cells transfected with GFP-APRc fusion constructs (WT and mutants) showed a smaller solidity and form factor values compared with the respective control constructs, except for GFP_APRc$_{87\text{-}231}$_3xFLAG (D140N). **C** and **D.** Graphic representation of the values of nuclei size parameters area **(C)** and perimeter **(D)**. Nuclei of cells transfected with GFP_APRc$_{87\text{-}231}$_3xFLAG showed a higher area and perimeter compared with the respective control construct. Cells expressing the respective mutant form restored the phenotype. The same trend was observed for the nuclei of cells expressing GFP_APRc$_{99\text{-}231}$_3xFLAG(D140N). Regarding the nuclei of cells transfected with GFP_APRc$_{110\text{-}231}$_TwinStrep, both WT and mutant displayed a smaller area and perimeter values. At least 400 nuclei were counted for each sample (n=2). Each value represents mean +/- SD. Brown-Forsythe and Welsh one-way ANOVA multiple-comparisons test was used to determine the significance between controls and GFP-APRc-fusion constructs. *p<0.05; **p<0.01; ***p<0.001; ****p<0.0001; ns: non-significant.

Solidity is calculated by *Area/Convex Area*, where *Convex Area* is the area bounded by the smallest polygon that borders all the points of the nuclei. The more irregular and ramified is the nuclei, the bigger is the convex area, thus yielding a solidity value lower than 1, which is observed when nuclei are condensed or even fragmented. On the other hand, form factor, also known as circularity, is calculated by $4\pi \times Area/Perimeter^2$. A perfectly circular object has a form factor equal to 1, while an irregular object (as a condensed/fragmented nuclei) displays a form factor value lower than 1. Taking into account the definition of these two descriptors, both are associated with the nuclear shape. We also analyzed the area and perimeter of the nuclei of these cells, being these two values correlated with the nuclei size.

As shown in **Figure 27**, the nuclei of cells transfected with GFP_APRc$_{87-231}$_3xFLAG showed a significant reduction in solidity (**Figure 27A**) and form factor (**Figure 27B**) values compared to GFP_3xFLAG. However, these nuclei shape parameter values were not significantly different in the active site mutant. Regarding the values of area and perimeter of the cells expressing GFP_APRc$_{87-231}$_3xFLAG(D140N) (**Figure 27C** and **27D**), the trend was the same, without a statistical difference compared with the control (GFP_3xFLAG). However, and somewhat surprisingly, the area and perimeter values of GFP_APRc$_{87-231}$_3xFLAG were higher compared with the control construct. Taking this together with the data from **Figure 26B**, where the WT showed a higher percentage of condensed nuclei compared with the mutant, it appears that the catalytic activity of the protease is somehow relevant for the induction of changes in nuclear shape and size.

In cells expressing GFP_APRc$_{99-231}$_3xFLAG or the mutant, the solidity and form factor values were significantly lower than the respective control. However, for the area and perimeter, only the WT displays significant differences when compared to control. These results suggest that the catalytic mutant effect in inducing nuclear morphological changes is less pronounced, which is consistent with the observed reduction in the percentage of nuclear condensation in mutant-expressing cells (Figure 26B).

Analyzing the results regarding cells expressing GFP_APRc$_{110-231}$_TwinStrep or the mutant, there was a significant decrease in all tested parameters compared with GFP_TwinStrep-expressing cells.

Altogether, and although the catalytic activity of APRc appears to be determinant for most of these morphological changes, other protein-protein interactions established by APRc might also contribute to the observed phenotype. This is supported by the fact that expression of the mutant forms not necessarily reverted the phenotype to levels observed in cells expressing GFP only.

### 3.5.2. DNA laddering assay

During apoptosis, a specific nuclease is responsible for cleaving chromosomal DNA strand, generating DNA fragments (DNA ladders), a biochemical hallmark of apoptotic cells (Zhang and Xu, 2000). Since we observed that the expression of various forms of APRc on HEK293 cells induced nuclear condensation and a decrease in the nuclear size, we next assessed if APRc expression would lead to DNA fragmentation. HEK293 cells were transiently transfected with several forms of APRc and the corresponding mutants, and cellular extracts were prepared at 48h post-transfection as described in section 2.2.12. As shown in **Figure 28**, no apparent DNA laddering was observed for the tested constructs. However, this sample preparation protocol resulted in extremely viscous samples, probably due to the presence of high-weight genomic DNA, fragments of cells, or even cellular components as lipids and proteins, which hindered their application in the agarose gel. To overcome this, a different strategy should be used in the future, such as the phenol-chloroform extraction, for a more efficient separation between the aqueous phase (DNA) and organic phase (lipids and proteins).

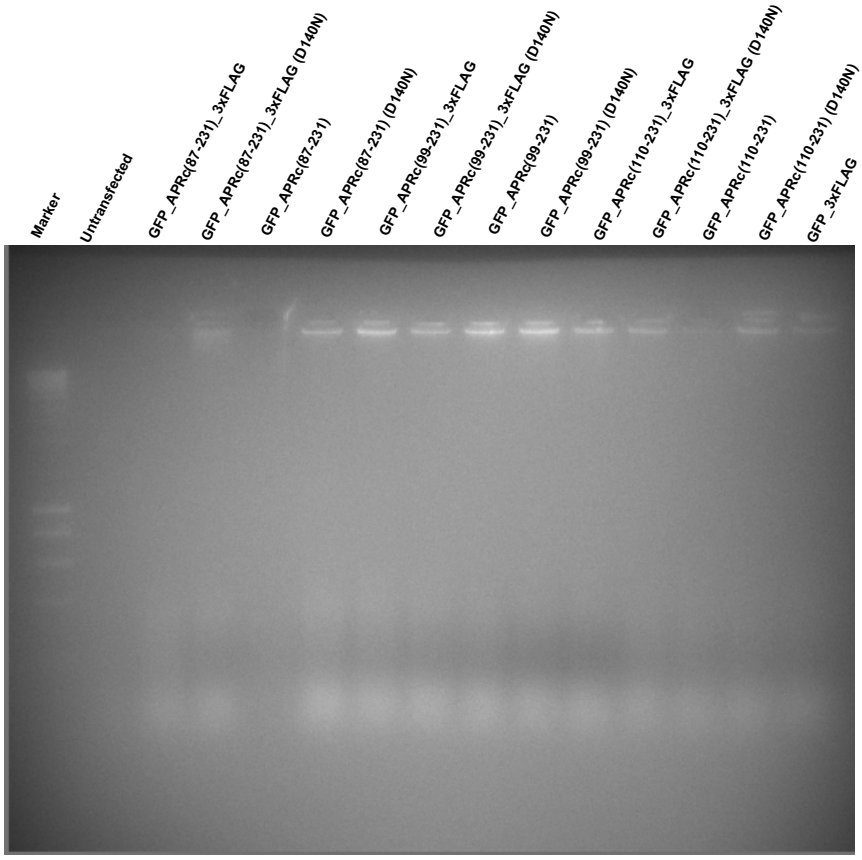


**Figure 28.** Analysis of DNA fragmentation on HEK293 cells transfected with various forms of GFP-APRc. HEK293 cells were transiently transfected with various constructs of APRc, represented on the top of the figure. At 48h post-transfection, cell lysates were prepared as described in section 2.2.12 and separated in an agarose gel.

### 3.5.3. Analysis of apoptosis-related proteins

During apoptosis, the cells exhibit other biochemical modifications, such as activation of proteolytic cascades, leading to the amplification of cell death signaling pathways. This proteolytic cascade is mainly coordinated by caspases that, when activated, can activate other caspases leading to cell death (Elmore, 2007). Caspase-3 is considered an executioner caspase, being cleaved and activated by other caspases (initiator caspases). This caspase catalyzes the cleavage of several cellular proteins, leading to some of the hallmarks of apoptosis, such as chromatin condensation and DNA fragmentation (Porter and Jänicke, 1999; Elmore, 2007). One of the cellular substrates of caspase-3 is PARP, a nuclear protein with an important role in DNA repair and stability. Cleavage of PARP, by executioner caspase-3, leads to its inactivation and generation of cleavage fragments, playing an important role in programmed cell death (Chaitanya et al., 2010).

The detection of activated caspases, or even its cleaved substrates, is one of the methodologies used to detect apoptosis. Thus, GFP_APRc$_{87-231}$_3xFLAG, GFP_APRc$_{99-231}$_3xFLAG, and the control construct (GFP_3xFLAG) were transiently transfected on HEK293 cells. At 48h post-transfection, total protein fractions were collected and evaluated by parallel Western blot analysis, using anti-caspase-3, anti-PARP, anti-cleaved PARP, and anti-APRc (to confirm APRc autoprocessing in these assays (**Supplementary Figure 7**)). However, no specific signal was detected for any of the apoptosis-related proteins (data not shown). To overcome this, we decided to concentrate the protein samples by using acetone precipitation, or by cell sorting through flow cytometry to analyze GFP-positive cells. However, none of these strategies were successful, as no signal was detected in Western blot analysis.

We next sought to use an immunofluorescence assay to detect cleaved caspase-3 and cleaved PARP as an alternative approach. HEK293 cells were transiently transfected with GFP_APRc$_{87-231}$_3xFLAG, GFP_APRc$_{87-231}$_3xFLAG (D140N), and the control GFP_3xFLAG. At 48h post-transfection, the cells were fixed and then stained with DAPI and with anti-cleaved caspase-3 (**Figure 29**) or anti-cleaved PARP antibodies (**Figure 30**).

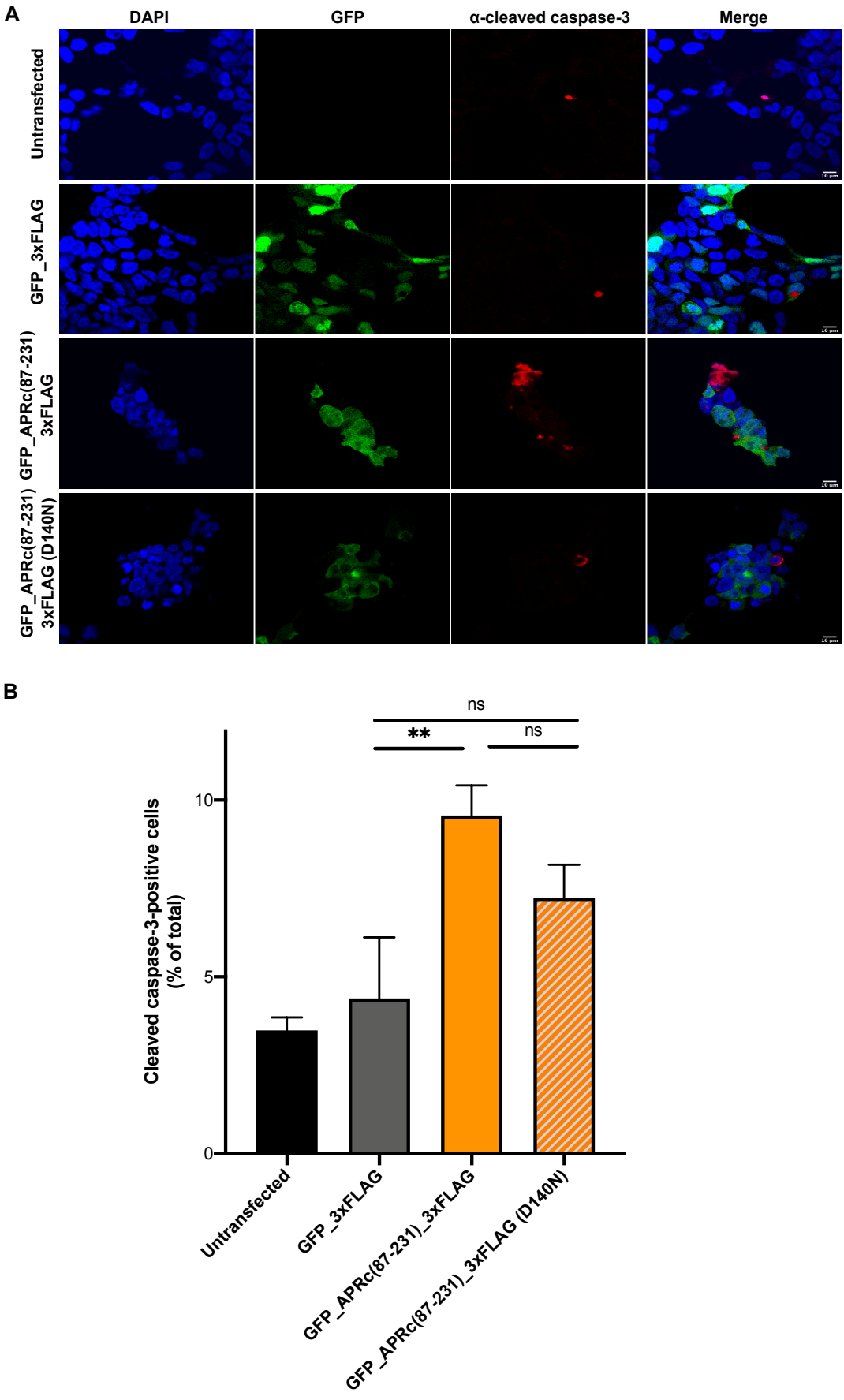
A
DAPI
GFP
α-cleaved caspase-3
Merge
Untransfected
GFP_3xFLAG
GFP_APRc(87-231) 3xFLAG
GFP_APRc(87-231) 3xFLAG (D140N)
B
ns
**
ns
Cleaved caspase-3-positive cells (% of total)
10
5
0
Untransfected
GFP_3xFLAG
GFP_APRc(87-231)_3xFLAG
GFP_APRc(87-231)_3xFLAG (D140N)

**Figure 29** (previous page)**.** Detection of cleaved caspase-3 on HEK293 cells transfected with different GFP_APRc-fusion constructs.
HEK293 cells were transiently transfected with GFP_APRc$_{87-231}$3XFLAG constructs (WT and mutant) and with the control GFP_3xFLAG. At 48h post-transfection, the cells were fixed, permeabilized, and stained for confocal microscopy analysis with DAPI (blue) and anti-cleaved caspase-3 (red). **A.** Immunofluorescence confocal microscopy images of HEK293 cells transfected with GFP_APRc-fusion constructs. Each row shows, from left to right, nuclei staining, GFP, α-cleaved caspase-3 staining, and the merged image. Scale bar = 10 µm. **B.** Quantification of cleaved caspase-3 positive cells. The levels of cleaved caspase-3 were increased in HEK293 cells transfected with the GFP_ APRc$_{87-231}$_3xFLAG, compared to control. Cells expressing GFP_ APRc$_{87-231}$_3xFLAG (D140N) did not show significant differences compared to WT, or the control. At least 300 nuclei were counted from each sample (n=3). Each value represents mean +/- SD. Kruskal-Wallis one-way ANOVA multiple-comparisons test was used to determine the significance between control constructs and APRc constructs. Mann-Whitney test was performed to determine the significance between WT and mutant constructs. **p<0.01; ns: non-significant.

As shown in **Figure 29**, cells expressing the construct GFP_APRc$_{87-231}$_3xFLAG displayed a significant increase in cleaved caspase-3-positive cells, compared to the control GFP_3xFLAG. Although not statistically different, there was a slight decrease in the percentage of cleaved caspase-3-positive cells in cells expressing the active site mutant. Compared with GFP_3xFLAG, the activity of APRc appears to significantly impact the proteolytic cleavage of caspase-3, which might explain the apoptotic-like phenotype observed in these cells.

Regarding the levels of cleaved PARP (**Figure 30**), there were no significant differences in the percentage of cleaved PARP-positive cells between the different tested conditions. However, the percentage of cleaved PARP-positive cells in the WT condition is slightly higher than in the mutant or control conditions. Additional assays are needed to validate this trend.

Together, the cleaved caspase-3 and cleaved PARP data provide additional evidence that the rickettsial retropepsin APRc might be indeed implicated in the induction of apoptosis in mammalian cells.

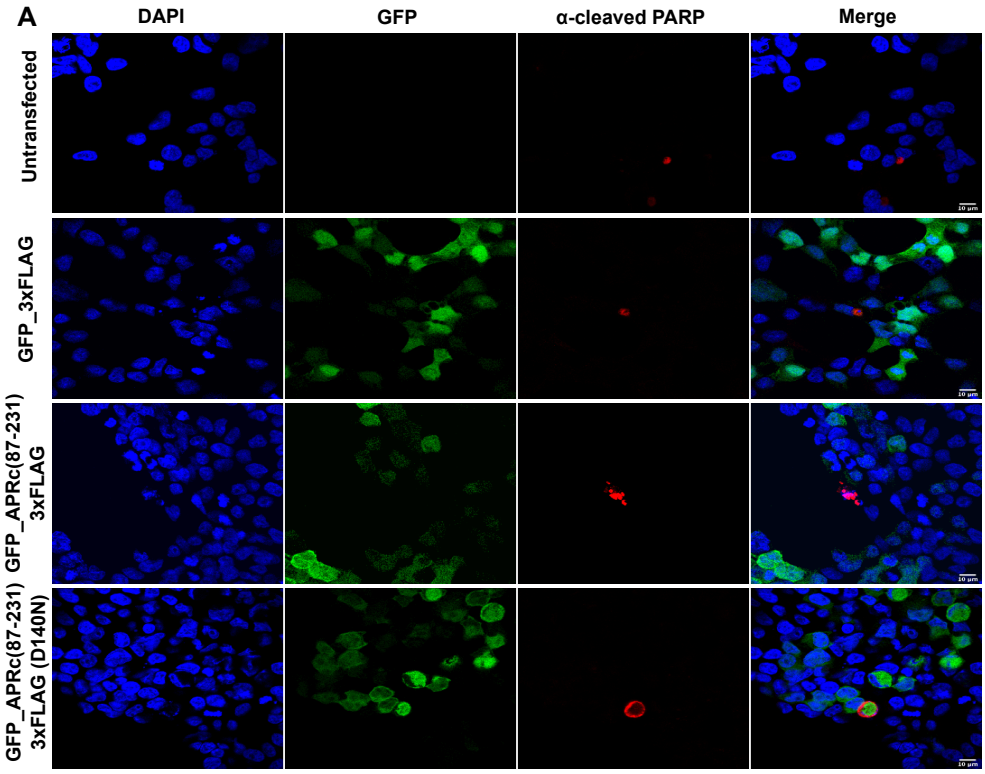
A
DAPI
GFP
α-cleaved PARP
Merge
Untransfected
GFP_3xFLAG
GFP_APRc(87-231) 3xFLAG
GFP_APRc(87-231) 3xFLAG (D140N)

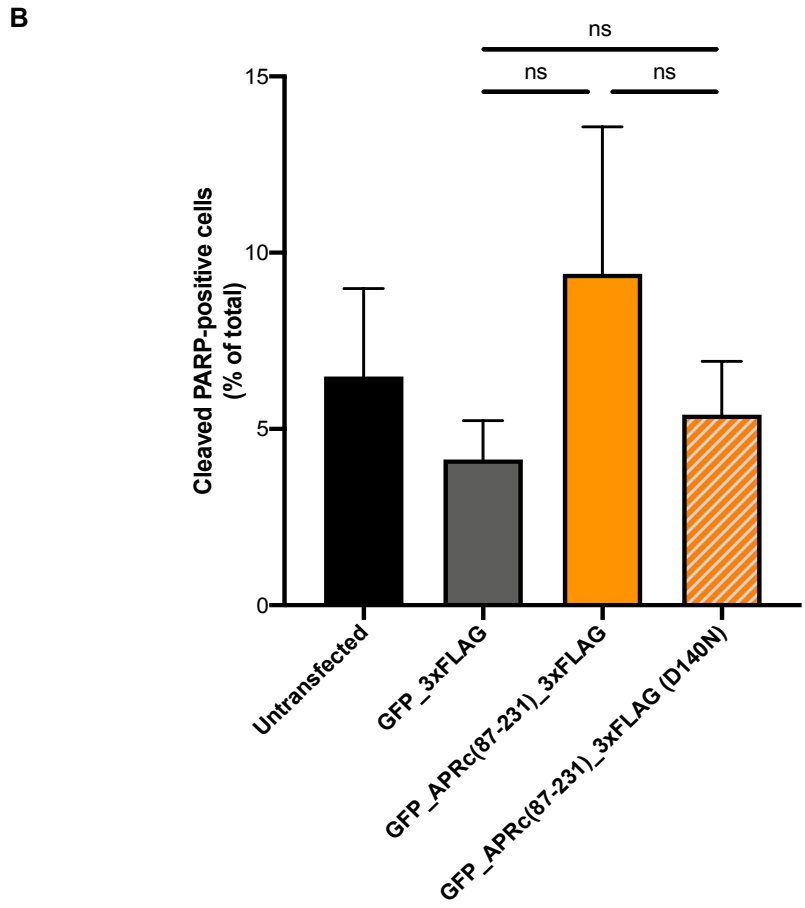
B
ns
ns
ns
Cleaved PARP-positive cells (% of total)
15
10
5
0
Untransfected
GFP_3xFLAG
GFP_APRc(87-231)_3xFLAG
GFP_APRc(87-231)_3xFLAG (D140N)

**Figure 30** (previous page)**.** Detection of cleaved PARP in HEK293 cells transfected with different GFP_APRc-fusion constructs.
HEK293 cells were transiently transfected with GFP_APRc$_{87-231}$3xFLAG constructs (WT and mutant) and with the control GFP_3xFLAG. At 48h post-transfection, cells were fixed, permeabilized, and stained for confocal microscopy analysis with DAPI (blue) and anti-cleaved PARP (red). **A.** Immunofluorescence confocal microscopy images of HEK293 cells transfected with GFP_APRc-fusion constructs. Each row shows, from left to right, nuclei staining, GFP, anti-cleaved PARP staining, and the merged image. Scale bar = 10 µm. **B.** Quantification of cleaved PARP-positive cells. The levels of cleaved-PARP in HEK293 cells were not significantly different between APRc constructs or the control. At least 300 nuclei were counted from each sample (n=3). Each value represents mean +/- SD. Kruskal-Wallis one-way ANOVA multiple-comparisons test was used to determine the significance between control constructs and APRc constructs. Mann-Whitney test was performed to determine the significance between WT and mutant constructs. ns: non-significant.

### 3.5.4. Annexin V-APC conjugate/DAPI detection with flow cytometry

To provide additional evidence that the expression of APRc induces apoptosis, changes at the cell surface were assessed by flow cytometry using annexin V and DAPI staining. Together with DAPI, annexin V binding allows determining if cells are viable, apoptotic or necrotic due to differences in the integrity and permeability of the plasma membrane. DAPI entry in cells depends on their permeability; live or early apoptotic cells have an intact membrane, and thus DAPI cannot stain these cells. On the other hand, membrane integrity is compromised in late apoptotic and necrotic cells, allowing the entry of the otherwise cell-impermeant fluorescent stain that binds to DNA. Therefore, DAPI staining is a good indicator of cell viability, separating live from dead cells. To assess if cells undergo apoptosis or another cell death process, a fluorescent conjugate of annexin V can be used. Annexin V is a protein with a high affinity for phosphatidylserine, a phospholipid that in healthy cells is located on the inner leaflet of the plasma membrane. However, during apoptosis, phosphatidylserine is translocated to the outer leaflet of the membrane, allowing the binding of the annexin conjugate (Elmore, 2007). The exposure of this phospholipid at the cell surface is a common feature of apoptotic cells, not observed in necrotic cells.

HEK293 cells were transiently transfected with GFP_APRc$_{87-231}$_3xFLAG, GFP_APRc$_{87-231}$_3xFLAG (D140N), and the control GFP_3xFLAG, and analyzed at 48h post-transfection. Moreover, to define the quadrants on the flow cytometry dot plots, annexin V-APC/DAPI double staining was also performed under control conditions: untransfected cells (negative control) and untransfected cells stimulated with hydrogen peroxide (positive control for cell death). For flow cytometry analysis, all GFP-positive cells (*GFP All*) were taken into account (**Supplementary Figure 8** and **Supplementary Table 1**). In cells expressing GFP_APRc$_{87-231}$_3xFLAG, both the WT and mutant forms, the level of early apoptosis (annexin V-APC$^+$/DAPI$^-$) was slightly higher than the control (GFP_3xFLAG) (**Figure 31**), although this difference was not statistically significant (**Figure 32)**. **Figure 31** illustrates two representative dot plots from cells expressing GFP_APRc$_{87-231}$_3xFLAG, since two assays were carried out on different days. These

results illustrate a similar trend towards an increased percentage of annexin V-APC$^{+}$/DAPI$^{-}$ in APRc-expressing cells compared to control. Moreover, we have also evaluated if this trend was maintained regardless of protein expression levels. As illustrated in **Supplementary Figure 8,** in the two additional quadrants (low GFP-expression, *GFP-Low*; and high GFP-expression, *GFP-High*) analyzed, an increased percentage of early apoptotic cells in APRc-expressing cells was always observed, compared to GFP_3xFLAG-expressing cells. Therefore, the presence of the protease itself (even without catalytic activity) might be sufficient to interfere with cellular processes that result in the translocation of phosphatidylserine to the external surface of the plasma membrane, providing additional evidence for the role of APRc in inducing programmed cell death.

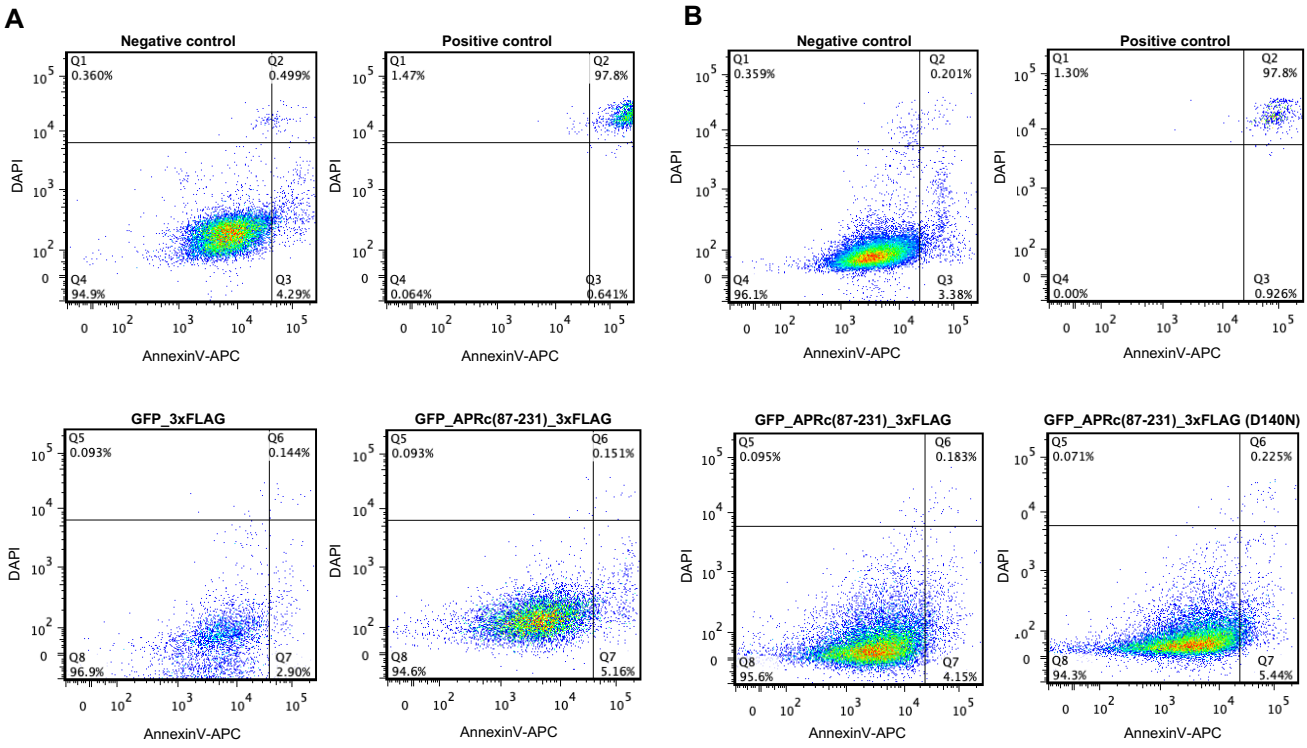


**Figure 31.** Detection of cell apoptosis in HEK293 cells by annexin V-APC/DAPI staining assay.
Cells were transiently transfected with different constructs (indicated on the top of each dot plot). At 48h post-transfection, HEK293 cells were stained with annexin V and DAPI, and analyzed by flow cytometry. According to the fluorescence intensity, live cells (annexin V$^{-}$/DAPI$^{-}$) can be discriminated from early apoptotic cells (annexin V$^{+}$/DAPI$^{-}$), late apoptotic cells (annexin V$^{+}$/DAPI$^{+}$) and necrotic cells (annexin V$^{-}$/DAPI$^{+}$). **A** and **B** represent results obtained from flow cytometry assays performed on different days, thus requiring duplicates of controls to be represented. Negative control corresponds to untransfected cells, while positive control corresponds to untransfected cells stimulated with hydrogen peroxide. 15,000-30,000 cells were analyzed by flow cytometry for each group condition and only GFP-positive cells were analyzed. APC, allophycocyanin.

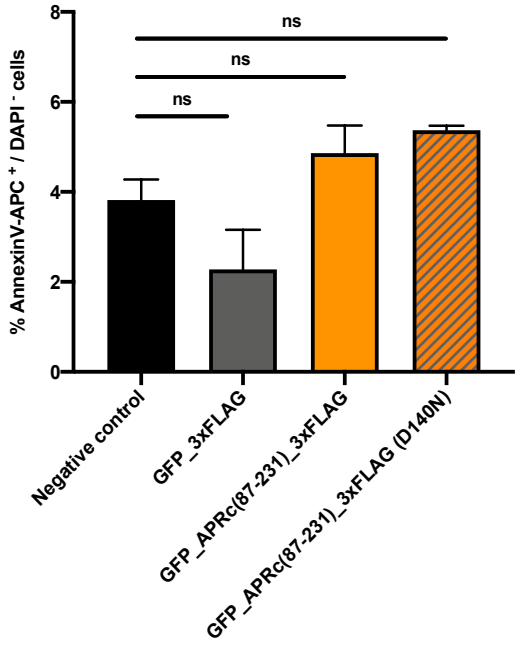


**Figure 32.** Quantitative analysis of early apoptosis in HEK293 cells.
Negative control corresponds to untransfected cells. Values of annexin $V^+$/$DAPI^-$ for each group are presented as mean +/- SD. Kruskal-Wallis one-way ANOVA multiple-comparisons test was used to determine the significance between groups. ns: non-significant.

HEK293 cells expressing GFP_APRc$_{99-231}$_3xFLAG were also analyzed in parallel. However, the percentage of cells annexin V-$APC^+$/$DAPI^-$ were similar to the control condition (GFP_3xFLAG) (data not shown). These results were unexpected, given the membrane blebbing and nuclear condensation phenotypes observed in the fluorescence microscopy analysis of cells expressing GFP_APRc$_{99-231}$_3xFLAG (**Figure 21**).

It is important to stress that these flow cytometry results are still preliminary, and there are several steps to be optimized. First, it would be important to evaluate other time points post-transfection or perform a time-course analysis. Apoptosis is a cell death process with time-sequential morphological and biochemical changes, ultimately leading to cell death. Not all the events occur simultaneously, and may even depend on a wide diversity of factors, such as cell line, stimulus intensity, or even exposure time (Sundquist et al., 2006). Thus, it would be important to perform a time-course study to ensure that the appropriate time point is not missed. Another strategy that could also be approached is using a suspension cell line (*e.g.*, Jurkat cell line). The detachment of adherent cells (*e.g.,* HEK293 cell line) is a critical step on the flow cytometry protocol. It can substantially interfere with cell membrane integrity and, consequently, with the results obtained by flow cytometry. By using cells in suspension, one could avoid the detachment step, thereby ensuring that the impact on membrane integrity is solely due to the expression of the target construct. One of the cytomorphological changes that occur at a late stage of apoptosis is the formation of apoptotic bodies. It is possible that

at 48h post-transfection, these apoptotic bodies were already released to the supernatant, being discarded when the cell medium was removed. Therefore, it will be interesting to analyze the supernatant of cell cultures in parallel, to determine if some of these released apoptotic bodies can be more effectively detected.

During the analysis of flow cytometry results, we faced another issue related to a signal spillover from GFP into the DAPI fluorescence channel, introducing bias in the data related to the intensity of DAPI in the analyzed samples. To correct this spillover, we performed fluorescence compensation, ensuring that the fluorescence detected by a specific detector derives from the measured fluorochrome. However, GFP's intensity was very high and, even with compensation, it was not possible to completely correct the spillover (particularly in control samples expressing GFP_3xFLAG). Therefore, one possible solution to overcome this problem would be to perform these assays with APRc constructs without GFP and compare it to untransfected cells.

# Chapter IV

# 4. Discussion and Future Perspectives

In recent years, many new rickettsial species associated with human diseases continue to be identified, supporting the evidence that rickettsial infections are globally emerging (European Centre for Disease Prevention and Control (ECDC), 2013). The knowledge about the mechanisms of pathogenicity in *Rickettsia* has significantly increased in the past years. However, it has not yet been developed a reliable protective vaccine or specific treatment against rickettsioses, reinforcing the importance of identifying new protein factors as targets to develop novel therapeutics.

Previous work in our laboratory has focused on the identification and characterization of a novel aspartic protease highly conserved in *Rickettsia*, named APRc. This enzyme shares several properties with retropepsin-like proteases, and might be a modulator of rickettsial surface virulence factors due to its ability to catalyze the processing of two autotransporter adhesin/invasion proteins, Sca5/OmpB and Sca0/OmpA (Cruz et al., 2014). In addition to cleaving rickettsial proteins, APRc might also play a role in other stages of the rickettsial infectious process. There is growing evidence that proteins with moonlighting activity are involved in bacterial pathogenicity (Henderson and Martin, 2011). Thus, we hypothesize that APRc could be a multifunctional protein in the rickettsial infection progression, as described in section 1.2.2.

Until now, the rickettsial retropepsin APRc was studied *in vitro* and in *E. coli*, with evidence of autoactivation and release of a mature active form (Cruz et al., 2014). Since *Rickettsia* are obligate intracellular bacteria that infect eukaryotic cells, it is relevant to extend these studies to mammalian cells to further understand the molecular and cellular mechanisms of APRc's autoactivation and activity in this context.

In this work, we provide evidence that different forms of the soluble domain of APRc undergo autoactivation within HEK293 cells and that this activation is dependent on the catalytic aspartate residue. This is in line with what has already been described in *E. coli* (Cruz et al., 2014). This autoprocessing activity in mammalian cells was either visualized by the presence of an activation product (for the entire soluble domain $APRc_{87-231}$), or by differences in the accumulation patterns between the WT and mutant forms of the shorter GFP_APRc fusion proteins ($APRc_{99-231}$ and $APRc_{110-231}$).

When the autoprocessing activity was analyzed *in vitro*, APRc underwent a multi-step activation, with an enrichment over time in different intermediate forms, culminating in the accumulation of the final activated product after 48 hours (**Figure 6**) (Cruz et al.,

2014). Interestingly, when the same soluble catalytic domain ($APRc_{87-231}$) is expressed in mammalian cells or *E. coli*, it is only observed the presence of the activation product, without the detection of intermediate forms (**Figure 15**) (Cruz et al., 2014). These results suggest that the protease autoprocessing may occur faster *in vivo* than *in vitro*. Moreover, it is important to stress that the activation product of APRc was detected in *E. coli* 3h after induction (Cruz et al., 2014), while in mammalian cells it was only observed at 48h post-transfection (**Figure 15B**). This may be explained by differences in the cellular complexity between these two cell types (*E. coli vs.* mammalian cells), or it may be due to an allosteric regulation of the protease autoprocessing, dependent on the cell type.

When comparing the different truncated forms of APRc, our results suggest that the autoprocessing of the longer form ($APRc_{87-231}$) is slower when compared with the shorter constructs ($APRc_{99-231}$ and $APRc_{110-231}$), for which no processing products were observed. Evidence from *E. coli* anticipates that the extension of the N-terminal region of the soluble domain of APRc may indeed impact autoprocessing activity (unpublished data). Combined with our results, this suggests that the N-terminal region of the soluble domain of APRc might represent a proregion/inhibitory sequence that regulates protease activation and exerts its role independently of the cellular context. Although further studies are required to corroborate this hypothesis, evidence for a similar mechanism in HIV-1 protease has been proposed (Partin et al., 1991; Huang and Chen, 2013). Indeed, the autoprocessing of HIV-1 protease was shown to progress faster upon deleting the transframe polypeptide, a region with 68 amino acids flanking the protease domain at its N-terminal (Partin et al., 1991).

HIV-1 protease is also able to undergo autoprocessing both in *E. coli* and mammalian cells. When expressed in *E. coli*, the mature form of the protease was detected in whole-cell lysates (Louis et al., 1999; Huang and Chen, 2010, 2013). In contrast, in mammalian cells, neither its precursor nor the cleavage products were detected. The activation and proteolytic activity of the protease is so exuberant that the precursor is only observed when inhibitors are used, suggesting that, as a result of its activity, HIV-1 protease completely self-degrades when expressed in this cell type (Lindsten et al., 2001; Huang and Chen, 2010). These observations on HIV-1 protease might help explain why there was no detection of cleavage products when the shorter constructs of APRc were expressed in mammalian cells. For these constructs, the activation and autolysis appear to occur faster, thereby hampering the detection of activation products by Western blotting. Although both proteases self-degrade due to proteolytic activity, there is a clear difference in the processing rate. When expressed in

mammalian cells, the activation and autolysis of APRc are only partial, suggesting that its processing in these cells is slower compared with that of HIV-1 protease.

Moreover, for some constructs of APRc, the presence of the C-terminal TwinStrep tag seems to somehow impact the conformation/activation of the protease. The expression of the construct GFP_APRc$_{87-231}$_TwinStrep did not result in the detection of the processing product (**Figure 15**), and a milder phenotype was observed upon expression of GFP_APRc$_{99-231}$_TwinStrep when compared with the untagged or 3xFLAG-tagged constructs (**Figure 21**). Distinctive observations were found when fluorescent proteins (YFP/CFP) were fused at the C-terminal of the HIV-1 protease. The tagged protease was active, both enzymatically and virologically, suggesting that the C-terminal extension has a low impact on HIV-1 protease activity (Koh et al., 2007). In contrast, our results indicate that for APRc the nature of the C-terminal tag may significantly impact activity and must be evaluated case by case.

To further understand the mechanism and dynamic of APRc autoprocessing activity, future experiments may include the use of inhibitors to validate if the intermediate forms of APRc are observed under these conditions. Moreover, the assessment of critical residues to APRc autoprocessing activity should also be performed. By mutating the already identified cleavage sites of APRc (Cruz et al., 2014) (**Figure 4**), we would be able to confirm if the N-terminal processing is indeed sequence-dependent, as already observed in *E. coli* (unpublished data).

Interestingly, APRc activation (at 48h post-transfection) was concomitant with an evident impact on cell morphology. The cells expressing the different GFP_APRc-fusion WT constructs exhibited dramatic morphological alterations, such as membrane blebbing, nuclear condensation, and the presence of fragmented cellular material, suggesting induction of a cell death process (**Figures 17, 18, 21** and **24**). These results anticipate that autoprocessing is a critical step for rendering APRc in an active form, available to cleave mammalian substrates, and likely promoting cell death with features resembling those of apoptosis. In order to provide more evidence that the expression of APRc induces apoptosis, additional assays were performed. Although no apparent DNA fragmentation was observed, the expression of APRc contributed significantly to nuclear condensation and alterations of nuclear shape and size (**Figures 26** and **27**). Moreover, a significant increase in cleaved caspase-3-positive cells upon expression of the WT version of GFP_APRc-fusion construct was observed, and the percentage of cleaved PARP-positive cells in the WT condition was also slightly higher (although not statistically significant) (**Figures 29** and **30**); however, additional assays are needed to confirm this trend. We also demonstrated that the expression of APRc contributed to an increase in the percentage of annexin V-APC$^{+}$/DAPI$^{-}$ cells (**Figures 31** and **32**). These data suggest

that APRc may be implicated in specific cellular processes that result in alterations in plasma membrane composition, providing additional evidence for the possibility of APRc inducing apoptosis in expressing cells. Altogether, and although additional assays are needed to confirm this cell death phenotype, these data support the hypothesis that APRc may be a potential trigger of apoptosis in HEK293 cells.

There is again some parallel between our observations and what has been described for HIV-1 protease. As detailed in section 1.2.1.2, HIV-1 protease expression also induces a mechanism of cell death. Some of the morphological changes detected in mammalian cells expressing this retroviral protease are hallmarks of apoptosis, such as nuclear condensation, DNA fragmentation, and PARP cleavage (Nie et al., 2002; Rumlová et al., 2014). HIV-1 infection leads to cell death of a specific type of cells, $CD4^+$ T cells, which are involved in the immune response against infections (Okoye and Picker, 2013; Vidya Vijayan et al., 2017). The depletion of infected $CD4^+$ T cells may be associated with the activation/activity of the HIV-1 protease since several studies indicate that HIV-1 protease induces cell death through several pathways (Baum et al., 1990; Strack et al., 1996; Blanco et al., 2003; Rumlová et al., 2014; Benko et al., 2016). Apoptosis is known to be dynamically regulated during rickettsial infection, as shown by Curto and colleagues when infected macrophages were analyzed (Curto et al., 2019b). This evidence raises the exciting possibility that, as shown for HIV-1 protease, APRc might also be involved in modulating cell death processes during rickettsial infection by targeting specific host proteins.

The catalytic activity of APRc appears to be determinant for most of the observed morphological changes. Nonetheless, the expression of the mutant forms not necessarily reverted the phenotype to levels observed in cells expressing GFP only, suggesting that other protein-protein interactions established by APRc might also contribute to the observed phenotype. Curiously, the cells transfected with the mutant forms of some of the GFP_APRc fusion constructs displayed a speckled-like pattern of GFP (**Figures 16-18, 20, 21** and **24**). A similar phenotype was previously observed in HIV-1 protease-expressing cells and correlated with the co-localization of the protease with a mitochondrial marker and detection in the mitochondrial fraction (Rumlová et al., 2014). We sought to investigate if APRc could also have a similar localization in HEK293 cells. However, our results suggest that the pattern observed on APRc-expressing cells does not correspond to a mitochondrial localization. Therefore, additional experiments are required to further assess if this speckled-like pattern corresponds indeed to a specific intracellular localization of APRc.

Supported by our observations, it will be important to understand in more detail this novel function of APRc as a trigger of cell death. One of the potential approaches could

be to perform an AP-SWATH analysis to identify APRc interactors in host cells. Another experiment that could also be further pursued is the quantitative proteomic profiling of cells transfected with the WT and corresponding mutant of APRc to evaluate differences in proteomic signatures in response to the transient expression of APRc. Both strategies would provide complementary data that would connect the protease to biological pathways, revealing if/how the protease can be modulated, and even unveiling targeted proteins/complexes as possible therapeutic targets. Moreover, and since endothelial cells and macrophages have great importance during rickettsial infection (Chan et al., 2010; Curto et al., 2016), it will be critical to assess if this cell death phenotype induced by APRc is also detected in these cell types.

With this work, we provide evidence for a potentially novel function of APRc as a modulator of cell death processes, raising exciting questions on the role of this highly conserved protease as a virulence factor in rickettsial infections.

# Chapter V

## 5. Bibliography

Adams, L. D.; Tomasselli, A. G.; Robbins, P.; Moss, B.; Heinrikson, R. HIV-1 Protease Cleaves Actin During Acute Infection of Human T-Lymphocytes. *AIDS Res. Hum. Retroviruses* **1992**, *8* (2), 291–295.

Aistleitner, K.; Clark, T.; Dooley, C.; Hackstadt, T. Selective Fragmentation of the *trans* -Golgi Apparatus by *Rickettsia rickettsii*. *PLoS Pathog.* **2020**, *16* (5), e1008582.

Alix, E.; Chesnel, L.; Bowzard, B. J.; Tucker, A. M.; Delprato, A.; Cherfils, J.; Wood, D. O.; Kahn, R. A.; Roy, C. R. The Capping Domain in RalF Regulates Effector Functions. *PLoS Pathog.* **2012**, *8* (11), e1003012.

Álvarez-Hernández, G.; Roldán, J.; Milan, N.; Lash, R.; Behravesh, C.; Paddock, C. Rocky Mountain Spotted Fever in Mexico: Past, Present, and Future. *Lancet Infect. Dis.* **2017**, *17* (6), e189–e196.

Álvarez, E.; Castelló, A.; Menéndez-Arias, L.; Carrasco, L. HIV Protease Cleaves Poly(A)-Binding Protein. *Biochem. J.* **2006**, *396* (2), 219–226.

Andersson, S. G. E.; Zomorodipour, A.; Andersson, J. O.; Sicheritz-Pontén, T.; Alsmark, U. C. M.; Podowski, R. M.; Näslund, A. K.; Eriksson, A.-S.; Winkler, H. H.; Kurland, C. G. The Genome Sequence of *Rickettsia prowazekii* and The Origin of Mitochondria. *Nature* **1998**, *396*, 133–140.

Ashida, H.; Mimuro, H.; Ogawa, M.; Kobayashi, T.; Sanada, T.; Kim, M.; Sasakawa, C. Cell Death and Infection: A Double-Edged Sword for Host and Pathogen Survival. *J. Cell Biol.* **2011**, *195* (6), 931–942.

Atkin-Smith, G. K.; Poon, I. K. H. Disassembly of the Dying: Mechanisms and Functions. *Trends Cell Biol.* **2017**, *27* (2), 151–162.

Azad, A. F. Pathogenic Rickettsiae as Bioterrorism Agents. *Clin. Infect. Dis.* **2007**, *45* (Supplement_1), S52–S55.

Azad, A. F.; Beard, C. B. Rickettsial Pathogens and Their Arthropod Vectors. *Emerg. Infect. Dis.* **1998**, *4* (2), 179–186.

Banga, S.; Gao, P.; Shen, X.; Fiscus, V.; Zong, W.-X.; Chen, L.; Luo, Z.-Q. *Legionella pneumophila* Inhibits Macrophage Apoptosis by Targeting Pro-Death Members of The Bcl2 Protein Family. *Proc. Natl. Acad. Sci.* **2007**, *104* (12), 5121–5126.

Baron, S. Bacterial Pathogenesis. In *Medical Microbiology*; University of Texas Medical Branch at Galveston: Galveston (TX), 1996.

Baum, E. Z.; Bebernitz, G. A.; Gluzman, Y. Isolation of Mutants of Human Immunodeficiency Virus Protease Based on the Toxicity of the Enzyme in *Escherichia coli*. *Proc. Natl. Acad. Sci.* **1990**, *87* (14), 5573–5577.

Bechah, Y.; Capo, C.; Mege, J.; Raoult, D. Epidemic Typhus. *Lancet Infect. Dis.* **2008**, *8* (7), 417–426.

Bechelli, J.; Smalley, C.; Milhano, N.; Walker, D. H.; Fang, R. *Rickettsia massiliae* and *Rickettsia conorii* Israeli Spotted Fever Strain Differentially Regulate Endothelial Cell Responses. *PLoS One* **2015**, *10* (9), 1–15.

Benko, Z.; Elder, R. T.; Li, G.; Liang, D.; Zhao, R. Y. HIV-1 Protease in the Fission Yeast *Schizosaccharomyces pombe*. *PLoS One* **2016**, *11* (3), 1–22.

Bielaszewska, M.; Rüter, C.; Kunsmann, L.; Greune, L.; Bauwens, A.; Zhang, W.; Kuczius, T.; Kim, K. S.; Mellmann, A.; Schmidt, M. A.; et al. Enterohemorrhagic *Escherichia coli* Hemolysin Employs Outer Membrane Vesicles to Target Mitochondria and Cause Endothelial and Epithelial Apoptosis. *PLoS Pathog.* **2013**, *9* (12), e1003797.

Blanco, R.; Carrasco, L.; Ventoso, I. Cell Killing by HIV-1 Protease. *J. Biol. Chem.* **2003**, *278* (10), 1086–1093.

Blanton, L. S. The Rickettsioses. A Pratical Update. *Infect. Dis. Clin. North Am.* **2019**, *33*, 213–229.

Blasche, S.; Mörtl, M.; Steuber, H.; Siszler, G.; Nisa, S.; Schwarz, F.; Lavrik, I.; Gronewold, T. M. A.; Maskos, K.; Donnenberg, M. S.; et al. The *E. coli* Effector Protein NleF Is a Caspase Inhibitor. *PLoS One* **2013**, *8* (3), e58937.

Brik, A.; Wong, C.-H. HIV-1 Protease: Mechanism and Drug Discovery. *Org. Biomol. Chem.* **2003**, *1* (1), 5–14.

Brodsky, I. E.; Palm, N. W.; Sadanand, S.; Ryndak, M. B.; Sutterwala, F. S.; Flavell, R. A.; Bliska, J. B.; Medzhitov, R. A *Yersinia* Secreted Effector Protein Promotes Virulence by Preventing Inflammasome Recognition of The Type III Secretion System. *Cell Host Microbe* **2010**, *7* (5), 376–387.

Cardwell, M. M.; Martinez, J. J. The Sca2 Autotransporter Protein from *Rickettsia conorii* Is Sufficient To Mediate Adherence to and Invasion of Cultured Mammalian Cells. *Infect. Immun.* **2009**, *77* (12), 5272–5280.

Centers for Disease Control and Prevention (CDC). *Rickettsia parkeri* Rickettsiosis. https://www.cdc.gov/ticks/tickbornediseases/rickettsiosis.html (accessed May 2, 2020).

Centers for Disease Control and Prevention (CDC). Epidemiology and Statistics. Rocky Mountain Spotted Fever (RMSF). https://www.cdc.gov/rmsf/stats/index.html (accessed May 2, 2020).

Chaitanya, G. V.; Alexander, J. S.; Babu, P. P. PARP-1 Cleavage Fragments: Signatures of Cell-Death Proteases in Neurodegeneration. *Cell Commun. Signal.* **2010**, *8*, 31.

Chan, Y.; Cardwell, M. M.; Hermanas, T. M.; Uchlyama, T.; Martinez, J. J.

Rickettsial Outer-Membrane Protein B (rOmpB) Mediates Bacterial Invasion through Ku70 in an Actin, c-Cbl, Clathrin and Caveolin 2-Dependent Manner. *Cell. Microbiolgy* **2009**, *11* (4), 629–644.

Chan, Y. G.-Y.; Riley, S. P.; Martinez, J. J. Adherence to and Invasion of Host Cells by Spotted Fever Group *Rickettsia* Species. *Front. Microbiol.* **2010**, *1*, 139.

Chapman, A. S.; Bakken, J. S.; Folk, S. M.; Paddock, C. D.; Bloch, K. C.; Krusell, A.; Sexton, D. J.; Buckingham, S. C.; Marshall, G. S.; Storch, G. A.; et al. Diagnosis and Management of Tickborne Rickettsial Diseases: Rocky Mountain Spotted Fever, Ehrlichioses, and Anaplasmosis--United States: A Practical Guide for Physicians and Other Health-Care and Bublic Health Professionals. *MMWR Recomm. Reports* **2006**, *55* (RR-4), 1–27.

Chatterjee, A.; Mridula, P.; Mishra, R. K.; Mittal, R.; Hosur, R. V. Folding Regulates Autoprocessing of HIV-1 Protease Precursor. *J. Biol. Chem.* **2005**, *280* (12), . 11369 – 11378.

Cherry, E.; Liang, C.; Rong, L.; Quan, Y.; Inouye, P.; Li, X.; Morin, N.; Kotler, M.; Wainberg, M. A. Characterization of Human Immunodeficiency Virus Type-1 (HIV-1) Particles That Express Protease-Reverse Transcriptase Fusion Proteins. *J. Mol. Biol.* **1998**, *284*, 43–56.

Clifton, D. R.; Goss, R. A.; Sahni, S. K.; Van Antwerp, D.; Baggs, R. B.; Marder, V. J.; Silverman, D. J.; Sporn, L. A. NF-κB-Dependent Inhibition of Apoptosis Is Essential for Host Cell Survival during *Rickettsia rickettsii* Infection. *Proc. Natl. Acad. Sci. U. S. A.* **1998**, *95* (8), 4646–4651.

Clifton, D. R.; Rydkina, E.; Freeman, R. S.; Sahni, S. K. NF-κB Activation during *Rickettsia rickettsii* Infection of Endothelial Cells Involves the Activation of Catalytic IκB Kinases IKKα and IKKβ and Phosphorylation-Proteolysis of the Inhibitor Protein IκBα. *Infect. Immun.* **2005**, *73* (1), 155–165.

Cruz, R.; Huesgen, P.; Riley, S. P.; Wlodawer, A.; Faro, C.; Overall, C. M.; Martinez, J. J.; Simões, I. RC1339/APRc from *Rickettsia conorii* Is a Novel Aspartic Protease with Properties of Retropepsin-Like Enzymes. *PLoS Pathog.* **2014**, *10* (8), e1004324.

Curto, P.; Simões, I.; Riley, S. P.; Martinez, J. J. Differences in Intracellular Fate of Two Spotted Fever Group *Rickettsia* in Macrophage-Like Cells. *Front. Cell. Infect. Microbiol.* **2016**, *6*, 80.

Curto, P.; Santa, C.; Allen, P.; Manadas, B.; Simões, I.; Martinez, J. J. A Pathogen and a Non-Pathogen Spotted Fever Group *Rickettsia* Trigger Differential Proteome Signatures in Macrophages. *Front. Cell. Infect. Microbiol.* **2019a**, *9* (43), 1–26.

Curto, P.; Riley, S. P.; Simões, I.; Martinez, J. J. Macrophages Infected by a

Pathogen and a Non-Pathogen Spotted Fever Group *Rickettsia* Reveal Differential Reprogramming Signatures Early in Infection. *Front. Cell. Infect. Microbiol.* **2019b**, *9* (97).

D'Arcy, M. S. Cell Death: A Review of The Major Forms of Apoptosis, Necrosis and Autophagy. *Cell Biol. Int.* **2019**, *43* (6), 582–592.

Darke, P. L.; Leu, C.-T.; J.Davis, L.; Heimbac, J. C.; Diehl, R. E.; Hill, W. S.; Dixon, R. A. F.; Sigal, I. S. Human Immunodeficiency Virus Protease. Bacterial Expression and Characterization of the Purified Aspartic Protease. *J. Biol. Chem.* **1989**, *264* (4), 2307–2312.

Dewoody, R.; Merritt, P. M.; Houppert, A. S.; Marketon, M. M. YopK Regulates The *Yersinia pestis* Type III Secretion System From Within Host Cells. *Mol. Microbiol.* **2011**, *79* (6), 1445–1461.

Dieme, C.; Bechah, Y.; Socolovschi, C.; Audoly, G.; Berenger, J. M.; Faye, O.; Raoult, D.; Parola, P. Transmission Potential of *Rickettsia felis* Infection by *Anopheles gambiae* Mosquitoes. *Proc. Natl. Acad. Sci. U. S. A.* **2015**, *112* (26), 8088–8093.

Dong, F.; Pirbhai, M.; Xiao, Y.; Zhong, Y.; Wu, Y.; Zhong, G. Degradation of the Proapoptotic Proteins Bik, Puma, and Bim with Bcl-2 Domain 3 Homology in *Chlamydia trachomatis*-Infected Cells. *Infect. Immun.* **2005**, *73* (3), 1861–1864.

Dortet, L.; Mostowy, S.; Louaka, A. S.; Gouin, E.; Nahori, M.-A.; Wiemer, E. A. C.; Dussurget, O.; Cossar, P. Recruitment of the Major Vault Protein by InlK: A *Listeria monocytogenes* Strategy to Avoid Autophagy. *PLoS Pathog.* **2011**, *7* (8), e1002168.

Drane, P.; Bravard, A.; Bouvard, V.; May, E. Reciprocal Down-Regulation of *p53* and *SOD2* Gene Expression-Implication in p53 Mediated Apoptosis. *Oncogene* **2001**, *20* (4), 430–439.

Dunn, B. M.; Goodenow, M. M.; Gustchina, A.; Wlodawer, A. Retroviral Proteases. *Genome Biol.* **2002**, *3* (4).

Elmore, S. Apoptosis: A Review of Programmed Cell Death. *Toxicol. Pathol.* **2007**, *35* (4), 495–516.

Engström, P.; Burke, T. P.; Mitchell, G.; Ingabire, N.; Mark, K. G.; Golovkine, G.; Iavarone, A. T.; Rape, M.; Cox, J. S.; Welch, M. D. Evasion of Autophagy Mediated by *Rickettsia* Surface Protein OmpB Is Critical for Virulence. *Nat. Microbiol.* **2019**, *4* (12), 2538–2551.

European Centre for Disease Prevention and Control (ECDC). *Epidemiological Situation of Rickettsioses in EU/EFTA Countries*; **2013**.

Fang, R.; Ismail, N.; Soong, L.; Popov, V. L.; Whitworth, T.; Bouyer, D. H.; Walker, D. H. Differential Interaction of Dendritic Cells with *Rickettsia conorii*: Impact on Host Susceptibility to Murine Spotted Fever Rickettsiosis. *Infect. Immun.* **2007**, *75* (6), 3112–

3123.

Ferreira, B. R.; Silva, J. S. Successive Tick Infestations Selectively Promote a T-Helper 2 Cytokine Profile in Mice. *Immunology* **1999**, *96* (3), 434–439.

Fields, K. A.; Heinzen, R. A.; Carabeo, R. The Obligate Intracellular Lifestyle. *Front. Microbiol.* **2011**, *2*.

Finlay, B. B.; McFadden, G. Anti-Immunology: Evasion of the Host Immune System by Bacterial and Viral Pathogens. *Cell* **2006**, *124* (4), 767–782.

Fish, A. I.; Riley, S. P.; Singh, B.; Riesbeck, K.; Martinez, J. J. The *Rickettsia conorii* Adr1 Interacts with the C-Terminus of Human Vitronectin in a Salt-Sensitive Manner. *Front. Cell. Infect. Microbiol.* **2017**, *7*, 61.

Garza, D. A.; Riley, S. P.; Martinez, J. J. Expression of *Rickettsia* Adr2 Protein in *E. coli* Is Sufficient to Promote Resistance to Complement-Mediated Killing, but Not Adherence to Mammalian Cells. *PLoS One* **2017**, *12* (6), 1–15.

Ge, J.; Xu, H.; Li, T.; Zhou, Y.; Zhang, Z.; Li, S.; Liu, L.; Shao, F. A *Legionella* Type IV Effector Activates The NF-KappaB Pathway by Phosphorylating The IkappaB Family of Inhibitors. *Proc. Natl. Acad. Sci. U. S. A.* **2009**, *106* (33), 13725–13730.

George, F.; Brouqui, P.; Boffa, M. C.; Mutin, M.; Drancourt, M.; Brisson, C.; Raoult, D.; Sampol, J. Demonstration of *Rickettsia conorii*-Induced Endothelial Injury *in vivo* by Measuring Circulating Endothelial Cells, Thrombomodulin, and von Willebrand Factor in Patients with Mediterranean Spotted Fever. *Blood* **1993**, *82* (7), 2109–2116.

Gillespie, J. J.; Ammerman, N. C.; Dreher-Lesnick, S. M.; Rahman, M. S.; Worley, M. J.; Setúbal, J. C.; Sobral, B. S.; Azad, A. F. An Anomalous Type IV Secretion System in *Rickettsia* Is Evolutionarily Conserved. *PLoS One* **2009a**, *4* (3), e4833.

Gillespie, J. J.; Ammerman, N. C.; Beier-Sexton, M.; Sobral, B. S.; Azad, A. F. Louse- and Flea-Borne Rickettsioses: Biological and Genomic Analyses. *Vet. Res.* **2009b**, *40* (2), 12.

Gong, B.; Shelite, T.; Mei, F. C.; Ha, T.; Hu, Y.; Xu, G.; Chang, Q.; Wakamiya, M.; Ksiazek, T. G.; Boor, P. J.; et al. Exchange Protein Directly Activated by cAMP Plays a Critical Role in Bacterial Invasion During Fatal Rickettsioses. *Proc. Natl. Acad. Sci. U. S. A.* **2013**, *110* (48), 19615–19620.

Goodall, K. J.; Finch-Edmondson, M. L.; Vuuren, J. van; Yeoh, G. C.; Gentle, I. E.; Vince, J. E.; Ekert, P. G.; Vaux, D. L.; Callus, B. A. Cycloheximide Can Induce Bax/Bak Dependent Myeloid Cell Death Independently of Multiple BH3-Only Proteins. *PLoS One* **2016**, *11* (11), e0164003

Guerrero, S.; Batisse, J.; Libre, C.; Bernacchi, S.; Marquet, R.; Paillart, J.-C. HIV-1 Replication and the Cellular Eukaryotic Translation Apparatus. *Viruses* **2015**, *7* (1), 199–218.

Guillotte, M. L.; Gillespie, J. J.; Chandler, C. E.; Rahman, M. S.; Ernst, R. K.; Azad, A. F. *Rickettsia* Lipid A Biosynthesis Utilizes the Late Acyltransferase LpxJ for Secondary Fatty Acid Addition. *J. Bacteriol.* **2018**, *200* (19), e00334-18.

Hackstadt, T. The Biology of Rickettsiae. *Infect. Agents Dis.* **1996**, *5* (3), 127–143.

Haglund, C. M.; Choe, J. E.; Skau, C. T.; Kovar, D. R.; Welch, M. D. *Rickettsia* Sca2 Is a Bacterial Formin-like Mediator of Actin-Based Motility. *Nat. Cell Biol.* **2010**, *12* (11), 1057–1063.

He, X.; Zhang, W.; Chang, Q.; Su, Z.; Gong, D.; Zhou, Y.; Xiao, J.; Drelich, A.; Liu, Y.; Popov, V.; et al. A New Role for Host Annexin A2 in Establishing Bacterial Adhesion to Vascular Endothelial Cells: Lines of Evidence from Atomic Force Microscopy and an *in vivo* Study. *Lab. Investig.* **2019**, *99* (11), 1650–1660.

Henderson, B.; Martin, A. Bacterial Virulence in the Moonlight: Multitasking Bacterial Moonlighting Proteins Are Virulence Determinants in Infectious Disease. *Infect. Immun.* **2011**, *79* (9), 3476–3491.

Hillman, R. D.; Baktash, Y. M.; Martinez, J. J. OmpA-Mediated Rickettsial Adherence to and Invasion of Human Endothelial Cells Is Dependent Upon Interaction with A2β1 Integrin. *Cell. Microbiolgy* **2013**, *15* (5), 727–741.

Huang, L.; Chen, C. Autoprocessing of Human Immunodeficiency Virus Type 1 Protease Miniprecursor Fusions in Mammalian Cells. *AIDS Res. Ther.* **2010**, *7*, 1–10.

Huang, L.; Chen, C. Understanding HIV-1 Protease Autoprocessing for Novel Therapeutic Development. *Future Med. Chem.* **2013**, *5* (11), 1215–1229.

Huang, L.; Sayer, J. M.; Swinford, M.; Louis, J. M.; Chen, C. Modulation of Human Immunodeficiency Virus Type 1 Protease Autoprocessing by Charge Properties of Surface Residue 69. *J. Virol.* **2009**, *83* (15), 7789–7793.

Humann, J.; Lenz, L. L. Bacterial Peptidoglycan-Degrading Enzymes and Their Impact on Host Muropeptide Detection. *J. Innate Immun.* **2009**, *1* (2), 88–97.

Humpolíčková, J.; Weber, J.; Starková, J.; Mašínová, E.; Günterová, J.; Flaisigová, I.; Konvalinka, J.; Majerová, T. Inhibition of the Precursor and Mature Forms of HIV-1 Protease as a Tool for Drug Evaluation. *Sci. Rep.* **2018**, *8*, 10438.

Israël, A. The IKK Complex, a Central Regulator of NF-KappaB Activation. *Cold Spring Harb. Perspect. Biol.* **2010**, *2* (3), a000158.

Jäger, S.; Cimermancic, P.; Gulbahce, N.; Johnson, J. R.; McGovern, K. E.; Clarke, S. C.; Shales, M.; Mercenne, G.; Pache, L.; Li, K.; et al. Global Landscape of HIV-Human Protein Complexes. *Nature* **2012**, *481* (7381), 365–370.

Jeffery, C. Moonlighting Proteins. *Trends Biochem. Sci.* **1999**, *24* (1), 8–11.

Johnson, J. W.; Fisher, J. F.; Mobashery, S. Bacterial Cell-Wall Recycling. *Ann. N. Y. Acad. Sci.* **2013**, *1277* (1), 54–75.

Johnson, M. C. Mechanisms for Env Glycoprotein Acquisition by Retroviruses. *AIDS Res. Hum. Retroviruses* **2011**, *23* (3), 239–247.

Jones, K. E.; Patel, N. G.; Levy, M. A.; Storeygard, A.; Balk, D.; Gittleman, J. L.; Daszak, P. Global Trends in Emerging Infectious Diseases. *Nature* **2008**, *451* (7181), 990–993.

Joshi, S. G.; Kovács, A. D. *Rickettsia rickettsii* Infection Causes Apoptotic Death of Cultured Cerebellar Granule Neurons. *J. Med. Microbiol.* **2007**, *56* (1), 138–141.

Joshi, S. G.; Francis, C. W.; Silverman, D. J.; Sahni, S. K. Nuclear Factor κB Protects against Host Cell Apoptosis during *Rickettsia rickettsii* Infection by Inhibiting Activation of Apical and Effector Caspases and Maintaining Mitochondrial Integrity. *Infect. Immun.* **2003**, *71* (7), 4127–4136.

Joshi, S. G.; Francis, C. W.; Silverman, D. J.; Sahni, S. K. NF-κB Activation Suppresses Host Cell Apoptosis during *Rickettsia rickettsii* Infection via Regulatory Effects on Intracellular Localization or Levels of Apoptogenic and Anti-Apoptotic Proteins. *FEMS Microbiol. Lett.* **2004**, *234* (2), 333–341.

Kazimírová, M.; Štibrániová, I. Tick Salivary Compounds: Their Role in Modulation of Host Defences and Pathogen Transmission. *Front. Cell. Infect. Microbiol.* **2013**, *3*, 43.

Kepp, O.; Galluzzi, L.; Lipinski, M.; Yuan, J.; Kroemer, G. Cell Death Assays for Drug Discovery. *Nat. Rev. Drug Discov.* **2011**, *10* (3), 221–237.

Kleba, B.; Clark, T. R.; Lutter, E. I.; Ellison, D. W.; Hackstadt, T. Disruption of the *Rickettsia rickettsii* Sca2 Autotransporter Inhibits Actin-Based Motility. *Infect. Immun.* **2010**, *78* (5), 2240–2247.

Koh, Y.; Matsumi, S.; Das, D.; Amano, M.; Davis, D. A.; Li, J.; Leschenko, S.; Baldridge, A.; Shioda, T.; Yarchoan, R.; et al. Potent Inhibition of HIV-1 Replication by Novel Non-Peptidyl Small Molecule Inhibitors of Protease Dimerization. *J. Biol. Chem.* **2007**, *282* (39), 28709–28720.

Konvalinka, J.; Kräusslich, H.-G.; Müller, B. Retroviral Proteases and Their Roles in Virion Maturation. *Virology* **2015**, *479–480*, 403–417.

Labbé, K.; Saleh, M. Cell Death in the Host Response to Infection. *Cell Death Differ.* **2008**, *15* (9), 1339–1349.

Latz, E.; Xiao, T. S.; Stutz, A. Activation and Regulation of The Inflammasomes. *Nat. Rev. Immunol.* **2013**, *13* (6), 397–411.

Lee, A. S. Y.; Kranzusch, P. J.; Doudna, J. A.; Cate, J. H. D. eIF3d Is an mRNA Cap-Binding Protein That Is Required for Specialized Translation Initiation. *Nature* **2016**, *536* (7614), 96–99.

Legendre, K. P.; Macaluso, K. R. *Rickettsia felis*: A Review of Transmission Mechanisms of an Emerging Pathogen. *Trop. Med. Infect. Dis.* **2017**, *2* (4).

Lehman, S. S.; Noriea, N. F.; Aistleitner, K.; Clark, T. R.; Dooley, C. A.; Nair, V.; Kaur, S. J.; Rahman, M. S.; Gillespie, J. J.; Azad, A. F.; et al. The Rickettsial Ankyrin Repeat Protein 2 Is a Type IV Secreted Effector That Associates with the Endoplasmic Reticulum. *MBio* **2018**, *9* (3), e00975-18.

Li, H.; D. H. Walker. Characterization of Rickettsial Attachment to Host Cells by Flow Cytometry. *Infect. Immun.* **1992**, *60* (5), 2030–2035.

Li, H.; Walker, D. H. rOmpA Is a Critical Protein for the Adhesion of *Rickettsia rickettsii* to Host Cells. *Microb. Pathog.* **1998**, *24* (5), 289–298.

Li, J.; Yuan, J. Caspases in Apoptosis and Beyond. *Oncogene* **2008**, *27* (48), 6194–6206.

Li, M.; Gustchina, A.; Cruz, R.; Simões, M.; Curto, P.; Martinez, J. J.; Faro, C.; Simões, I.; Wlodawera, A. Structure of RC1339/APRc from *Rickettsia conorii*, a Retropepsin-like Aspartic Protease. *Acta Crystallogr. Sect. D Biol. Crystallogr.* **2015**, *71* (10), 2109–2118.

Lindsten, K.; Uhlíková, T.; Konvalinka, J.; Massuci, M. G.; Dantuma, N. P. Cell-Based Fluorescence Assay for Human Immunodeficiency Virus Type 1 Protease Activity. *Antimicrob. Agents Chemother.* **2001**, *45* (9), 2616–2622.

Lloyd, R. E. Translational Control by Viral Proteinases. *Virus Res.* **2006**, *119* (1), 76–88.

López-Otín, C.; Bond, J. S. Proteases: Multifunctional Enzymes in Life and Disease. *J. Biol. Chem.* **2008**, *283* (45), 30433–30437.

Louis, J. M.; McDonald, R. A.; Nashed, N. T.; Wondrak, E. M.; Jerina, D. M.; Oroszlan, S.; Mora, P. T. Autoprocessing of the HIV-1 Protease Using Purified Wild-Type and Mutated Fusion Proteins Expressed at High Levels in *Escherichia coli*. *Eur. J. Biochem.* **1991**, *199* (2), 361–369.

Louis, J. M.; Marius Clore, G.; Gronenborn, A. M. Autoprocessing of HIV-1 Protease Is Tightly Coupled to Protein Folding. *Nat. Struct. Biol.* **1999**, *6* (9), 868–875.

Lv, Z.; Chu, Y.; Wang, Y. HIV Protease Inhibitors: A Review of Molecular Selectivity and Toxicity. *HIV/AIDS - Res. Palliat. Care* **2015**, *7*, 95–104.

Maina, A. N.; Klein, T. A.; Kim, H. C.; Chong, S. T.; Yang, Y.; Mullins, K.; Jiang, J.; St. John, H.; Jarman, R. G.; Hang, J.; et al. Molecular Characterization of Novel Mosquito-Borne *Rickettsia* spp. from Mosquitoes Collected at the Demilitarized Zone of the Republic of Korea. *PLoS One* **2017**, *12* (11), 1–16.

Martinez, J. J.; Cossart, P. Early Signaling Events Involved in the Entry of *Rickettsia conorii* into Mammalian Cells. *J. Cell Sci.* **2004**, *117* (21), 5097–5106.

Martinez, J. J.; Seveau, S.; Veiga, E.; Matsuyama, S.; Cossart, P. Ku70, a Component of DNA-Dependent Protein Kinase, Is a Mammalian Receptor for *Rickettsia*

*conorii*. *Cell* **2005**, *123* (6), 1013–1023.

Mattei, S.; Anders, M.; Konvalinka, J.; Kräusslich, H.-G.; Briggs, J. A. G.; Müller, B. Induced Maturation of Human Immunodeficiency Virus. *J. Virol.* **2014**, *88* (23), 13722–13731.

Mattick, J. S.; Makunin, I. V. Non-Coding RNA. *Hum. Mol. Genet.* **2006**, *15 Spec No 1*, R17-29.

Mayer, C. Bacterial Cell Wall Recycling. *eLS*. July 16, 2012.

McClure, E. E.; Chávez, A. S. O.; Shaw, D. K.; Carlyon, J. A.; Ganta, R. R.; Noh, S. M.; Wood, D. O.; Bavoil, P. M.; Brayton, K. A.; Martinez, J. J.; et al. Engineering of Obligate Intracellular Bacteria: Progress, Challenges and Paradigms. *Nat. Rev. Microbiol.* **2017**, *15* (9), 544–558.

McLeod, M. P.; Qin, X.; Karpathy, S. E.; Gioia, J.; Highlander, S. K.; Fox, G. E.; McNeill, T. Z.; Jiang, H.; Muzny, D.; Jacob, L. S.; et al. Complete Genome Sequence of *Rickettsia typhi* and Comparison with Sequences of Other *Rickettsia*. *J. Bacteriol.* **2004**, *186* (17), 5842–5855.

Montgomery, R. R.; Lusitani, D.; Chevance, A. de B.; Malawista, S. E. Tick Saliva Reduces Adherence and Area of Human Neutrophils. *Infect. Immun.* **2004**, *72* (5), 2989–2994.

Mous, J.; Heimer, E. P.; Grice, S. F. Le. Processing Protease and Reverse Transcriptase from Human Immunodeficiency Virus Type I Polyprotein in *Escherichia coli*. *J. Virol.* **1988**, *62* (4), 1433–1436.

Mukaida, N.; Wang, Y.-Y.; Li, Y.-Y. Roles of Pim-3, a Novel Survival Kinase, in Tumorigenesis. *Cancer Sci.* **2011**, *102* (8), 1437–1442.

Müller, U.; Vogel, P.; Alber, G.; Schaub, G. The Innate Immune System of Mammals and Insects. *Contrib. Microbiol.* **2008**, *15*, 21–44.

Naderer, T.; Fulcher, M. C. Targeting Apoptosis Pathways in Infections. *J. Leukoc. Biol.* **2018**, *103* (2), 275–285.

Narra, H. P.; Schroeder, C. L. C.; Sahni, A.; Rojas, M.; Khanipov, K.; Fofanov, Y.; Sahni, S. K. Small Regulatory RNAs of *Rickettsia conorii*. *Sci. Rep.* **2016**, *6* (36728).

Nie, Z.; Phenix, B. N.; Lum, J. J.; Alam, A.; Lynch, D. H.; Beckett, B.; Krammer, P. H.; Sekaly, R. P.; Badley, A. D. HIV-1 Protease Processes Procaspase 8 to Cause Mitochondrial Release of Cytochrome c, Caspase Cleavage and Nuclear Fragmentation. *Cell Death Differ.* **2002**, *9* (11), 1172–1184.

Ogawa, M.; Yoshimori, T.; Suzuki, T.; Sagara, H.; Mizushima, N.; Sasakawa, C. Escape of Intracellular *Shigella* From Autophagy. *Science* **2005**, *307* (5710), 727–731.

Okoye, A. A.; Picker, L. J. CD4(+) T-Cell Depletion in HIV Infection: Mechanisms of Immunological Failure. *Immunol. Rev.* **2013**, *254* (1), 54–64.

Pallett, M. A.; Crepin, V. F.; Serafini, N.; Habibzay, M.; Kotik, O.; Sanchez-Garrido, J.; Santo, J. P. Di; Shenoy, A. R.; Berger, C. N.; Frankel, G. Bacterial Virulence Factor Inhibits Caspase-4/11 Activation in Intestinal Epithelial Cells. *Mucosal Immunol.* **2017**, *10* (3), 602–612.

Pan, Y.-Y.; Wang, S.-M.; Huang, K.-J.; Chiang, C.-C.; Wang, C.-T. Placement of Leucine Zipper Motifs at the Carboxyl Terminus of HIV-1 Protease Significantly Reduces Virion Production. *PLoS One* **2012**, *7* (3), e32845.

Parola, P.; Paddock, C. D.; Raoult, D. Tick-Borne Rickettsioses Around the World: Emerging Diseases Challenging Old Concepts. *Clin. Microbiol. Rev.* **2005**, *18* (4), 719–756.

Parola, P.; Paddock, C. D.; Socolovschi, C.; Labruna, M. B.; Mediannikov, O.; Kernif, T.; Abdad, M. Y.; Stenos, J.; Bitam, I.; Fournier, P. E.; et al. Update on Tick-Borne Rickettsioses around the World: A Geographic Approach. *Clin. Microbiol. Rev.* **2013**, *26* (4), 657–702.

Partin, K.; Zybarth, G.; Ehrlich, L.; DeCrombrugghe, M.; Wimmer, E.; Carter, C. Deletion of Sequences Upstream of the Proteinase Improves the Proteolytic Processing of Human Immunodeficiency Virus Type 1. *Proc. Natl. Acad. Sci. U. S. A.* **1991**, *88* (11), 4776-4780.

Patel, J. G.; Narra, H. P.; Sepuru, K. M.; Sahni, A.; Golla, S. R.; Sahni, A.; Singh, A.; Schroeder, C. L. C.; Chowdhury, I. H.; Popov, V. L.; et al. Evolution, Purification, and Characterization of RC0497: A Peptidoglycan Amidase from the Prototypical Spotted Fever Species *Rickettsia conorii*. *Biol. Chem.* **2020**, *401* (2), 249–262.

Polager, S.; Ginsberg, D. NF-κB at the Crossroads of Life and Death. *Trends Cell Biol.* **2008**, *18* (11), 528–535.

Porter, A. G.; Jänicke, R. U. Emerging Roles of Caspase-3 in Apoptosis. *Cell Death Differ.* **1999**, *6*, 99–104.

Rahman, M. S.; Gillespie, J. J.; Kaur, S. J.; Sears, K. T.; Ceraul, S. M.; Beier-Sexton, M.; Azad, A. F. *Rickettsia typhi* Possesses Phospholipase A2 Enzymes That Are Involved in Infection of Host Cells. *PLoS Pathog.* **2013**, *9* (6), e1003399.

Raoult, D.; Roux, V. Rickettsioses as Paradigms of New or Emerging Infectious Diseases. *Clin. Microbiol. Rev.* **1997**, *10* (4), 694–719.

Rapaport, D. How Does the TOM Complex Mediate Insertion of Precursor Proteins into the Mitochondrial Outer Membrane? *J. Cell Biol.* **2005**, *171* (3), 419–423.

Ratner, L.; Haseltine, W.; Patarca, R.; Livak, K. J.; Starcich, B.; Josephs, S. F.; Doran, E. R.; Rafalski, J. A.; Whitehorn, E. A.; Baumeister, K.; et al. Complete Nucleotide Sequence of the AIDS Virus, HTLV-III. *Nature* **1985**, *313*, 277–284.

Rawlings, N. D.; Barrett, A. J.; Thomas, P. D.; Huang, X.; Bateman, A.; Finn, R. D.

The MEROPS Database of Proteolytic Enzymes, Their Substrates and Inhibitors in 2017 and a Comparison with Peptidases in the PANTHER Database. *Nucleic Acids Res.* **2018**, *46*, D624–D632.

Reed, S. C. O.; Lamason, R. L.; Risca, V. I.; Abernathy, E.; Welch, M. D. *Rickettsia* Actin-Based Motility Occurs in Distinct Phases Mediated by Different Actin Nucleators. *Curr. Biol.* **2014**, *24* (1), 98–103.

Rennoll-Bankert, K. E.; Rahman, M. S.; Guillotte, M. L.; Lehman, S. S.; Beier-Sexton, M.; Gillespie, J. J.; Azad, A. F. RalF-Mediated Activation of Arf6 Controls *Rickettsia typhi* Invasion by Co-Opting Phosphoinositol Metabolism. *Infect. Immun.* **2016**, *84* (12), 3496–3506.

Renvoisé, A.; Rolain, J.; Socolovschi, C.; Raoult, D. Widespread Use of Real-time PCR for Rickettsial Diagnosis. *FEMS Immunol. Med. Microbiol.* **2011**, *64* (1), 126–129.

Riley, S. P.; Goh, K. C.; Hermanas, T. M.; Cardwell, M. M.; Chan, Y.; Martinez, J. J. The *Rickettsia conorii* Autotransporter Protein Sca1 Promotes Adherence to Nonphagocytic Mammalian Cells. *Infect. Immun.* **2010**, *78* (5), 1895–1904.

Riley, S. P.; Patterson, J. L.; Martinez, J. J. The Rickettsial OmpB β-Peptide of *Rickettsia conorii* Is Sufficient to Facilitate Factor H-Mediated Serum Resistance. *Infect. Immun.* **2012**, *80* (8), 2735–2743.

Riley, S. P.; Patterson, J. L.; Martinez, J. J. Pathogenic *Rickettsia* Species Acquire Vitronectin From Human Serum to Promote Resistance to Complement-Mediated Killing. *Cell. Microbiolgy* **2014**, *16* (6), 649–661.

Rogers, L. D.; Overall, C. M. Proteolytic Post-Translational Modification of Proteins: Proteomic Tools and Methodology. *Mol. Cell. Proteomics* **2013**, *12* (12), 3532–3542.

Rumlová, M.; Křížová, I.; Keprová, A.; Hadravová, R.; Doležal, M.; Strohalmová, K.; Pichová, I.; Hájek, M.; Ruml, T. HIV-1 Protease-Induced Apoptosis. *Retrovirology* **2014**, *11* (37).

Sahni, A.; Patel, J.; Narra, H. P.; Schroeder, C. L. C.; Walker, D. H.; Sahni, S. K. Fibroblast Growth Factor Receptor-1 Mediates Internalization of Pathogenic Spotted Fever Rickettsiae Into Host Endothelium. *PLoS One* **2017**, *12* (8), 1–16.

Sahni, S. K.; Narra, H. P.; Sahni, A.; Walker, D. H. Recent Molecular Insights Into Rickettsial Pathogenesis and Immunity. *Future Microbiol.* **2013**, *8* (10), 1265–1288.

Sainski, A. M.; Dai, H.; Natesampillai, S.; Pang, Y. P.; Bren, G. D.; Cummins, N. W.; Correia, C.; Meng, X. W.; Tarara, J. E.; Ramirez-Alvarado, M.; et al. Casp8p41 Generated by HIV Protease Kills CD4 T Cells through Direct Bak Activation. *J. Cell Biol.* **2014**, *206* (7), 867–876.

Sebastiani, A.; Gölz, C.; Sebastiani, P. G.; Bobkiewicz, W.; Behl, C.; Mittmann, T.;

Thal, S. C.; Engelhard, K. Sequestosome 1 Deficiency Delays, but Does Not Prevent Brain Damage Formation Following Acute Brain Injury in Adult Mice. *Frontiers in Neuroscience*. 2017, p 678.

Secades, P.; Guijarro, J. A. Purification and Characterization of an Extracellular Protease from the Fish Pathogen *Yersinia ruckeri* and Effect of Culture Conditions on Production. *Appl. Environ. Microbiol.* **1999**, *65* (9), 3969–3975.

Seelmeier, S.; Schmidt, H.; Turk, V.; Helm, K. von der. Human Immunodeficiency Virus Has an Aspartic-Type Protease That Can Be Inhibited by Pepstatin A. *Proc. Natl. Acad. Sci.* **1988**, *85* (18), 6612–6616.

Seibel, N. M.; Eljouni, J.; Nalaskowski, M. M.; Hampe, W. Nuclear Localization of Enhanced Green Fluorescent Protein Homomultimers. *Anal. Biochem.* **2007**, *368* (1), 95–99.

Sekeyová, Z.; Danchenko, M.; Filipčík, P.; Fournier, P. E. Rickettsial Infections of the Central Nervous System. *PLoS Negl. Trop. Dis.* **2019**, *13* (8), 1–18.

Sharma, A. K.; Dhasmana, N.; Dubey, N.; Kumar, N.; Gangwal, A.; Gupta, M.; Singh, Y. Bacterial Virulence Factors: Secreted for Survival. *Indian J. Microbiol.* **2016**, *57* (1), 1–10.

Shoeman, R. L.; Höner, B.; Stoller, T. J.; Kesselmeier, C.; Miedel, M. C.; Traub, P.; Graves, M. C. Human Immunodeficiency Virus Type 1 Protease Cleaves the Intermediate Filament Proteins Vimentin, Desmin, and Glial Fibrillary Acidic Protein. *Proc. Natl. Acad. Sci.* **1990**, *87* (16), 6336–6340.

Socolovschi, C.; Mediannikov, O.; Raoult, D.; Parola, P. The Relationship Between Spotted Fever Group Rickettsiae and *Ixodid* Ticks. *Vet. Res.* **2009**, *40* (2), 34.

Socolovschi, C.; Pagés, F.; Raoult, D. *Rickettsia felis* in *Aedes albopictus* Mosquitoes, Libreville, Gabon. *Emerg. Infect. Dis.* **2012a**, *18* (10), 1687–1689.

Socolovschi, C.; Pages, F.; Ndiath, M. O.; Ratmanov, P.; Raoult, D. *Rickettsia* Species in African *Anopheles* Mosquitoes. *PLoS One* **2012b**, *7* (10), e48254.

Sousa, R. de; Nóbrega, S. D.; Bacellar, F.; Torgal, J. Mediterranean Spotted Fever in Portugal: Risk Factors for Fatal Outcome in 105 Hospitalized Patients. *Ann. N. Y. Acad. Sci.* **2003**, *990* (1), 285–294.

Sporn, L. A.; Sahni, S. K.; Lerner, N. B.; Marder, V. J.; Silverman, D. J.; Turpin, L. C.; Schwab, A. L. *Rickettsia rickettsii* Infection of Cultured Human Endothelial Cells Induces NF-κB Activation. *Infect. Immun.* **1997**, *65* (7), 2786–2791.

Strack, P. R.; Frey, M. W.; Rizzo, C. J.; Cordova, B.; George, H. J.; Meade, R.; Ho, S. P.; Corman, J.; Tritch, R.; Korant, B. D. Apoptosis Mediated by HIV Protease Is Preceded by Cleavage of Bcl-2. *Proc. Natl. Acad. Sci.* **1996**, *93* (18), 9571–9576.

Sundquist, T.; Moravec, R.; Niles, A.; O'Brien, M.; Riss, T. Timing Your Apoptosis

Assays. *Cell Notes* **2006**, No. 16, 18–21.

Swanstrom, R.; Wills, J. W. Synthesis, Assembly, and Processing of Viral Proteins. In *Retroviruses*; Coffin, J. M., Hughes, S. H., Varmus, H. E., Eds.; Cold Spring Harbor (NY): Cold Spring Harbor Laboratory Press, 1997.

Tessmer, U.; Kräusslich, H.-G. Cleavage of Human Immunodeficiency Virus Type 1 Proteinase from the N-Terminally Adjacent p6* Protein Is Essential for Efficient Gag Polyprotein Processing and Viral Infectivity. *J. Virol.* **1998**, *72* (4), 3459–3463.

Thomas, P.; Smart, T. G. HEK293 Cell Line: A Vehicle for the Expression of Recombinant Proteins. *J. Pharmacol. Toxicol. Methods* **2005**, *51*, 187–200.

Uchida, N.; Hoshino, S.; Imataka, H.; Sonenberg, N.; Katada, T. A Novel Role of the Mammalian GSPT/eRF3 Associating with Poly(A)-Binding Protein in Cap/Poly(A)-Dependent Translation. *J. Biol. Chem.* **2002**, *277* (52), 50286–50292.

Uchiyama, T.; Kawano, H.; Kusuhara, Y. The Major Outer Membrane Protein rOmpB of Spotted Fever Group Rickettsiae Functions in the Rickettsial Adherence to and Invasion of Vero Cells. *Microbes Infect.* **2006**, *8* (3), 801–809.

Uchlyama, T. Tropism and Pathogenicity of Rickettsiae. *Front. Microbiol.* **2012**, *3*, 230.

Valbuena, G.; Walker, D. H. Changes in The Adherens Junctions of Human Endothelial Cells Infected with Spotted Fever Group Rickettsiae. *Virchows Arch.* **2005**, *446* (4), 379–382.

Valenzuela, J. G. Exploring Tick Saliva: From Biochemistry to 'Sialomes' and Functional Genomics. *Parasitology* **2004**, *129* (S1), S83–S94.

Vellaiswamy, M.; Kowalczewska, M.; Merhej, V.; Nappez, C.; Vincentelli, R.; Renesto, P.; Raoult, D. Characterization of Rickettsial Adhesin Adr2 Belonging to a New Group of Adhesins in α-Proteobacteria. *Microb. Pathog.* **2011**, *50* (5), 233–242.

Ventoso, I.; Blanco, R.; Perales, C.; Carrasco, L. HIV-1 Protease Cleaves Eukaryotic Initiation Factor 4G and Inhibits Cap-Dependent Translation. *Proc. Natl. Acad. Sci. U. S. A.* **2001**, *98* (23), 12966–12971.

Ventoso, I.; Navarro, J.; Muñoz, M. A.; Carrasco, L. Involvement of HIV-1 Protease in Virus-Induced Cell Killing. *Antiviral Res.* **2005**, *66* (1), 47–55.

Vidya Vijayan, K. K.; Karthigeyan, K. P.; Tripathi, S. P.; Hanna, L. E. Pathophysiology of CD4+ T-Cell Depletion in HIV-1 and HIV-2 Infections. *Front. Immunol.* **2017**, *8*, 580.

Vogt, V. M. Retroviral Virions and Genomes. In *Retroviruses*; Coffin, J. M., Hughes, S. H., Varmus, H. E., Eds.; Cold Spring Harbor (NY): Cold Spring Harbor Laboratory Press, 1997.

Wagner, R. N.; Reed, J. C.; Chanda, S. K. HIV-1 Protease Cleaves the Serine-

Threonine Kinases RIPK1 and RIPK2. *Retrovirology* **2015**, *12* (1), 1–16.

Walker, D. H.; Ismail, N. Emerging and Re-Emerging Rickettsioses: Endothelial Cell Infection and Early Disease Events. *Nat. Rev. Microbiol.* **2008**, *6* (5), 375–386.

Walker, D. H.; Hudnall, S. D.; Szaniawski, W. K.; Feng, H. M. Monoclonal Antibody-Based Immunohistochemical Diagnosis of Rickettsialpox: The Macrophage Is the Principal Target. *Mod. Pathol. An Off. J. United States Can. Acad. Pathol.* **1999**, *12* (5), 529–533.

Walsh, D.; Mohr, I. Viral Subversion of the Host Protein Synthesis Machinery. *Nat. Rev. Microbiol.* **2011**, *9* (12), 860–875.

Weinert, L. A.; Werren, J. H.; Aebi, A.; Stone, G. N.; Jiggins, F. M. Evolution and Diversity of *Rickettsia* Bacteria. *BMC Biol.* **2009**, *7* (6).

Whitworth, T.; Popov, V. L.; Yu, X.-J.; Walker, D. H.; Bouyer, D. H. Expression of the *Rickettsia prowazekii pld* or *tlyC* Gene in *Salmonella enterica* Serovar Typhimurium Mediates Phagosomal Escape. *Infect. Immun.* **2005**, *73* (10), 6668–6673.

Wilson, J.; Schurr, M.; LeBlanc, C.; Ramamurthy, R.; Buchanan, K.; Nickerson, C. Mechanisms of Bacterial Pathogenicity. *Postgrad. Med. J.* **2002**, *78* (918), 216–224.

Wolf, A. J.; Underhill, D. M. Peptidoglycan Recognition by the Innate Immune System. *Nat. Rev. Immunol.* **2018**, *18* (4), 243–254.

Wood, D. O.; Azad, A. F. Genetic Manipulation of Rickettsiae: A Preview. *Infect. Immun.* **2000**, *68* (22), 6091–6093.

World Health Organization (WHO). Mosquito-borne diseases. https://www.who.int/neglected_diseases/vector_ecology/mosquito-borne-diseases/en/ (accessed May 2, 2020).

Wu, Y.-W.; Li, F. Bacterial Interaction with Host Autophagy. *Virulence* **2019**, *10* (1), 352–362.

Yatim, K. M.; Lakkis, F. G. A Brief Journey through the Immune System. *Clin. J. Am. Soc. Nephrol.* **2015**, *10* (7), 1274–1281.

Ying, S.; Seiffert, B. M.; Häcker, G.; Fischer, S. F. Broad Degradation of Proapoptotic Proteins with the Conserved Bcl-2 Homology Domain 3 during Infection with *Chlamydia trachomatis*. *Infect. Immun.* **2005**, *73* (3), 1399–1403.

Yoshikawa, Y.; Ogawa, M.; Hain, T.; Yoshida, M.; Fukumatsu, M.; Kim, M.; Mimuro, H.; Nakagawa, I.; Yanagawa, T.; Ishii, T.; et al. *Listeria M+monocytogenes* ActA-Mediated Escape from Autophagic Recognition. *Nat. Cell Biol.* **2009**, *11* (10), 1233–1240.

Yrlida, U.; Wicka, M. J. *Salmonella*-Induced Apoptosis of Infected Macrophages Results in Presentation of a Bacteria-Encoded Antigen after Uptake by Bystander Dendritic Cells. *J. Exp. Med.* **2000**, *191* (4), 613–624.

Zhang, J.; Lu, G.; Li, J.; Kelly, P.; Li, M.; Wang, J.; Huang, K.; Qiu, H.; You, J.; Zhang, R.; et al. Molecular Detection of *Rickettsia felis* and *Rickettsia bellii* in Mosquitoes. *Vector-Borne Zoonotic Dis.* **2019**, *19* (11), 802–809.

Zhang, J. H.; Xu, M. DNA Fragmentation in Apoptosis. *Cell Res.* **2000**, *10* (3), 205–211.

Zhao, Y.; Valbuena, G.; Walker, D. H.; Gazi, M.; Hidalgo, M.; DeSousa, R.; Oteo, J. A.; Goez, Y.; Brasier, A. R. Endothelial Cell Proteomic Response to *Rickettsia conorii* Infection Reveals Activation of the Janus Kinase (JAK)-Signal Transducer and Activator of Transcription (STAT)-Inferferon Stimulated Gene (ISG)15 Pathway and Reprogramming Plasma Membrane Integrin. *Mol. Cell. Proteomics* **2016**, *15* (1), 289–304.

Zhao, Y.; Fang, R.; Zhang, J.; Zhang, Y.; Bechelli, J.; Smalley, C.; Valbuena, G.; Walker, D. H.; Oteo, J. A.; Brasier, A. R. Quantitative Proteomics of the Endothelial Secretome Identifies RC0497 as Diagnostic of Acute Rickettsial Spotted Fever Infections. *Am. J. Pathol.* **2020**, *190* (2), 306–322.

Zhu, N.; Wang, Z. An Assay for DNA Fragmentation in Apoptosis without Phenol/Chloroform Extraction and Ethanol Precipitation. *Anal. Biochem.* **1997**, *246*, 155–158.

# Chapter VI

# 6. Supplementary Material

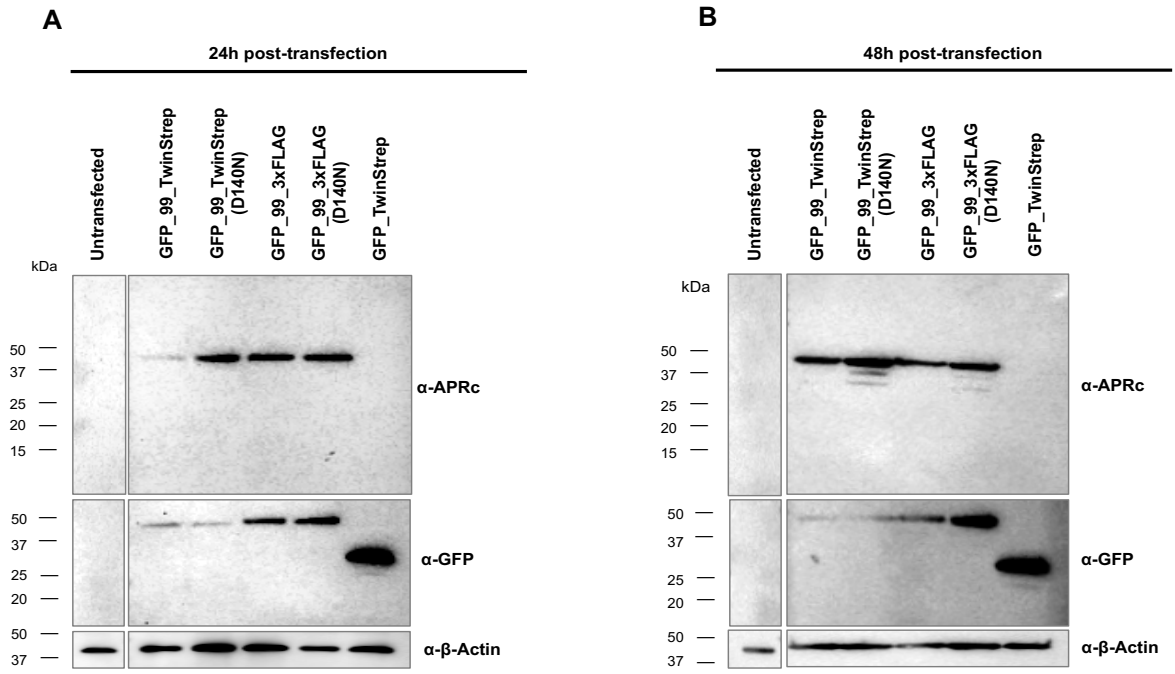


**Supplementary Figure 1.** Autoprocessing of GFP_APRc$_{99\text{-}231}$-fusion proteins in HEK293 cells.
HEK293 cells were transiently transfected with pcDNA3.1(+)-N-eGFP-derived vectors expressing the indicated constructs using the calcium phosphate method. Protein extracts were prepared at 24h (**A**) and 48h (**B**) post-transfection and analyzed by SDS-PAGE and Western blotting. 40µL of each sample was examined in parallel with anti-APRc antibody, anti-GFP antibody, and anti-β-actin antibody (as a loading control). Molecular mass markers (kDa) are indicated at the left of each membrane.

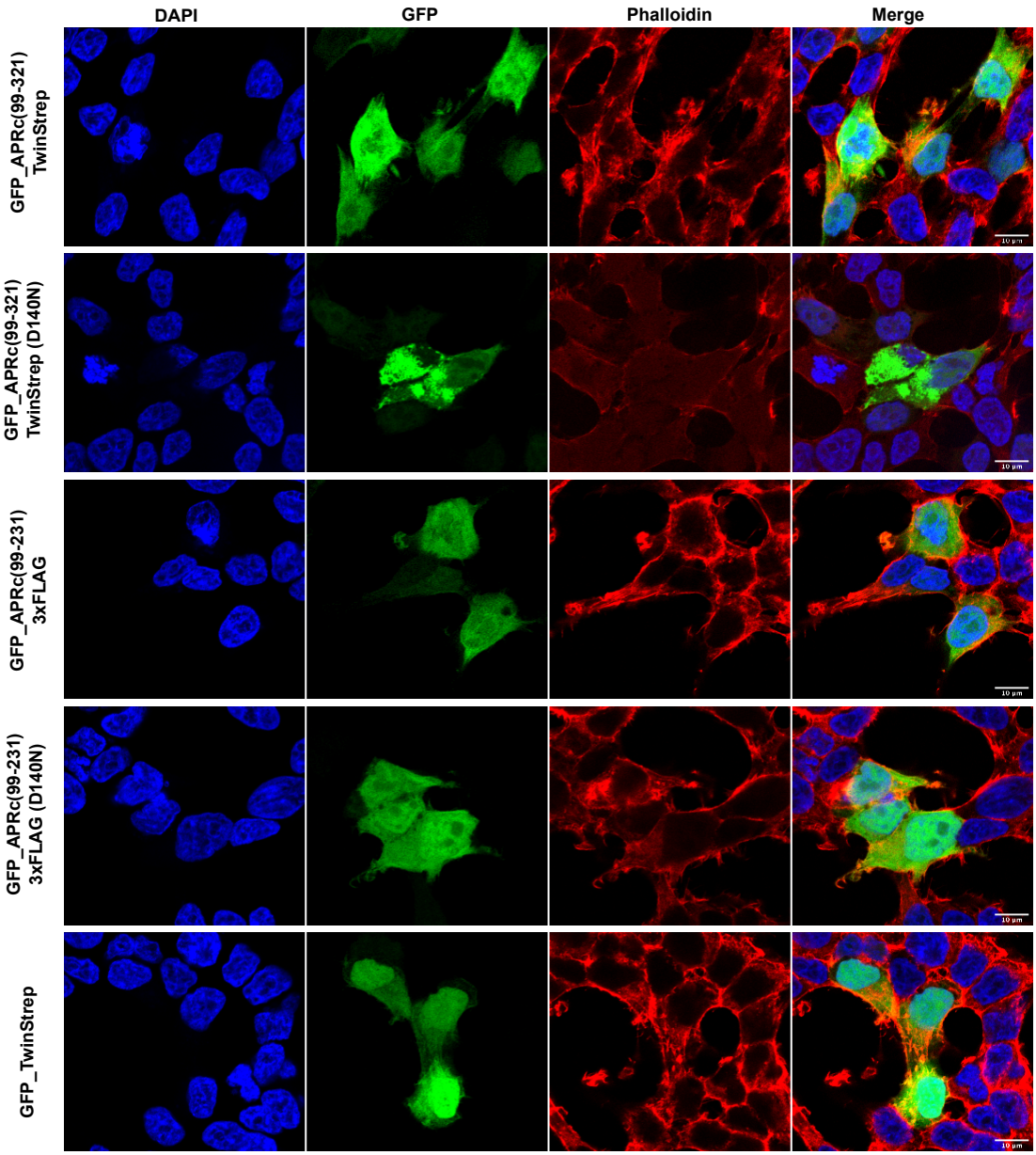


**Supplementary Figure 2.** Confocal microscopy analysis of the expression of GFP_APRc$_{99-231}$-fusion constructs in HEK293 cells at 24h post-transfection.
HEK293 cells were transiently transfected with pcDNA3.1(+)-N-eGFP-derived vectors expressing the indicated constructs using the calcium phosphate method. At 24h post-transfection, the cells were fixed, permeabilized, and double stained for confocal microscopy analysis with DAPI (blue) to stain the nuclei and phalloidin (red) to stain the actin cytoskeleton. Representative images of a single slice from the z stacks. Each row shows, from left to right, nuclei staining, GFP, phalloidin staining, and the merged image. Scale bar = 10 µm.

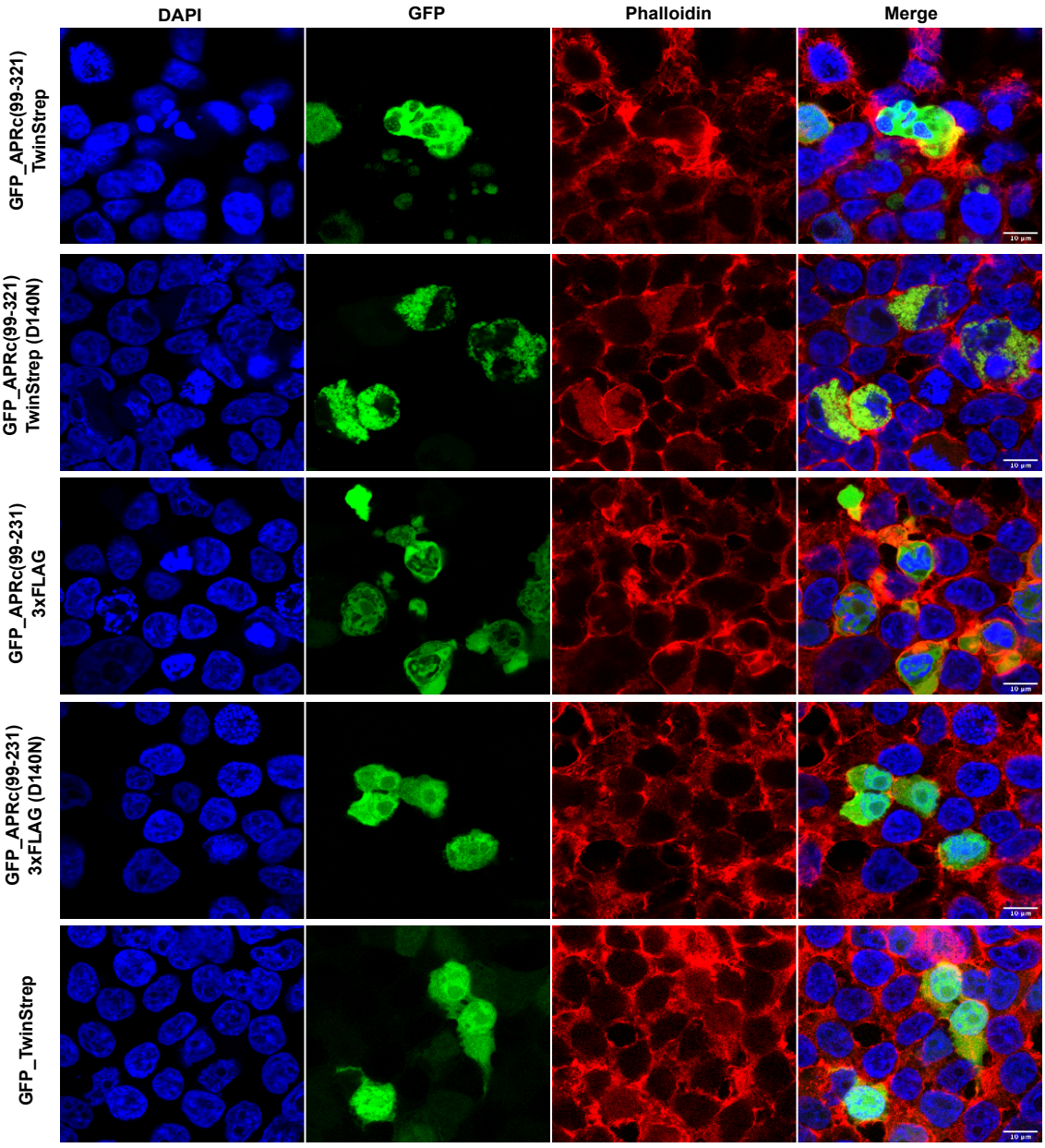


**Supplementary Figure 3.** Confocal microscopy analysis of the expression of GFP_APRc$_{99-231}$-fusion constructs in HEK293 cells at 48h post-transfection.
HEK293 cells were transiently transfected with pcDNA3.1(+)-N-eGFP-derived vectors expressing the indicated constructs using the calcium phosphate method. At 48h post-transfection, the cells were fixed, permeabilized, and double stained for confocal microscopy analysis with DAPI (blue) to stain the nuclei and phalloidin (red) to stain the actin cytoskeleton. Representative images of a single slice from the z stacks. Each row shows, from left to right, nuclei staining, GFP, phalloidin staining, and the merged image. Scale bar = 10 µm.

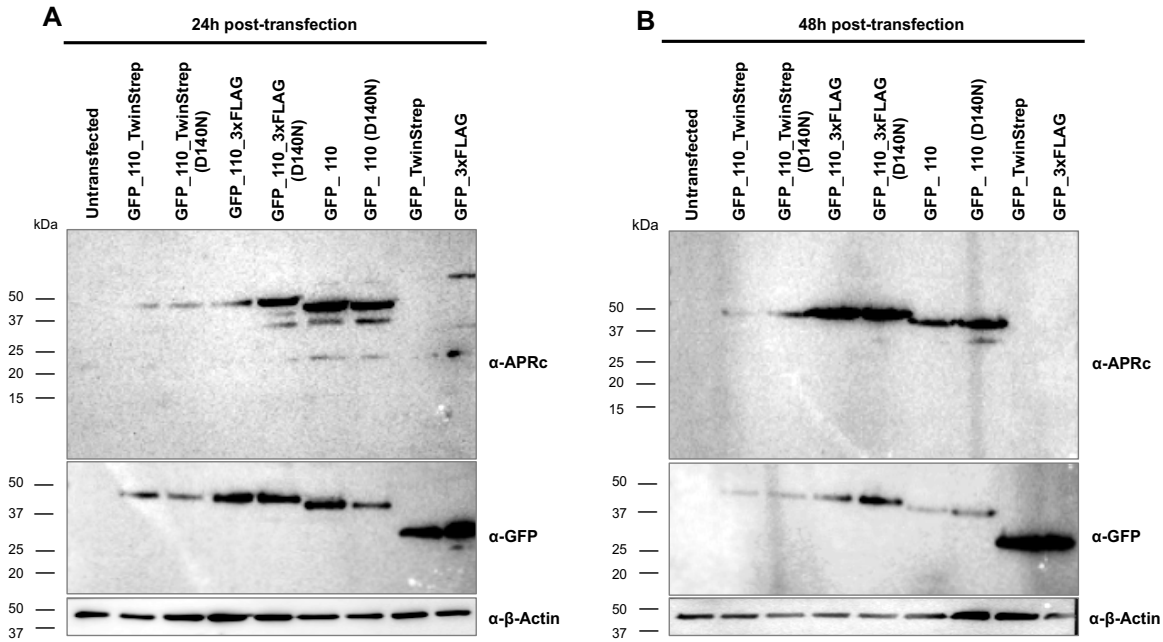


**Supplementary Figure 4.** Autoprocessing of GFP_APRc$_{110-231}$-fusion proteins in HEK293 cells. HEK293 cells were transiently transfected with pcDNA3.1(+)-N-eGFP-derived vectors expressing the indicated constructs using the calcium phosphate method. Protein extracts were prepared at 24h (**A**) and 48h (**B**) post-transfection and analyzed by SDS-PAGE and Western blotting. 40µL of each sample was examined in parallel with anti-APRc antibody, anti-GFP antibody, and anti-β-actin antibody (as a loading control). Molecular mass markers (kDa) are indicated at the left of each membrane.

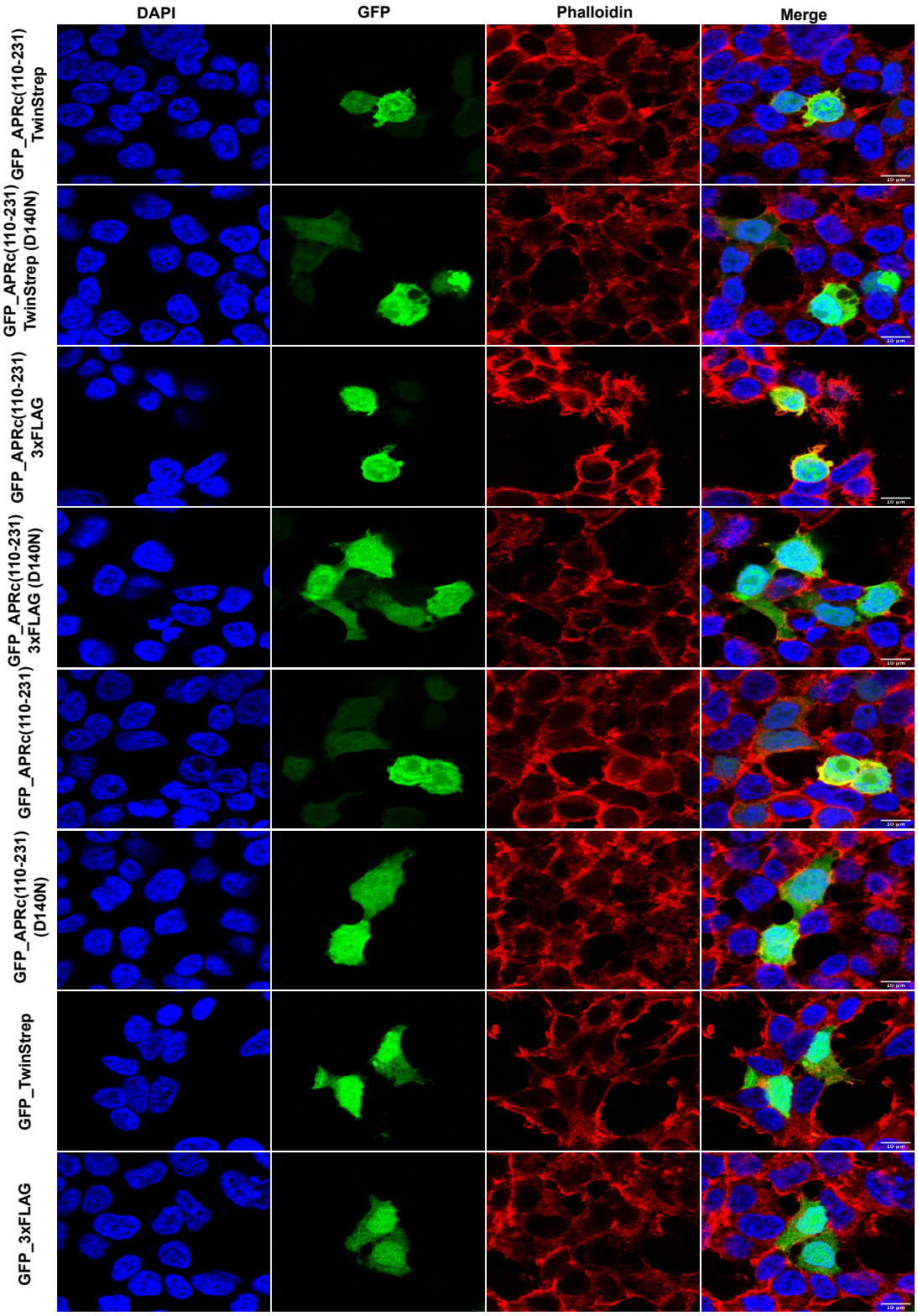


**Supplementary Figure 5.** Confocal microscopy analysis of the expression of GFP_APRc$_{110-231}$-fusion constructs in HEK293 cells at 24h post-transfection.
HEK293 cells were transiently transfected with pcDNA3.1(+)-N-eGFP-derived vectors expressing the indicated constructs using the calcium phosphate method. At 24h post-transfection, the cells were fixed, permeabilized, and double stained for confocal microscopy analysis with DAPI (blue) to stain the nuclei and phalloidin (red) to stain the actin cytoskeleton. Representative images of a single slice from the z stacks. Each row shows, from left to right, nuclei staining, GFP, phalloidin staining, and the merged image. Scale bar = 10 µm.

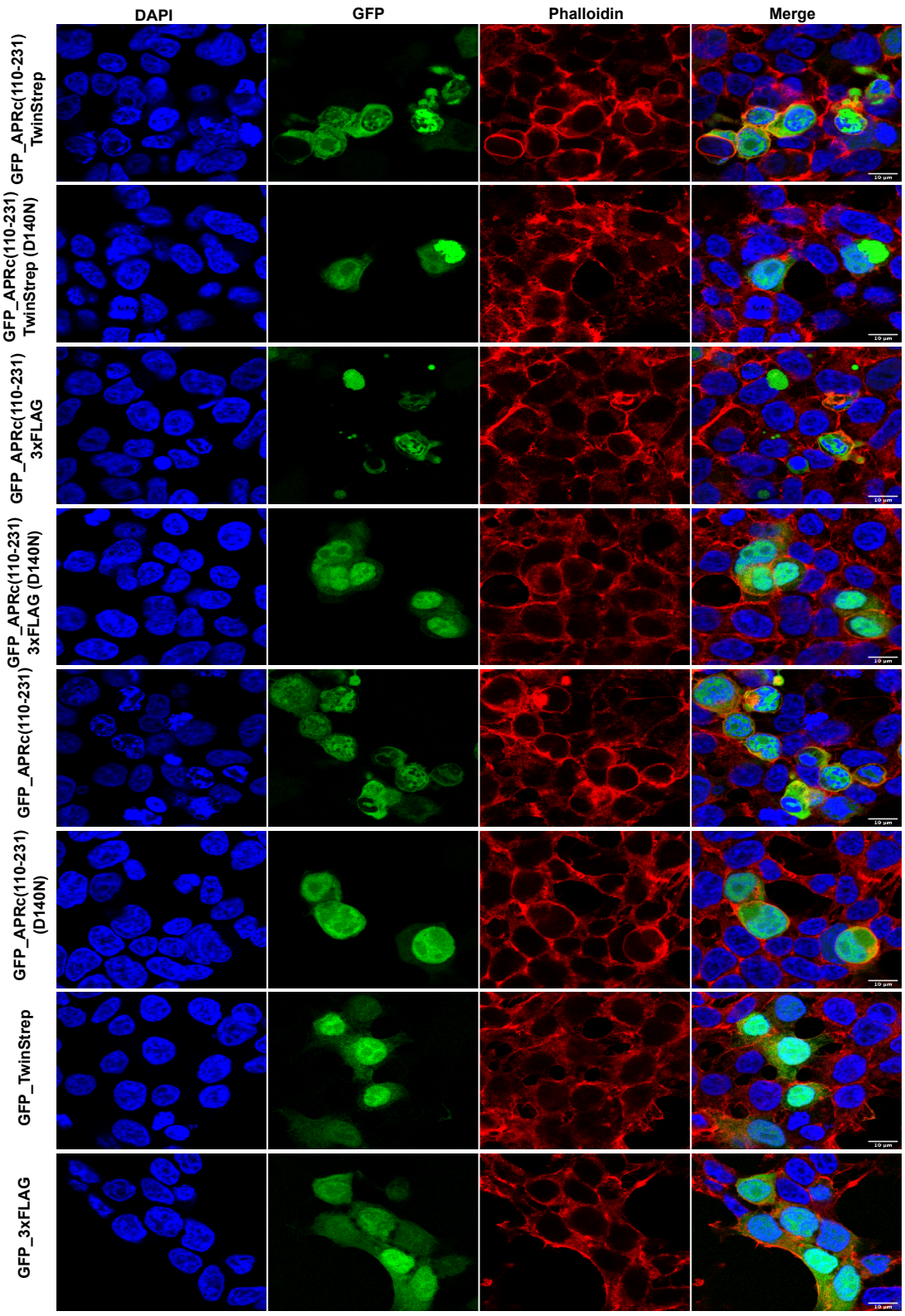


**Supplementary Figure 6.** Confocal microscopy analysis of the expression of GFP_APRc$_{110-231}$-fusion constructs in HEK293 cells at 48h post-transfection.
HEK293 cells were transiently transfected with pcDNA3.1(+)-N-eGFP-derived vectors expressing the indicated constructs using the calcium phosphate method. At 48h post-transfection, the cells were fixed, permeabilized, and double stained for confocal microscopy analysis with DAPI (blue) to stain the nuclei and phalloidin (red) to stain the actin cytoskeleton. Representative images of a single slice from the z stacks. Each row shows, from left to right, nuclei staining, GFP, phalloidin staining, and the merged image. Scale bar = 10 µm.

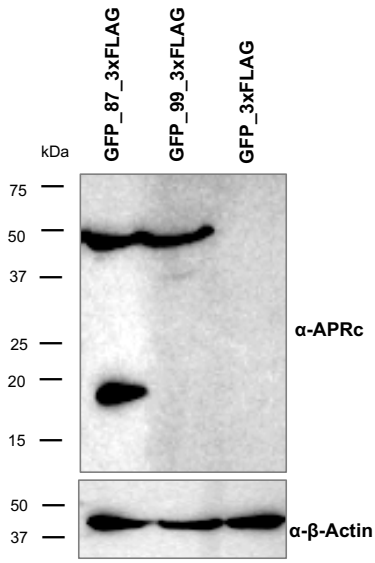


**Supplementary Figure 7.** Autoprocessing of different GFP_APRc-fusion constructs in HEK293 cells upon transfection with Lipofectamine 3000.
HEK293 cells were transiently transfected with pcDNA3.1(+)-N-eGFP-derived vectors expressing the indicated constructs using the Lipofectamine 3000. Protein extracts were prepared at 48h post-transfection and analyzed by SDS-PAGE and Western blotting. 40µL of each sample was examined in parallel with anti-APRc antibody and anti-β-actin antibody (as a loading control). Molecular mass markers (kDa) are indicated at the left.

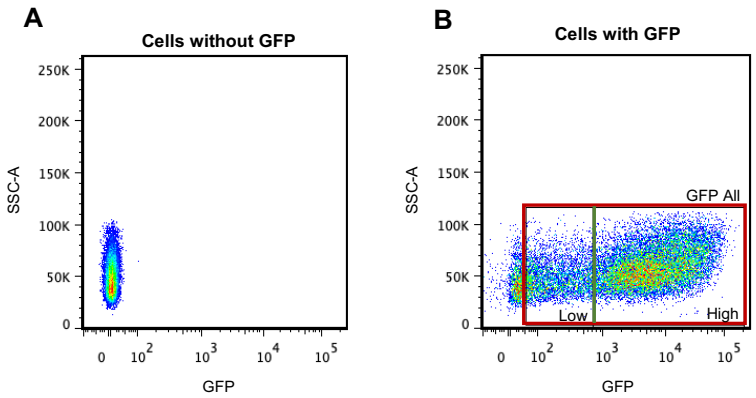


**Supplementary Figure 8.** Separation of flow cytometry results intro subgroups of transfected cells, according to GFP intensity.
Taking into account the dot plot represented in **A** (baseline of GFP intensity value), three subgroups of transfected cells were defined **(B)**: *GFP All* (all transfected cells), *GFP High* (transfected cells with high levels of accumulation of GFP-fusion proteins), and *GFP Low* (transfected cells low levels of accumulation of GFP- fusion proteins).

**Supplementary Table 1.** Annexin V/DAPI detection by flow cytometry in HEK293 cells.
Percentage of annexin V+/DAPI- cells for each group are presented for each independent replicate. The distinction by GFP intensity is represented in **Supplementary Figure 8**. [(1)] Correspond to values represented in **Figure 32**.

**% AnnexinV$^+$/DAPI$^-$**

| | Negative control | GFP_3xFLAG | GFP_APRc(87-231) 3xFLAG | GFP_APRc(87-231) 3xFLAG (D140N) |
|---|---|---|---|---|
| | 3.79 / 4.29 / 3.38 [(1)] | | | |
| **GFP All** | | 1.65 / 2.90 [(1)] | 5.27 / 5.16 / 4.15 [(1)] | 5.44 / 5.30 [(1)] |
| **GFP High** | | 1.44 / 2.70 | 4.43 / 4.24 /3.36 | 5.01 / 4.71 |
| **GFP Low** | | 2.49 / 3.56 | 8.55 /8.06 /7.63 | 6.98 / 7.41 |